Matrix-Assisted Laser Desorption/Ionization

11

Learning Objectives

- Pulsed laser light as a source of energy for desorption and ionization
- Ion formation from thin solid layers
- Matrix assistance as a key to soft desorption/ionization
- Ionization in an inherently pulsed mode
- Applications for small molecules, synthetic polymers, and biomolecules
- Vacuum and atmospheric pressure sources for MALDI
- MALDI imaging techniques

Laser desorption/ionization (LDI) was introduced in the late 1960s [1–3], long before the advent of field desorption (FD, Chap. 8), *californium plasma desorption* (^{252}Cf-PD, Sect. 10.8) or *fast atom bombardment* (FAB, Chap. 10). While low-mass organic salts and light-absorbing organic molecules are easily accessible by LDI [2, 3], it takes a serious effort to obtain useful mass spectra of biomolecules [4], in particular when the mass of the analyte exceeds 2000 u [5, 6]. FAB and ^{252}Cf-PD therefore represented the standard in all life science-related fields of mass spectrometry until the late 1980s, while LDI was regarded rather exotic [7].

The admixture of strongly light-absorbing compounds to the sample prior to preparation for laser desorption effected a tremendous change of what was possible in mass spectrometry. Two approaches were independently developed: (*i*) the admixture of ultrafine cobalt powder (particle size about 30 nm) to analyte solutions in glycerol [8, 9], and (*ii*) the cocrystallization of the analyte with an organic matrix [10–13]. When combined with a *time-of-flight* (TOF, Sect. 4.2) mass analyzer, both methods are capable of producing mass spectra of proteins of about 100,000 u molecular weight. Nonetheless, the application of the "*ultrafine-metal-plus-liquid-matrix*" method remained an exception because the versatility of an organic matrix

J.H. Gross, *Mass Spectrometry*, DOI 10.1007/978-3-319-54398-7_11

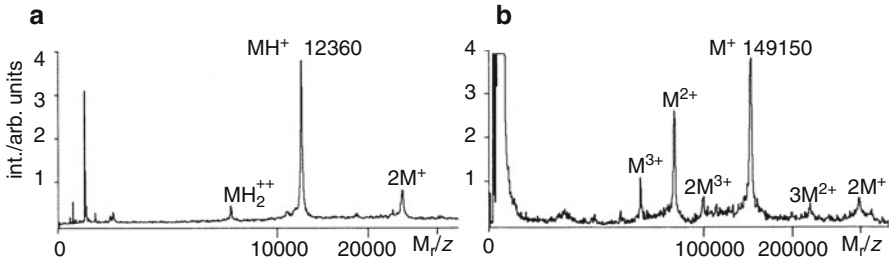

Fig. 11.1 MALDI-TOF mass spectra of (**a**) porcine cytochrome C from 2,5-dihydroxybenzoic acid matrix at a laser wavelength of 337 nm and (**b**) a monoclonal antibody from nicotinic acid matrix at 266 nm. These spectra from one of the landmark papers during the early phase of MALDI development impressively demonstrate the enormous potential of the method (Reproduced from Ref. [16] by permission. © John Wiley & Sons, 1991)

and the sensitivity of *matrix-assisted laser desorption/ionization* (MALDI) [10, 11, 14, 15] made it by far superior to the admixture of cobalt powder (Fig. 11.1) [16–19]. In its present state, MALDI represents a major analytical tool in the modern life sciences [20–25] and in polymer science [24–27].

11.1 Ion Sources for LDI and MALDI

The basic setup of LDI/MALDI ion sources is comparatively simple (Fig. 11.2) [28]. Both LDI and MALDI make use of the absorption of laser light by a solid sample layer. The energy uptake upon laser irradiation then causes evaporation and eventually ionization of the sample. The pulse of laser light is focused onto a small spot which is typically 0.05–0.2 mm in diameter [29]. As laser irradiance is a critical parameter in MALDI, a variable beam attenuator in the laser optical path is employed to adjust the irradiance. Then, the laser attenuation is individually optimized for each measurement. LDI/MALDI ion sources are generally operated at ambient temperature.

Although lasers of both ultraviolet (UV) and infrared (IR) wavelengths are in use, UV lasers are by far the most important light sources in analytical LDI-MS and MALDI-MS. Among these, nitrogen lasers and frequency-tripled or quadrupled Nd:Yag lasers serve for the majority of applications [30]. IR-MALDI is dominated by Er:Yag lasers [30, 31] while TEA-CO_2 lasers (cf. IRMPD in Sect. 9.12) are rarely used (Table 11.1) [17, 32].

Photon energy We can calculate the energy per photon of the widely employed frequency-tripled Nd:Yag laser by using the relationship $E = h\nu$ and substituting $\nu = c/\lambda$ (Sect. 2.10.6). For a wavelength $\lambda = 355$ nm and with $h = 4.14 \times 10^{-15}$ eVs ($= 6.63 \times 10^{-34}$ Js) we obtain $E = 4.14 \times 10^{-15}$ eVs $\times$ (2.99×10^{8} m s^{-1}/ 3.55×10^{-7} m) = 3.49 eV (Table 11.1). This tells us, on the one hand, that the photon energy is substantial, but on the other, that a single photon

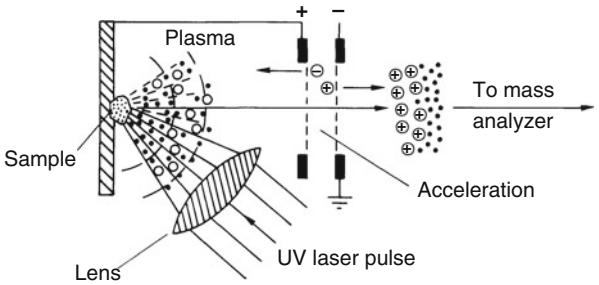

Fig. 11.2 Simplistic laser desorption ion source for nonresonant light absorption by a solid; in practice, the solid is supplied as a thin microcrystalline layer. Here, positive ions are continuously being extracted as long as the supply is sustained by the laser desorption plasma (Reproduced from Ref. [28] by permission. © Elsevier Science, 1994)

Table 11.1 Lasers for laser desorption/ionization

Spectral range	Wavelength	Photon energy	Laser type
UV	193 nm	6.4 eV	ArF Excimer laser
UV	248 nm	5.0 eV	KrF Excimer laser
UV	266 nm	4.7 eV	Frequency-quadrupled Nd:YAG laser
UV	308 nm	3.8 eV	XeCl Excimer laser
UV	337 nm	3.7 eV	Nitrogen laser[a]
UV	355 nm	3.5 eV	Frequency-tripled Nd:YAG laser[a]
IR	1.06 μm	1.2 eV	Nd:YAG laser[b]
IR	2.94 μm	0.4 eV	Er:YAG laser[b]
IR	1.7–2.5 μm	0.7–0.5 eV	Optical parametric oscillator (OPO) laser
IR	10.6 μm	0.1 eV	CO_2 laser

[a]most frequently used UV lasers
[b]most frequently used IR lasers

will not be able to cause ionization. Unlike photoionization, MALDI relies on the coincidence of a large number of photon absorptions across a macroscopic area.

UV lasers are emitting pulses of 3–10 ns duration, while those of IR lasers are in the range of 6–200 ns. Short pulses are needed to effect sudden ablation of the sample layer. In addition, an extremely short time interval of ion generation basically avoids thermal degradation of the analyte, e.g., a 10 ns laser pulse would require the high rate constant of 10^8 s^{-1} to complete decomposition. On the other hand, substantially longer irradiation would simply cause heating of the bulk material. In case of IR-MALDI, a slight decrease in threshold fluence has been observed with shorter laser pulses [33]. Furthermore, a short time interval of ion generation means a better definition of the starting pulse, which is relevant when a TOF analyzer is being used. Fortunately, the introduction of delayed extraction

techniques (Sect. 4.2.6) has greatly reduced the influence of the laser pulse duration on resolving power and mass accuracy [33].

Mostly UV MALDI
The majority of MALDI applications are run with UV lasers. IR-MALDI has been restricted to applications where the deeper penetration of IR radiation offers advantages, e.g., for the direct desorption of analytes from *sodium dodecyl sulfate* (SDS) gels or *thin layer chromatography* (TLC) plates.

11.2 Ion Formation

The mechanisms of ion formation in MALDI are a subject of continuing research [34–39]. The major concerns are the relationship between ion yield and laser fluence [29, 40], the temporal evolution of the desorption process and its implications upon ion formation [41], the initial velocity of the desorbing ions [33, 42, 43], and the question whether preformed ions or ions generated in the gas phase provide the major source of the ionic species detected in MALDI [44–46].

11.2.1 Ion Yield and Laser Fluence

Ion formation does not occur below a *threshold laser irradiance* of about 10^6 W cm^{-2}. At threshold, a sharp onset of desorption/ionization occurs and ion abundances rise to a high power (5th to 9th) of laser irradiance [17, 40, 47]. The threshold *laser fluence* for the detection of matrix and analyte ions not only depends on the actual matrix, but also on the molar matrix-to-analyte ratio, e.g., the minimum threshold laser fluence for cytochrome C was found at a molar matrix-to-sample ratio of 4000 : 1. Significantly higher or lower ratios require almost twice that laser fluence (Fig. 11.3) [48]. The increase at low analyte concentrations can be attributed to a decreasing detection efficiency because a larger volume of material has to be ablated in order to generate a sufficient number of analyte ions. At high analyte concentrations, the energy absorption per volume is reduced as the matrix becomes diluted with analyte molecules causing a higher threshold fluence. The total particle yield from laser desorption as a function of *laser fluence* has been determined by collecting the desorbed neutrals on a quartz crystal microbalance [49]. The study by Quist *et al.* [29] indicates that the desorption of neutrals occurs by thermal evaporation starting at laser fluences of about 11 mJ cm^{-2}. However, the ion-to-neutral ratio of the MALDI process was determined to be less than 10^{-5} [49].

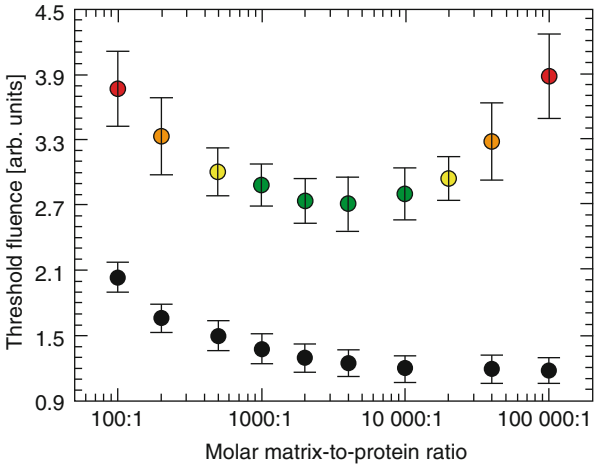

Fig. 11.3 Threshold fluence for positive ions of (*colored* ○) cytochrome c and (●) sinapinic acid as a function of the molar matrix-to-protein ratio. The range indicated by *green circles* provides optimum performance in terms of resolution and signal-to-noise ratio (Adapted from Ref. [48] by permission. © John Wiley & Sons, 1994)

Fluence and irradiance
The *fluence* is defined as energy per unit area; in MALDI typical fluences are in the range of 10–100 mJ cm^{-2}. The *irradiance* is fluence divided by the laser pulse duration; in MALDI the irradiances are in the range of 10^6–10^7 W cm^{-2} [37].

11.2.2 Effect of Laser Irradiation on the Surface

Best MALDI spectra in terms of resolution and low to absent ion fragmentation are obtained slightly above threshold for analyte ion formation [17, 47]. An evenly distributed shallow ablation of material from the upper layers of the sample is achieved if a comparatively homogeneous laser fluence is irradiated onto the target [29, 40, 50]. Ideal laser spot sizes are 100–200 µm as realized by 100–200 mm focal length of the commonly employed lenses [51]. Numerous single-shot spectra are then obtained from one spot. Such a laser spot size is also advantageous because a number of micrometer-sized crystrals are illuminated simultaneously thereby averaging out the effects of mutual orientation of crystal surfaces and laser beam axis [50, 52, 53]. On the other hand, an extremely sharp laser spot causes the eruption of material from a small area upon formation of a deep crater (Fig. 11.4). The MALDI spectra of cytochrome C (M_r = 12,360 u) demonstrate the superior quality of spectra obtained using an optimized spot size [54].

Although established over the years, nitrogen lasers inherently possess disadvantages in that *i*) their maximum repetition rate is limited to about 50 Hz, and *ii*) their average lifespan is only several 10^7 shots. Diode-pumped solid-state lasers such as the frequency-tripled Nd:YAG laser can deliver rates of > 1 kHz and have a hundred times longer lifespan. Especially in MALDI imaging and automated

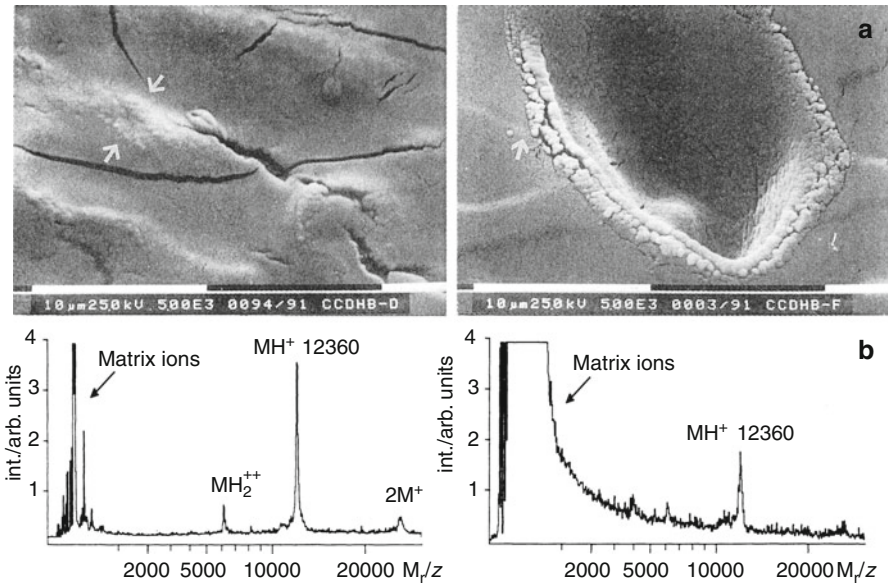

Fig. 11.4 Effect of focused and defocused laser beam. (**a**) SEM micrographs of DHB single crystals after exposure to 10 laser shots (337 nm) under focused (*right column*) and defocused (*left column*) irradiation with corresponding sum spectra of horse heart cytochrome C ($M_r = 12{,}360$ u); *black and white bars* correspond to 10 µm. (**b**) Resulting MALDI spectra (Reproduced from Ref. [54] by permission. © Elsevier Science, 1991)

high-throughput proteomics this number of shots is easily reached. Frequency-tripled Nd:YAG lasers unfortunately suffer from poor MALDI performance, e.g., they are of limited use with certain matrices and with highly relevant thin layer preparations. Their inferiority is not caused by the slight change from 337 nm to 355 nm wavelength but simply by their too small spot size. While nitrogen lasers deliver a moderately focused beam profile that also varies from shot to shot (Fig. 11.5), frequency-tripled Nd:YAG lasers yield sharp and too small irradiated spots. The insertion of a beam modulator to create beam profiles delivering a diffuse multispot pattern of similar overall diameter as a nitrogen laser solves this problem. This way, Bruker's Smartbeam™ Nd:YAG lasers even surpass the MALDI performance of nitrogen lasers (Fig. 11.6) [39, 55].

Use low laser fluence and acquire thousands of shots

MALDI spectra are acquired just above the threshold laser fluence for ion formation. Single-shot spectra therefore tend to exhibit a low signal-to-noise ratio (Sect. 1.6.3) due to poor ion statistics. With the 10–50 Hz repetition rates of nitrogen lasers, it was common to accumulate 50–200 single-shot spectra to create the final spectrum [53]. Nowadays, kHz shot rates of Nd:YAG lasers allow thousands of laser shots to be accumulated per final MALDI spectrum.

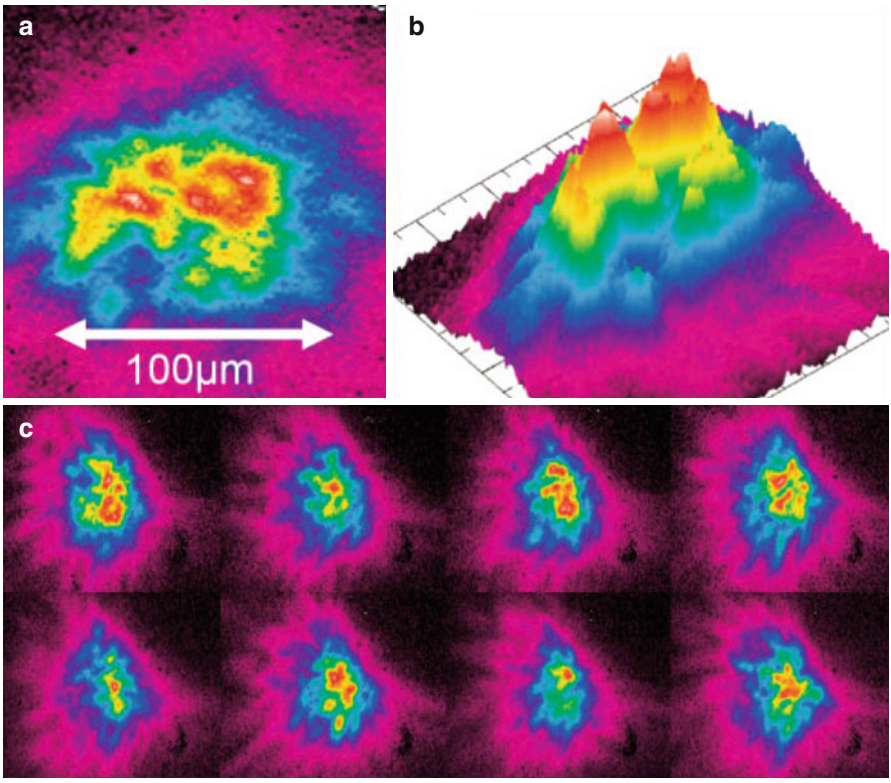

Fig. 11.5 Typical profile of a nitrogen laser. (**a**) View from top, (**b**) 3D view from the side, (**c**) beam profile of eight consecutive laser shots, demonstrating the shot-to-shot variation in the profile of the nitrogen laser. Different colors represent different intensities (Reproduced from Ref. [55] with permission. © Wiley, 2006)

11.2.3 Temporal Evolution of a Laser Desorption Plume

The desorption of ions and neutrals into the vacuum upon irradiation of a laser pulse proceeds as a jet-like *supersonic expansion* [43]: a small, but initially hot and very rapidly expanding plume is generated [15, 56]. The description of MALDI as an *energy-sudden* method [46] nicely expresses the explosive character of the plume formed by the nanosecond laser pulse. As the expansion is adiabatic, the process is accompanied by fast cooling of the plume [43].

Although the initial velocity of the desorbed ions is difficult to measure, reported values generally are in the range of 400–1200 m s^{-1}. The initial velocity is almost independent of the mass of the analyte ions but dependent on the matrix [37, 41–43, 52, 57, 58]. On the other hand, the initial analyte ion velocity is not independent of

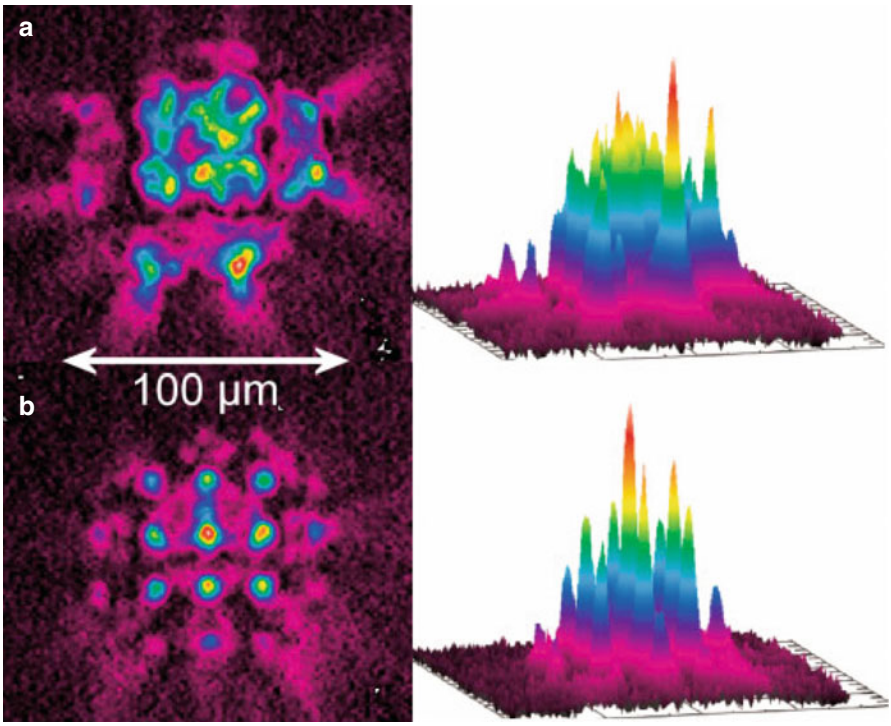

Fig. 11.6 Beam profiles of two differently structured beams of an Nd:YAG laser as employed in Bruker's Smartbeam lasers, (**a**) structured with FWHM of a Gaussian fit of the envelope of 60 µm and (**b**) with fit of 45 µm. The overlapping local maxima and the pattern are clearly visible (Reproduced from Ref. [55] with permission. © Wiley, 2006)

the compound class, i.e., peptides show a behavior different from oligosaccharides [15, 58]. The essential independence of mean ion velocities on the molecular weight of the analyte leads to an approximate linear increase of the mean initial kinetic energies of the analyte ions with mass. High-mass ions therefore carry tens of electronvolts of translational energy *before* ion acceleration [37, 47, 57]. The initial velocity of the ions is superimposed onto that obtained from ion acceleration, thereby causing considerable losses in resolution with continuous extraction TOF analyzers, in particular when operated in the linear mode.

Photographs of the plume Laser flash light photographs of the temporal evolution of a laser desorption plume are highly illustrative [59, 60]. The plume shown in Fig. 11.7 was generated from neat glycerol by an Er:Yag (2.94 µm) laser of 100 ns pulse width. Such laser pulse durations are typical for IR-MALDI. Glycerol was employed as a liquid matrix to provide a homogeneous sample and reproducible plume formation. Pulses of a frequency-doubled Nd:YAG laser (532 nm, 8 ns

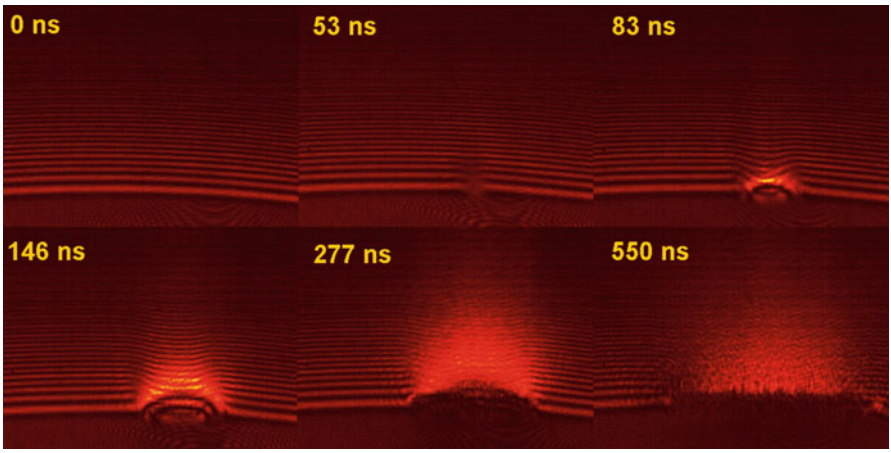

Fig. 11.7 Temporal evolution of a laser desorption plume generated by a 100-ns Er:Yag (2.94 μm) laser pulse from neat glycerol [60] (By courtesy of F. Hillenkamp and A. Leisner, University of Münster)

duration) served as the flashing light source for obtaining the photographs. Dark-field illumination was used to show the particulate components of the plume. In the beginning, the plume appears to consist of a continuous cloud of material of varying density, whereas individual micrometer-sized particles dominate later images. Interestingly, even after the exposure there was still some ejection of material observed [61].

Always vacuum MALDI?
Based on the understanding that mass analyzers require ions to be generated in vacuum, MALDI was initially developed as a vacuum ionization technique. In fact, most MALDI sources are operated in high vacuum and in combination with TOF analyzers. The MALDI-TOF-MS combination still defines the gold standard of MALDI-MS. Accordingly, most of this chapter implicitly is about vacuum MALDI. Nonetheless, it turned out that the MALDI process tolerates mbar-pressures and can also be performed at atmospheric pressure; the latter is referred to as atmospheric pressure MALDI (AP-MALDI, Sect. 11.8). The presence of gas can provide some collisional cooling of the freshly formed ions (cf. vacuum CI versus APCI in Sect. 7.8). This effect may even be increased at super-atmospheric pressure as demonstrated by running MALDI at 4–5 bar [62]. While from the user's perspective both vacuum MALDI and AP-MALDI may appear to work the same way, there are differences in the microscopic processes.

11.2.4 Processes of Ion Formation in MALDI

The pathways of ion formation in MALDI are numerous, i.e., no single process applies [15, 45, 46]. The promoting effect of decreasing pH of matrix-analyte solutions upon peptide ion yield indicates desorption of preformed $[M + H]^+$ ions. Similar observations are made for cationization products such as $[M + alkali]^+$ ions from oxygen-rich analytes. Nonetheless, gas phase processes – essentially some sort of CI in the dense desorption plume – cannot be excluded, because ions may be formed in the plasma plume even some hundred micrometers above the sample surface [63, 64]. Another study reveals a gradual increase of the initial ion velocities as the mass of oligosaccharides and synthetic polymers increases; they may even reach the high level characteristic for peptides and proteins. Introduction of a charged functional group via derivatization has the same effect on small oligosaccharides. This indicates that typical MALDI analytes require their incorporation as preformed ions into the matrix crystal to effectively become released into the gas phase, while gas phase cationization is viable for low-molecular-weight neutrals [43]. When non-carboxylic acid matrices are being used to protonate slightly basic analyte molecules, excited states of the matrix molecules may account for proton transfer [64, 65].

In case of UV light-absorbing analytes, direct photoionization can also occur. The frequently observed positive and negative radical ions $M^{+\bullet}$ [66, 67] and $M^{-\bullet}$ [68–70] can only be generated by removal or capture of an electron. Thus, $M^{+\bullet}$ and $M^{-\bullet}$ ions point towards the occurrence of photoionization [66], charge transfer, and electron capture in the gas phase [46, 66]. Which of the above processes contributes most to ion formation depends on the actual combination of matrix, analyte, and possibly present additives or contaminants.

11.2.5 "Lucky Survivor" Model of Ion Formation

The plasma emerging from a surface upon laser irradiation contains both positive and negative ions – it is neutral in total. Depending only on the polarity of the acceleration voltage one may either extract positive or negative ions, a situation similar to CI where an isobutane reagent gas plasma works equally well to deliver protonated species in PICI or deprotonated ions in NICI (Sect. 7.5). The starting conditions in MALDI, however, are quite different in that the analyte can be *multiply* protonated, deprotonated or otherwise charged by ion attachment in solution before its incorporation into the matrix crystals [15, 46]. Proof of multiple charging of macromolecules in solution phase is directly obtained from electrospray ionization mass spectra (Chap. 12).

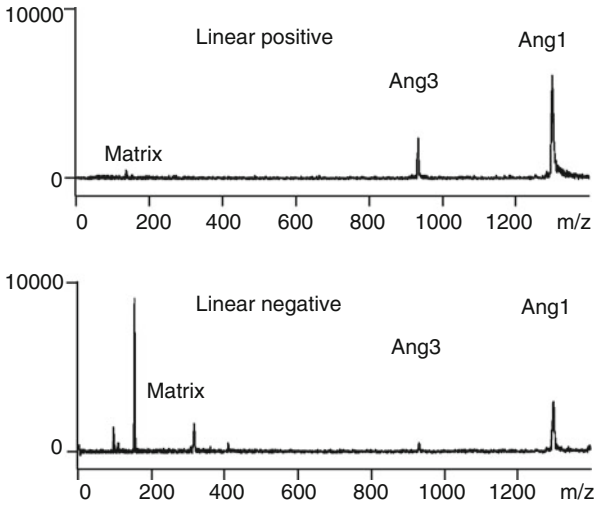

Fig. 11.8 MALDI mass spectra of a mixture of the small peptides angiotensin 1 (Ang1) and angiotensin 3 (Ang3) from DHB matrix as obtained on a linear TOF instrument in (**a**) positive-ion and (**b**) negative-ion mode under otherwise identical conditions (Reproduced from Ref. [46] with permission. © John Wiley & Sons, Ltd., 2000)

Peptide ion formation Although peptides and proteins are generally prepared for MALDI from acidified solutions, both singly protonated or deprotonated ions can normally be observed solely depending on the polarity of the extraction voltage. However, negative ion spectra tend to be less intensive for the same laser fluence, i.e., positive- and negative-ion mass spectra are not analogous (Fig. 11.8). Interestingly, the relative ion yields of both polarities are basically independent of the solvent composition, its pH, and of the solution phase acidity/basicity of the analyte.

In order to explain the above observations, we have to answer the following questions concerning the ionization process:

- Why are singly charged ions the (almost) only species observed in MALDI?
- How can charge separation be accomplished when mutual neutralization is considered to be the preferred process inside the plume?
- What are the fundamental processes limiting the ionic charge state to just one – either positive or negative?

The so-called *lucky survivor model* [46] explains this behavior in terms of mutual neutralization by recombination of cationic and anionic components of the plasma. Re-neutralization rates are higher, the higher the initial charge state of an ion. Thus, re-neutralization is slower for singly charged ions representing a late stage of the sequence, and therefore less probable to occur. Hence, singly charged ions generally are the "lucky survivors of the re-neutralization conflict" inside the laser plume (Fig. 11.9). As the fast moving electrons are most rapidly lost from the laser plume, an excess positive charge is established over time, which explains the lower abundance of negative ions in MALDI.

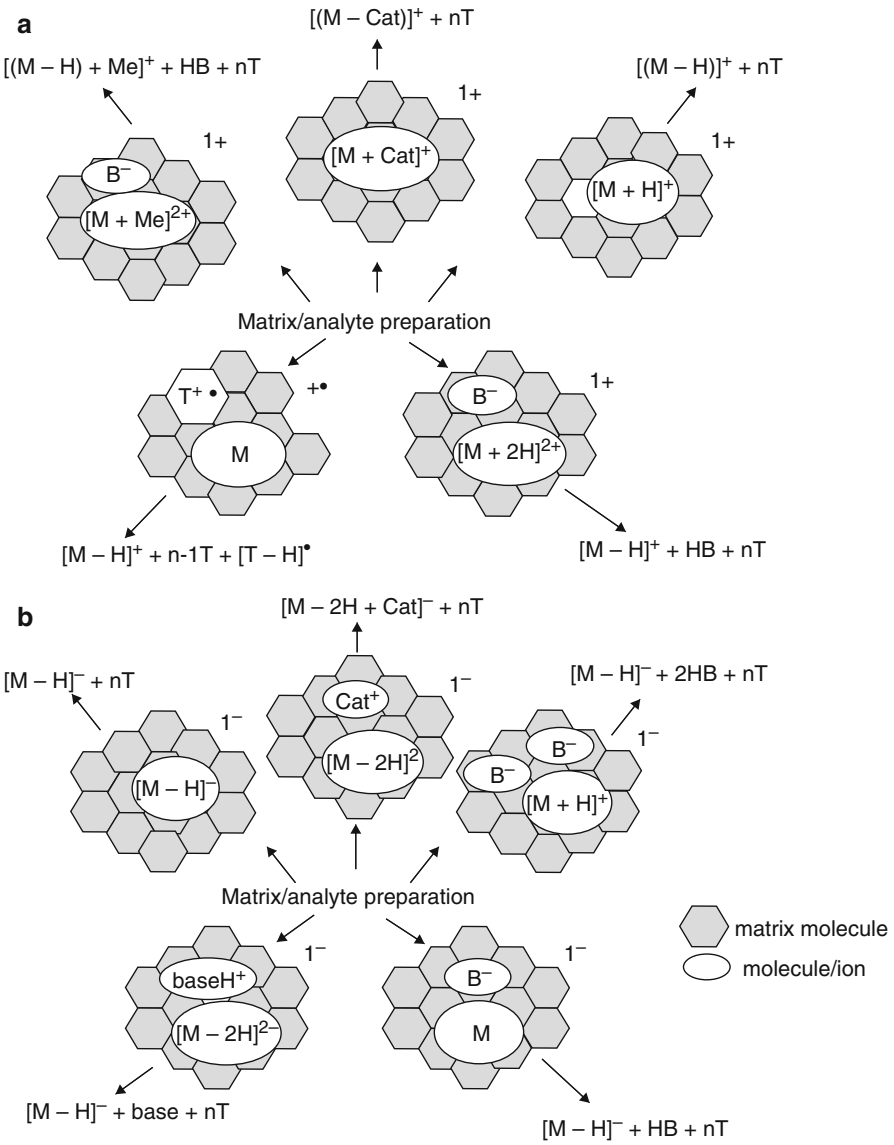

Fig. 11.9 Pathways of formation of singly charged ions from sample–matrix preparations according to the lucky survivor model. (**a**) Positive ion formation, (**b**) negative ion formation; M: analyte molecule, T: matrix molecule, Cat: small cation, Me: metal^{2+}, B: base (Adapted from Ref. [46] with permission. © John Wiley & Sons., Ltd., 2000)

11.3 MALDI Matrices

11.3.1 Role of the Solid Matrix

The role of the matrix in MALDI is analogous to that in FAB (Sect. 10.3). In contrast to FAB, MALDI matrices are generally crystalline solids of low vapor pressure in order not to be volatized in the ion source vacuum. While in principle any liquid can serve as a FAB matrix to moderate the energy of the impacting primary particles, the matrix in MALDI has to effectively absorb the laser light of the wavelength intended for use [71]. In UV-MALDI, the molecules need to possess a suitable chromophore, because energy uptake is based on the strong absorption, and thus the resulting electronic excitation of the matrices. Therefore, the structure of UV-MALDI matrices is based on some aromatic core suitably functionalized to achieve the desired properties.

In case of IR-MALDI, fewer restrictions apply because wavelengths around 3 μm are effectively absorbed by O–H and N–H stretch vibrations, while wavelengths around 10 μm cause excitation of C–O stretch and O–H bending vibrations [33, 36]. Therefore, malonic acid, succinic acid, malic acid, urea, and glycerol serve well as matrices in IR-MALDI [31, 32]. A matrix can serve as protonating or deprotonating agent or as electron-donating or -accepting agent.

Job of the matrix
It is evident that the first function of the matrix essentially is to dilute and isolate analyte molecules from each other. This occurs during solvent evaporation and concomitant formation of a solid solution. Then, upon laser irradiation, it functions as a mediator for energy absorption [46].

11.3.2 Matrices in UV-MALDI

Nicotinic acid (NA) was the first organic compound to be successfully employed as a matrix in UV-MALDI of peptides and proteins [12–14]. Ever since, better matrices have been sought, some of which now being widespread in use (Table 11.2 and Fig. 11.10). The currently most relevant matrices for UV-MALDI are HCCA, DHB, SA, DHAP, 3-HPA, DCTB, and dithranol. Nonetheless, even [60]fullerene [72] and porphyrins [73] have been used. Ionic liquids (ILs) have been employed as liquid MALDI matrices to achieve long-lasting signals on the same spot [74, 75].

Table 11.2 UV-MALDI matrices

Compound	Acronym	Application to	References
Nicotinic acid	NA	Peptides, proteins	[12–14]
Picolinic acid	PA	Oligonucleotides, DNA	[76]
3-Hydroxypicolinic acid	HPA, 3-HPA	Oligonucleotides, DNA	[77]
3-Aminopicolinic acid	3-APA	Oligonucleotides, DNA	[78]
6-Aza-2-thiothymine	ATT	Oligonucleotides, DNA	[79–81]
2,5-Dihydroxybenzoic acid	DHB	Proteins, oligosaccharides	[17, 54]
DHB-based mixtures	DHB/XY and super-DHB	Proteins, oligosaccharides	[82–86]
3-Aminoquinoline	3-AQ	Oligosaccharides	[87–89]
α-Cyano-4-hydroxycinnamic acid	α-CHC, α-CHCA, 4-HCCA, CHCA	Peptides, smaller proteins, triacylglycerols, numerous other compounds	[90–93]
4-Chloro-α-cyano-cinnamic acid	ClCCA	Peptides	[94, 95]
3,5-Dimethoxy-4-hydroxycinnamic acid	SA	Proteins	[96]
2-(4-Hydroxyphenylazo) benzoic acid	HABA	Peptides, proteins, glycoproteins, polystyrene	[71, 97]
2-Mercaptobenzothiazole	MBT	Peptides, proteins, synthetic polymers	[98]
5-Chloro-2-mercaptobenzothiazole	CMBT	Glycopeptides, phosphopeptides, and proteins	[98]
2,6-Dihydroxyacetophenone	DHAP	Glycopeptides, phosphopeptides, proteins	[99, 100]
2,4,6-Trihydroxyacetophenone	THAP	Solid-supported oligonucleotides	[101]
Dithranol (1,8,9-anthracenetriol)	None	Synthetic polymers	[102, 103]
9-Nitroanthracene	9-NA	Fullerenes and derivatives	[70, 104, 105]
Benzo[a]pyrene	None	Fullerenes and derivatives	[69]
2-[(2*E*)-3-(4-*tert*-Butylphenyl)-2-methylprop-2-enylidene]malonitrile	DCTB	Oligomers, polymers, dendrimers, small molecules	[106, 107]

Acronyms for matrices

It is common to use acronyms rather than compound names for most UV-MALDI matrices. However, these are not always consistently used, e.g., α-CHC, 4-HCCA, CHCA, and CCA all refer to α-cyano-4-hydroxycinnamic acid. Others may be easily confused, e.g., nicotinic acid (NA) and

(continued)

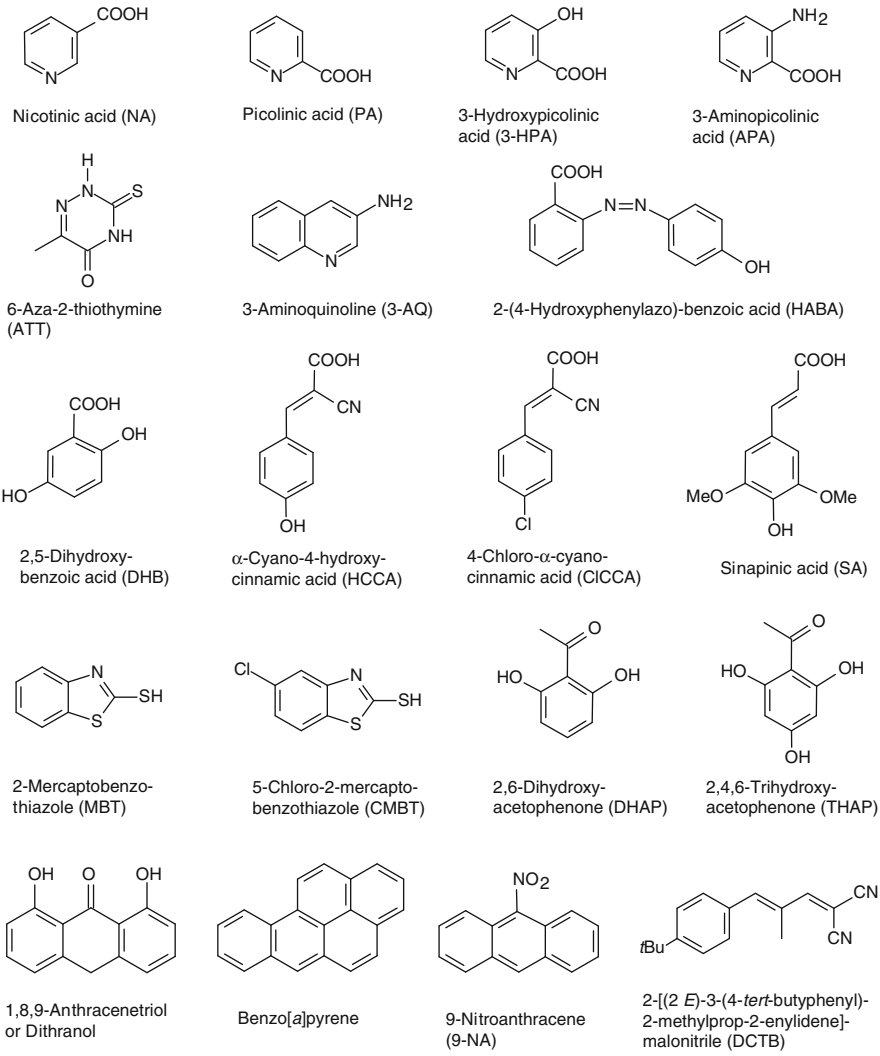

Fig. 11.10 Structures, names, and acronyms of common UV-MALDI matrices

9-nitroanthracene (9-NA), while some like dithranol or benzopyrene do not have an acronym, and others in fact can appear mysterious (DCTB).

Matrix is key to success

The choice of the right matrix is key to success in MALDI – and at the same time appears to be some kind of magic. For a first approach to a new analytical problem, it is recommended to try a matrix from the above

(continued)

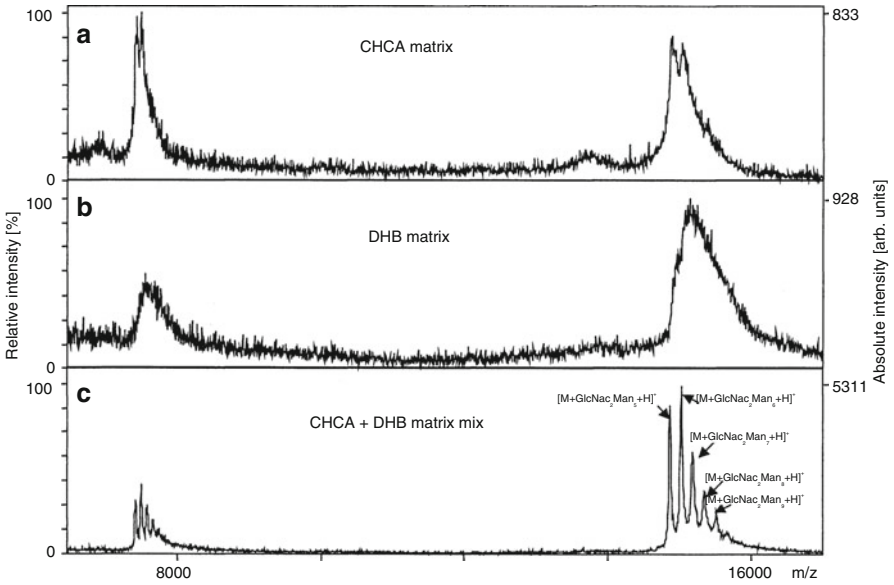

Fig. 11.11 Linear mode positive-ion MALDI-TOF spectra of ribonuclease B in 80 mM urea. (**a**) 300 fmol in CHCA, (**b**) 600 fmol in DHB, and (**c**) 300 fmol in CHCA/DHB matrix mix (Reproduced from Ref. [85] by permission. © Elsevier Science, 2003)

compilation. In general, highly polar analytes work better with highly polar matrices, and nonpolar analytes are preferably combined with nonpolar matrices. Matrix acidity data may help to judge its protonating effect [94, 108, 109]. While many compound classes may be analyzed using a variety of matrices, in less fortunate cases, only one specific analyte–matrix combination might yield useful MALDI spectra.

Only with the right matrix The choice of a matrix and optimized conditions of sample preparation have substantial influence on the analytical value of MALDI spectra. Even when employing standard matrices such as CHCA or DHB, significant improvements can be achieved, e.g., by appropriate mixing of the two matrices to analyze ribonuclease B (Fig. 11.11) [85].

11.3.3 Characteristics of MALDI Matrix Spectra

MALDI matrix (Ma) spectra are characterized by strong molecular and/or ions from protonation, cationization etc. The signals are accompanied by series of matrix cluster ions and some more abundant fragment ions [36]. In positive-ion MALDI, $[Ma_n + H]^+$ cluster ions predominate, while $[Ma_n - H]^-$ cluster ions are

preferably formed in negative-ion MALDI. The principal ion series may be accompanied by $[Ma_n + \text{alkali}]^+$ ions and some fragments of minor intensity, e.g., $[Ma_n + H - H_2O]^+$. In particular with aprotic matrices, radical ions tend to dominate. In addition, a "continuous" background is formed by clustering of radiolytic decomposition products of the matrix. In general, the spectrum of the neat matrix, i.e., its LDI spectrum, strongly depends on the actual laser fluence and on the presence of impurities. Thus, the "correct" LDI spectrum of the matrix compound largely differs from what is obtained under conditions applied to form analyte ions from that matrix, because then, a 10–100-fold increased matrix ion density causes numerous secondary processes to occur. This dramatic change in mass spectral appearance bears some similarity to the transition observed from EI to CI spectra of reagent gases (Sect. 7.2.2).

11.4 Sample Preparation

The standard method of sample preparation in LDI and MALDI involves deposition and subsequent evaporation of 0.5–2 µl of dilute sample(–matrix) solution on the surface of a *sample holder* or *MALDI target*, as it is often referred to. Both composition of the solution and surface characteristics of the target strongly effect the outcome of the MALDI-MS experiment.

11.4.1 MALDI Target

Sample introduction has undergone a dramatic change in MALDI. In first experiments, single samples were supplied on MALDI probes designed similar to FAB probes (Sect. 10.3). Soon, multi-sample probes were developed. Early commercial products provided approximately twenty spots on one target which could be rotated, shifted, or freely moved in *x*- and *y*-directions to bring any spot on its surface into the laser's focus. Driven by the needs of combinatorial chemistry, 96-spot targets were developed to allow for the transfer of samples from a complete standard well plate. Soon after, the current standard of 384-spot, occasionally even 1536-spot, targets was established (Fig. 11.12). To take full advantage of such targets it is recommended to combine robotic sample preparation with automated measurement of the MALDI spectra.

The spot size of MALDI preparations and thus the amount of sample necessary to yield a useful layer can be substantially reduced by so-called *AnchorChip*™ targets (Bruker Daltonik). Such targets bear small hydrophilic spots on a hydrophobic surface. As a result, the evaporating drop of matrix–analyte solution is "anchored" to such a point where it shrinks until the onset of crystallization exactly within this hydrophilic area (Fig. 11.13c) [110]. The resulting preparation covers a much smaller surface than that from a freely spreading drop. In addition to improved detection limits, this technique simplifies automated spot finding due to their precisely defined location on the target.

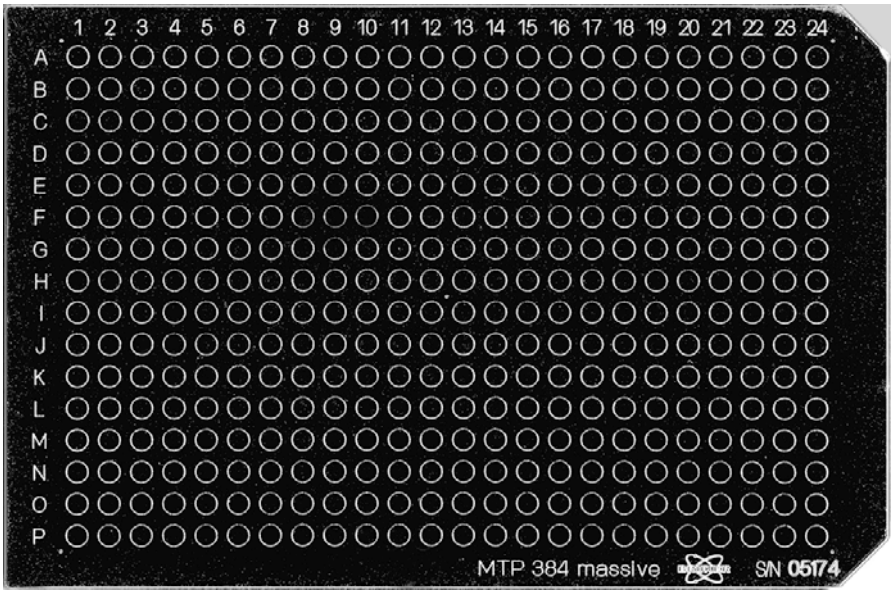

Fig. 11.12 Typical MALDI target: Bruker Scout384™ target offers a 16 × 24 spot array with up to 384 positions for sample preparation. Here, a standard nickel-coated massive aluminum version is shown; its dimensions are 84 × 128 mm with engraved marks of 3 mm in diameter

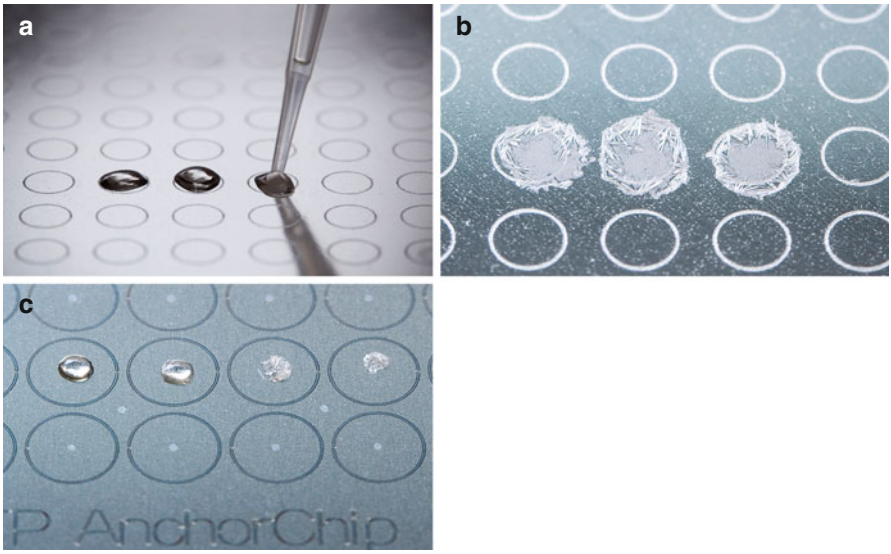

Fig. 11.13 Sample preparation for MALDI. (**a**) Pipetting of 1 µl of sample–matrix solution onto a standard MALDI target; (**b**) same spots after DHB has crystallized show large crystals on the rim and evenly distributed small crystals in the center; (**c**) cummulative effect of hydrophilic spots (*bright areas in circles*) present on a hydrophobic surface of an AnchorChip™ target on crystallizing DHB matrix

11.4.2 Standard Sample Preparation

The analyte should be soluble to at least about 0.1 mg ml^{-1} in some solvent. If a matrix is used, the matrix is dissolved to yield either a saturated solution or a concentration of about 10 mg ml^{-1}. The solution of the analyte is then admixed to that of the matrix. For optimized MALDI spectra, the molar matrix-to-analyte ratio is normally adjusted as to fall into the range from 1000 : 1 to 100,000 : 1 [16, 17, 54]. In this range, a good signal-to-noise ratio and a low degree of ion fragmentation are preserved. At very high sample concentrations the "matrix effect" is diminished and the spectra start resembling LDI spectra. Too low sample concentrations require additional laser irradiance for sufficient analyte ion production [48]. However, given a proper preparation, even a molar matrix-to-analyte ratio of 10^8 : 1 can produce useful results. A sufficient miscibility of analyte and matrix is also required [102].

Sample consumption Assuming a typical MALDI matrix with an M_r of about 200 g mol^{-1}, dissolution at 10 mg ml^{-1} in a suitable solvent yields a matrix solution that is 0.05 M in concentration, which is equal to 5×10^{-8} mol μl^{-1}. An average peptide of M_r around 2000 g mol^{-1} dissolved at 0.01 mg ml^{-1} results in 5×10^{-12} mol μl^{-1} (5 pmol μl^{-1}). Mixing the matrix with the analyte solution 1:1 (v/v) results in a molar matrix-to-analyte ratio of 10,000 : 1 for preparation on a target. Pipetting 1 µl of this mixture per spot onto a MALDI target corresponds to 2.5 pmol of sample per spot (Fig. 11.13). In fact, MALDI-TOF-MS of peptides can be extended to 1/1000th of this amount, and thus, may routinely deliver useful spectra down to a few fmol of peptide per spot, which is equal to a molar matrix-to-analyte ratio of 10,000,000 : 1.

The crystallization process is a critical parameter in LDI and MALDI sample preparation [54, 111, 112]. The conventional co-crystallization is usually termed *dried droplet preparation*. Dried droplet preparation yields comparatively large crystals, especially when slow evaporation, e.g., from aqueous solutions, is involved. Unfortunately, large crystals are detrimental for good shot-to-shot reproducibility and mass accuracy.

Evenly distributed thin layers of microcrystallites are therefore preferred [111, 113]. The original so-called *thin layer technique* involves preparation of a thin HCHA layer from solution in acetone on top of which the analyte is placed in a second step without re-dissolving the matrix [114, 115]. The formation of thin layers can also be assisted by (*i*) using volatile solvent(s) such as acetone, (*ii*) by eventually enforcing evaporation by gentle heating of the target or by a softly blowing hair dryer, and finally (*iii*) by using polished targets. Thus, the thin layer technique had a significant impact on MALDI sample preparation [114, 116].

Finally, (nano)electrospray deposition can be used to deposit the analytes onto different kinds of predeposited matrix layers. MALDI sample preparations where the analyte solution is deposited on top of a previously prepared matrix layer are generally termed *sandwich methods*. The base layer of matrix may be prepared either by the standard dried droplet technique or by thin layer preparation. For (nano)electrospray deposition of peptides, for example, a 10^{-5} M solution is

sprayed from a (nano)electrospray capillary onto the solid matrix layer. The advantage of nanoelectrospray over conventional electrospray is that very small droplets are formed, which arrive at the target as dry particles, and thus, do not wet and re-dissolve the matrix surface [45].

11.4.3 Cationization

Metal ions, in particular singly charged ions such as Na^+, K^+, Cs^+, and Ag^+ are sometimes added to the matrix–analyte solution to effect cationization of the neutral analyte [117]. This is advantageous when the analyte has a high affinity to a certain metal ion, e.g., towards alkali ions in case of oligosaccharides [6]. Addition of individual cations can also lead to a concentration of ions of a particular kind, e.g., promoting $[M + K]^+$ ions over all other alkali ion adducts upon addition of a potassium salt (Fig. 11.14).

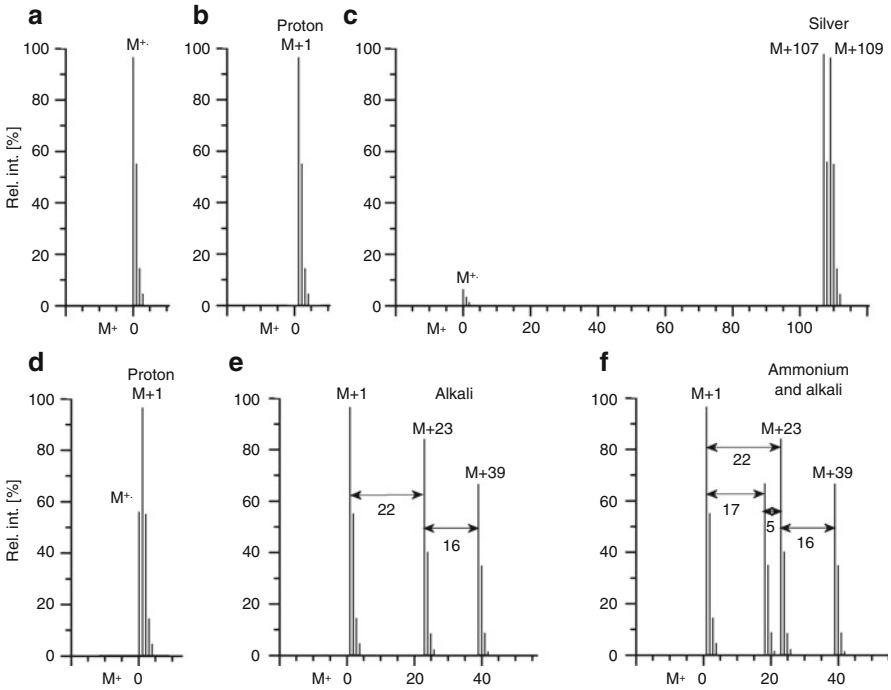

Fig. 11.14 Typical appearances of signals representing the intact molecular mass in case of (**a**) molecular ion formation, (**b**) protonation, (**c**) silver cationization, (**d**) molecular ion and protonation, (**e**) protonation plus alkali cationization, and (**f**) protonation, ammonium plus alkali adduct formation. The relative abundances of the respective contributions are subject to wide variations. The abscissa gives the corresponding M + X nominal mass value; artificial isotopic patterns are added for more realistic appearance

Silver ions (from silver trifluoroacetate or trifluoromethanesulfonate), Cu^+, and other transition metal ions in their 1+ oxidation state [118, 119] are frequently employed to obtain $[M + metal]^+$ ions from nonfunctionalized or at least nonpolar hydrocarbons [120], polyethylene [121, 122], or polystyrene (for an example see Sect. 11.6.1) [118, 119, 123–125].

Na^+ and K^+ are everywhere
Sodium and potassium are ubiquitous and the corresponding adducts are almost omnipresent given the analyte has some alkali ion affinity [126]. It is therefore advisable to know these typical mass differences by heart. Searching a spectrum for those frequent peak distances, e.g., +22 u and +16 u in case of $[M + Na]^+$ and $[M + K]^+$ ions accompanying $[M + H]^+$, reveals the true molecular mass. Other cations, e.g., Li^+ or Ag^+, are easily identifiable by their isotopic pattern.

Accurate mass data provided, the $\Delta(m/z)$ values between suspect pairs of peaks can be used to unequivocally identify $[M + Na]^+$, $[M + K]^+$, and other frequent cationization product ions the same way as we used the corresponding differences to verify the presence of certain elements by their characteristic $\Delta(m/z)$ between isotopes (Table 3.2) [127]. The most frequent pairs to be distinguished are collected below (Table 11.3).

11.4.4 Cation Exchange and the Need for Cation Removal

If an analyte molecule contains several acidic hydrogens, these can be exchanged by alkali ions without generating a charged species, e.g., [M – H + K] or [M – 2H + 2Na]. As a result, a single analyte species will form numerous ionic species thereby significantly decreasing the abundance of each species involved, e.g., $[M – 2H + Na]^-$, $[M – 2H + K]^-$, $[M – 3H + Na + K]^-$ etc. Fortunately, in MALDI, we only need to consider singly charged ions.

Challenging multiple cation exchange Oligonucleotides are important representatives of this type of compounds. Their extreme polarity and poly-anionic character alone make them very hard to analyze. Additionally, each added

Table 11.3 Characteristic mass differences to identify frequent cationization products

Pair of ions	Δm [u]
$M^{+\bullet}$ vs. $^{13}C\text{-}M^{+\bullet}$	1.0033
$M^{+\bullet}$ vs. $[M + H]^+$	1.0078
$[M + H]^+$ vs. $[M + NH_4]^+$	17.0265
$[M + H]^+$ vs. $[M + Na]^+$	21.9819
$[M + H]^+$ vs. $[M + K]^+$	37.9559
$[M + Na]^+$ vs. $[M + K]^+$	15.9739
$[M + H]^+$ vs. $[M + O + H]^+$	15.9949

nucleoside imports another exchangeable hydrogen via the phosphate residue. An oligonucleotide 11mer, for example, can theoretically appear as any ion from $[M - H]^-$, $[M - 2H + Na]^-$ up to $[M - 10H + 9Na]^-$, and, provided these are present, can repeat this exchange scheme with K^+ and NH_4^+ ions. Further, products of mixed exchange like $[M - 6H + 3Na + 2K]^-$ have to be considered. Thus, hydrogen-to-metal exchange may finally result in complete suppression of a useful signal as numerous, eventually unresolved, peaks each of very low intensity can appear just as a slight and broad bump in the baseline of the spectrum [128]. Mass spectral analysis of oligonucleotides is alternatively performed by electrospray ionization (ESI) and their sequencing is also dealt with in that context (Sect. 12.6.4).

On-target washing presents a simple but very effective approach to reduce the alkali ion content of MALDI sample preparations [129, 130]. For this purpose, 2–5 µl of alkali ion-free water containing 0.1–1% formic or trifluoroacetic acid is placed on top of the crystalline layer and removed after a few seconds by a microliter pipette or by blowing it off with a stream of pressurized air. The acidification avoids dissolution of the crystals in case of carboxylic acid matrix preparations.

Cation exchange resins can be added prior to preparation to substitute alkali ions for ammonium (Fig. 11.15) [30]. To take full effect, it is important to keep the cation exchange beads even on the target in order to capture the alkali ion contamination of the metal surface, too. No useful signals are obtained when the laser hits the cation exchange beads. Furthermore, there is a risk of ion source contamination as beads may occasionally fall off the surface, even as a result of laser shots.

Another approach is to use tips of microliter pipettes as miniature columns by filling them with *size exclusion chromatography* (SEC) stationary phase material or standard C_{18} reversed phase material [131, 132]. Such tips are also commercially available as ZipTips™ [128]. There is a risk of sample absorption on the column

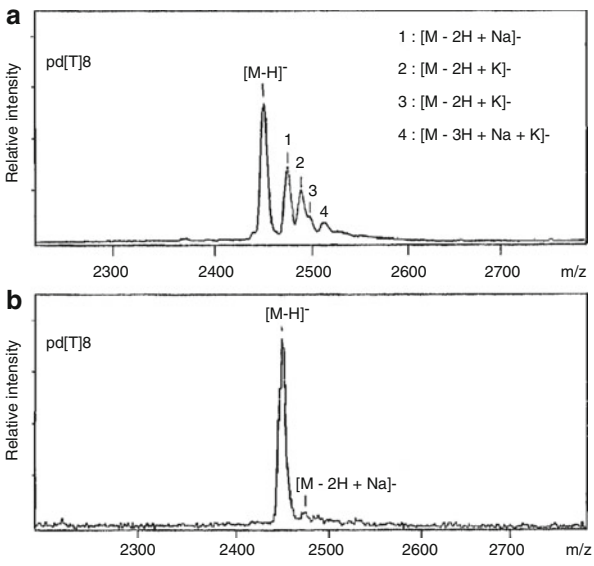

Fig. 11.15 Negative-ion MALDI spectra of the oligonucleotide pd$[T]_8$; (**a**) 5 pmol, (**b**) same as (**a**) after addition of 5–10 cation exchange beads to the sample preparation (Adapted from Ref. [30] by permission. © John Wiley & Sons, 1992)

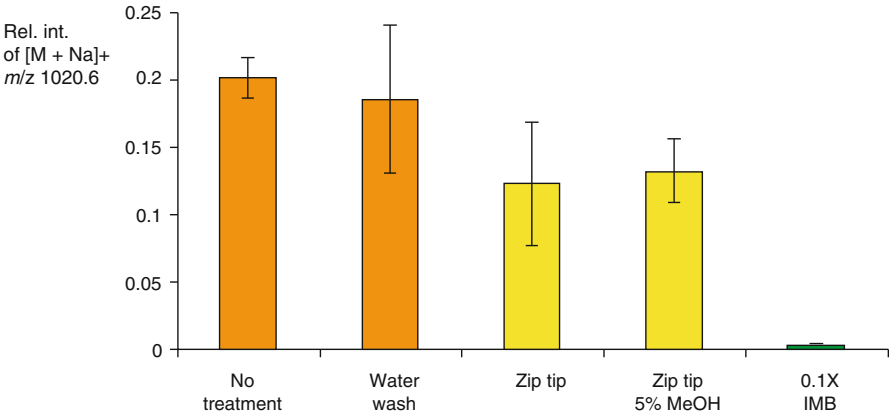

Fig. 11.16 Comparison of common alkali adduct suppression techniques. The ratio of the intensity of a peptide $[M + Na]^+$ peak, *m/z* 1020.6, to the sum of $[M + H]^+$ and $[M + Na]^+$ signal intensities is shown. *Error bars* represent standard deviation of three measurements (Adapted from Ref. [133] with permission. © John Wiley & Sons, Ltd, 2004)

material, which is particularly critical for minor components of complex mixtures – and the cost factor of these consumables should also be kept in mind.

Finally, it is advantageous to add a surfactant blend (Invitrosol-MALDI protein solubilizer B, IMB) prior to preparation (Fig. 11.16) [133].

Equally, sodium dodecyl sulfate contaminations should be removed from 2D gel electrophoresis before subjecting samples to MALDI-MS [134].

11.4.5 Anion Adducts

In negative-ion MALDI, analyte molecules do not exclusively form $[M - H]^-$ ions but also anion adducts with $[M + Cl]^-$, $[M + COOH]^-$, and $[M + CF_3COO]^-$ being most likely. Formiate and triflate adducts can be formed when matrix solutions are acidified by use of formic acid or trifluoroacetic acid (HTFA), respectively. Additionally, open-electron ions can be formed by electron capture (Sect. 7.6). It is therefore helpful to have accurate mass differences for their identification at hand (Table 11.4).

11.4.6 Solvent-Free Sample Preparation

If an analyte is absolutely insoluble or only soluble in solvents that are not acceptable for the standard MALDI sample preparation technique, it can alternatively be ground together with the solid matrix, preferably in a vibrating ball mill. The resulting fine powder is then spread onto the target. To avoid contamination, non-adherent material should be gently blown away from the target before insertion into the ion source [122, 135, 136] (Fig. 11.17).

Table 11.4 Characteristic mass differences to identify frequent negative adduct ions

Pair of ions	Δm [u]
$M^{-\bullet}$ vs. $^{13}C\text{-}M^{-\bullet}$	1.0033
$[M - H]^-$ vs. $M^{-\bullet}$	1.0078
$[M - H]^-$ vs. $[M + OH]^-$	18.0106
$[M - H]^-$ vs. $[M + {}^{35}Cl]^-$	35.9767
$[M - H]^-$ vs. $[M + COOH]^-$	46.0055
$[M - H]^-$ vs. $[M + {}^{79}Br]^-$	79.9261
$[M - H]^-$ vs. $[M + CF_3COO]^-$	113.9928

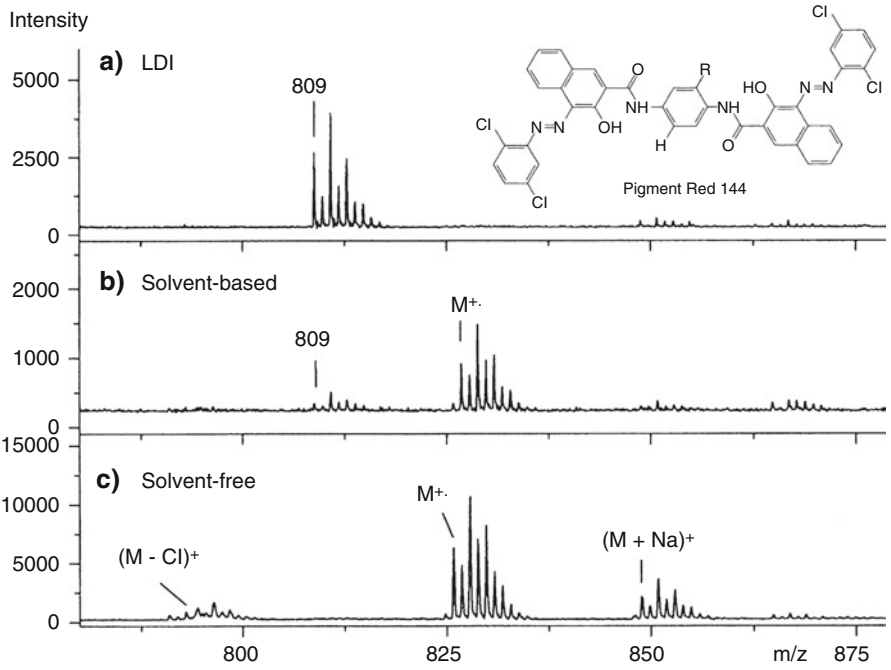

Fig. 11.17 Comparison of spectra of the organic dye Pigment Red 144 as obtained by (**a**) LDI, (**b**) solvent-based, and (**c**) solvent-free MALDI sample preparation (Adapted from Ref. [136] by permission. © John Wiley & Sons, 2001)

MALDI of an insoluble pigment The organic dye Pigment Red 144, has been subjected to mass analysis by LDI, solvent-based MALDI, and solvent-free MALDI [136]. Its monoisotopic molecular ion, $[C_{40}H_{23}Cl_5O_4N_6]^{+\bullet}$, is expected at *m/z* 826.0. Due to the strong light absorption of the pigment, the uptake of energy in LDI causes quantitative fragmentation to yield solely $[M - OH]^+$ ions. Here, solvent-based MALDI results in a poor sample preparation because of the unfavorable solvents needed, whereas solvent-free sample preparation yields a better spectrum exhibiting mainly $M^{+\bullet}$ and $[M + Na]^+$ ions of the pigment (Fig. 11.15).

11.4.7 Additional Methods of Sample Supply

Surface-adsorbed analytes can be examined by laser desorption techniques if they are supplied on a metal foil, a TLC plate [137], or at least on semiconducting material. Even the foil itself can be subject to LDI. This requires the foil to be fixed on top of a sample target, e.g., by means of (conducting) double-sided adhesive tape or some general-purpose adhesive. Care has to be taken not to produce sharp edges protruding from the surface because these might cause discharges in the ion source when the accelerating voltage is switched on. Furthermore, the mass calibration can be affected by such an unusually thick "sample layer". The latter two limitations are only relevant in case of on-axis MALDI-TOF analysis, while oaTOF analyzers and other setups with external MALDI ion sources are by far more robust in this respect.

Safety notice
Unconventional sample supply techniques on commercial MALDI instruments afford great care. Possible pitfalls include (*i*) blocking of the vacuum lock due to unacceptable thickness of the target, (*ii*) loss of the sample inside the ion source or inside the vacuum lock, (*iii*) damage to the instrument from electric discharges. It is therefore highly recommended to use dedicated sample holders when such are supplied by the instrument manufacturer.

11.5 Applications of LDI

Although LDI is also possible for peptides [5] and oligosaccharides [4, 6], it is suited much better for analyzing organic and inorganic salts [138–140], molecules with large conjugated π-electron systems [141–143], organic dyes as contained in ballpoint pen inks [144], porphyrins [145], or UV light-absorbing synthetic polymers [5, 56]. As interferences with matrix ions are excluded, LDI presents a useful and quick alternative to MALDI in the low-mass range. In addition, solvent-free sample preparation can be employed with insoluble analytes by simply grinding the solid onto the sample holder. However, LDI is a "harder" ionization method than MALDI and fragmentation has to be taken into account.

LDI of a polycyclic aromatic hydrocarbon Polycyclic aromatic hydrocarbons (PAHs) are easily detected by LDI due to their strong UV absorbance. The positive-ion LDI-TOF mass spectrum of 1,2,3,4,5,6-hexahydrophenanthro[1,10,9,8-*opqra*] perylene exclusively presents the molecular ion at *m*/*z* 356 (Fig. 11.18; for the EI spectrum cf. Sect. 2.1) [143].

Fullerene soot analyzed by LDI Fullerene soot as obtained by the Huffman-Krätschmer synthesis [146] can be characterized by positive- as well as negative-

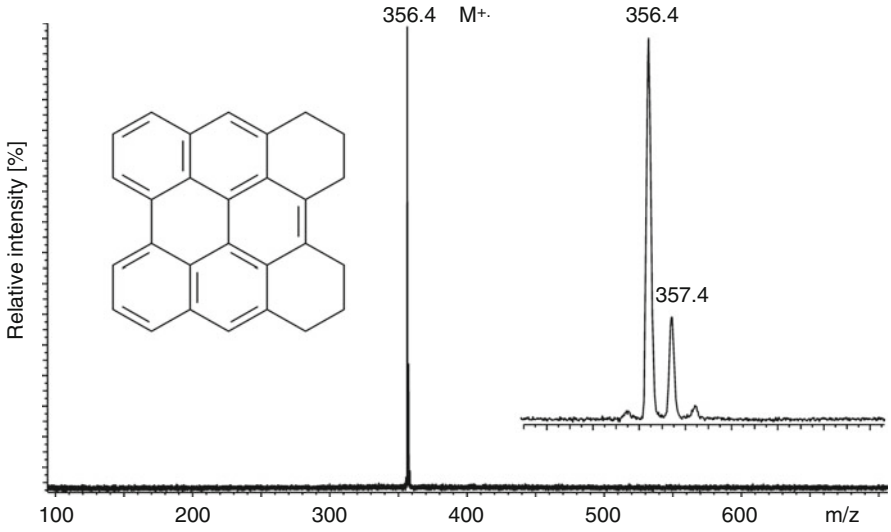

Fig. 11.18 Positive-ion LDI-TOF mass spectrum of 1,2,3,4,5,6-hexahydrophenanthro[1,10,9,8-*opqra*] perylene. The *inset* shows an expanded view of the molecular ion signal (Adapted from Ref. [143] with permission. © Elsevier Science, 2002)

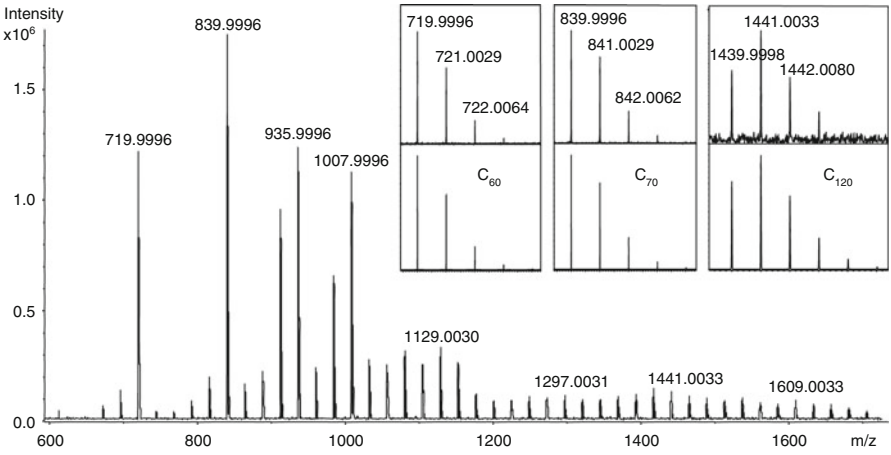

Fig. 11.19 Positive-ion LDI-FT-ICR mass spectrum of a fullerene soot. The *insets* show expanded views of the experimental (*upper parts*) and calculated (*lower parts*) isotopic patterns of $C_{60}^{+\bullet}$, $C_{70}^{+\bullet}$, and $C_{120}^{+\bullet}$. Sample courtesy of W. Krätschmer, Max Planck Institute for Nuclear Physics, Heidelberg (Reproduced from Ref. [148] by permission. © Wiley-VCH, Weinheim, 2009)

ion LDI-MS [141]. Such LDI spectra can exhibit fullerene molecular ion signals well beyond *m*/*z* 3000; among these, $C_{60}^{+\bullet}$ and $C_{70}^{+\bullet}$ are clearly accentuated (Fig. 11.19). Furthermore, such samples provide experimental carbon-only isotopic

patterns over a wide mass range (Sect. 3.2.1). The spectrum below was obtained on a FT-ICR mass spectrometer; hence the resolution is 175,000 at *m/z* 840, i.e., almost by a factor of 1000 higher than on early TOF instruments as used for the discovery of C_{60} and larger fullerenes [147]. The insets show expanded views of the $M^{+\bullet}$ ions for C_{60}, C_{70}, and C_{120} together with the corresponding calculated isotopic patterns. Note, that the accurate masses are lower than the nominal values by the mass of an electron, while the difference in mass of 1.0033 u between ^{12}C and ^{13}C can be recognized from the mass increment of the 1st and 2nd isotopic peaks, respectively.

11.6 Applications of MALDI

MALDI applications are growing at a rapid pace with thousands of publications annually. A single book chapter thus can impossibly cover all aspects of these developments. However, there are several excellent monographs on different aspects of MALDI that are highly recommended to anyone intending to pursue further studies of MALDI-MS [23–26, 149–152]. The following section will merely outline selected flagship applications of MALDI-MS.

11.6.1 General Protein Analysis by MALDI-MS

The success story of MALDI started with the demonstration of intact protein analysis by MALDI-TOF-MS. In their seminal work, F. Hillenkamp and M. Karas showed that MALDI is unique in that it can combine the ability for:

- desorbing ions of biomacromolecules into the gas phase,
- preserving their structural integrity, and
- being perfectly compatible with mass analyzers with almost unlimited *m/z* range and extraordinary sensitivity (Figs. 11.1 and 11.4) [11, 13, 14].

The analysis of intact proteins is often the first step in a series of analytical procedures revealing characteristics of cells, physiological pathways, diseases, or other aspects of interest in a biological or biomedical context. Often, the proteins are separated prior to MALDI-MS, e.g., by 2D gel electrophoresis. MALDI experiments must be carried out with highly purified proteins or mixtures containing only a limited number of proteins. In cases where the full mass range of proteins is needed, MALDI-TOF-MS would be the preferred choice.

The most commonly used matrices for MALDI of proteins are 3,5-dimethoxy-4-hydroxycinnamic acid (generally known as sinapinic acid (SA) [96]) and 2,5-dihydroxybenzoic acid (DHB) [17, 54]. Alternatively, for peptides, proteins, and glycoproteins one can use 2-(4-hydroxyphenylazo)benzoic acid (HABA) [71], 2-mercaptobenzothiazole (MBT), and 5-chloro-2-mercaptobenzothiazole (CMBT). For smaller proteins of up to about 6000 u good results can also be obtained using α-cyano-4-hydroxycinnamic acid (α-CHCA) [90].

11.6.2 Protein Fingerprints and MALDI Biotyping

Any organism bears a characteristic *protein fingerprint*. Protein fingerprints (and also those of carbohydrates) can be readily obtained by means of MALDI-MS. The necessary purification steps prior to MALDI analysis depend on the individual sample. For instance, the protein composition of a Mozzarella cheese will be able to reveal whether it was made from cow's milk or of that of a water buffalo [153], or whether feta cheese is "contaminated" with cow's milk [154]. MALDI spectra of protein extracts from different *Bacillus* species can be used to distinguish pathogenic from nonpathogenic bacteria, e.g., the protein fingerprints of chemically lysed *B. anthracis* (Sterne), *B. thuringiensis* (4A1), and *B. cereus* (6E1) are clearly different [155]; even different strains are distinguishable on the basis of particular biomarker proteins.

This field of MALDI-based mass spectrometry for the identification of biological species is known as *MALDI biotyping*. Instruments optimized for use in the clinical laboratory are available, e.g., the Bruker MALDI biotyper, a compact linear-mode MALDI instrument. MALDI biotyping is now well established for the identification of bacteria as it offers much faster and also cheaper means than immunoassays [156–158].

Microorganisms on fish In food analysis of fish and seafood products, differentiating between individual species of pathogenic and food-spoilage microorganisms and their rapid identification are particularly important. MALDI-TOF-MS protein fingerprinting was used to characterize the main 26 species responsible for seafood spoilage and associated pathogenic bacteria such as *Acinetobacter baumanii* and *Pseudomonas* species (Fig. 11.20) [159]. For this purpose, low-mass proteins were extracted from intact bacterial cells and subjected to MALDI analysis using α-CHCA matrix on a linear TOF instrument. Then, a library of specific MS fingerprints was compiled by comparing 10–35 characteristic peaks per organism in a range of m/z 2,000–10,000 from the protein fingerprint MALDI spectra.

MALDI-TOF spectra of intact parasites The selection of the proper matrix and the technique of sample preparation also matters in MALDI biotyping as is impressively demonstrated by the comparison of matrices for the identification of *Trypanosoma cruzi*, a protozoan flagellate parasite that causes Chagas disease (American trypanosomiasis). In this study, positive-ion MALDI spectra were obtained after using dried droplets or thin layer preparation in combination with DHB, SA, and CHCA [157]. Microscopic images of the preparations with SA and CHCA already showed differences in uniformity (Fig. 11.21). The superiority of SA by thin layer technique was directly reflected in the quality of the MALDI spectrum (Fig. 11.22). DHB neither formed a crystalline layer nor was it able to yield a useful spectrum.

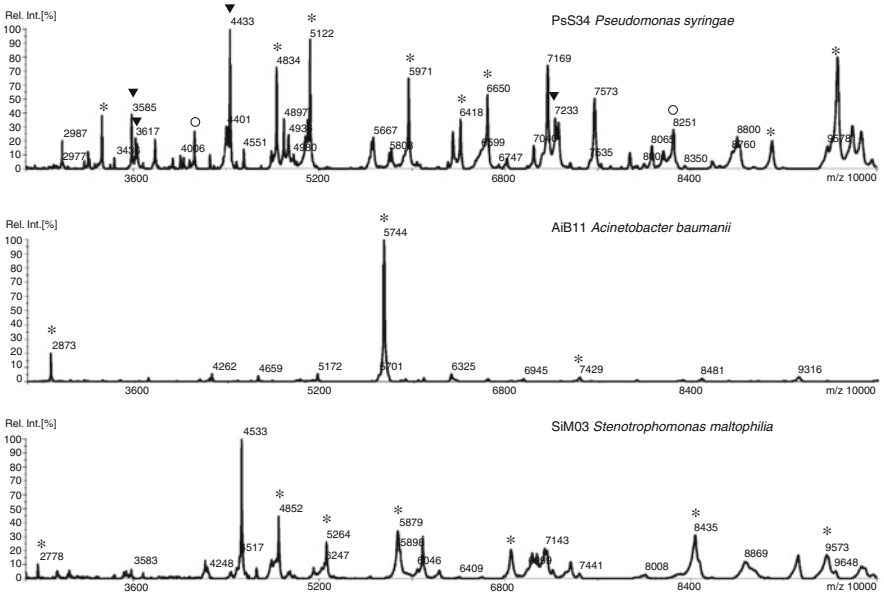

Fig. 11.20 Protein fingerprint MALDI-TOF spectra of *Pseudomonas syringae* (*top*), *Acetinobacter baumannii* (*center*) and *Stenotrophomonas maltophilia* (*bottom*) have clearly different appearances; species-specific peaks are indicated by *, genus-specific peaks by O, and other characteristic peaks by ▼ (Adapted from Ref. [159] with permission. © American Chemical Society, 2010)

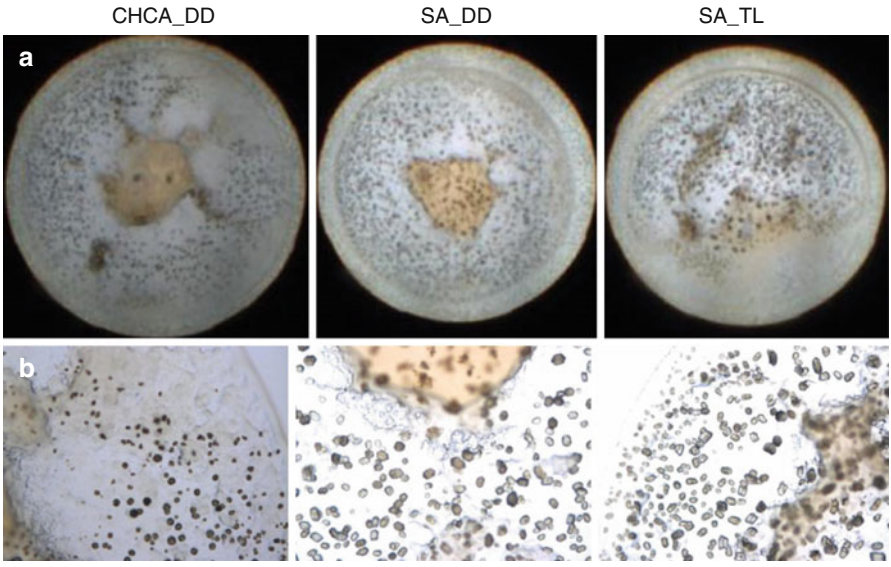

Fig. 11.21 Microscopic images of intact parasite cells embedded in different matrices imaged at two levels of resolution (**a**) ×10 and (**b**) ×100; DD: dried droplet preparation, TL: thin layer method. Matrices were dissolved in acetonitrile : water = 7 : 3 with 0.1% of trifluoroacetic acid. The superior uniformity of the thin layer sample deposition is visible and notably affects the quality of the MALDI spectrum (Fig. 11.22) (Adapted from Ref. [157] with permission. © Wiley, 2016)

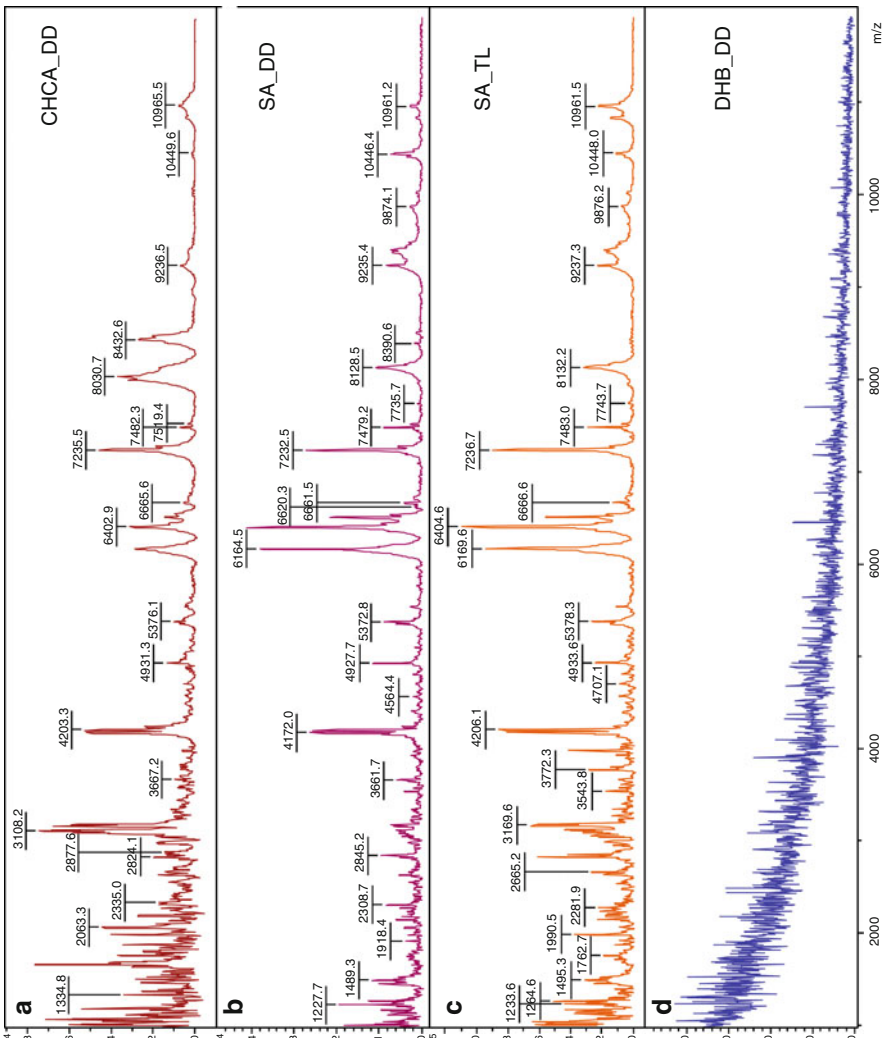

Fig. 11.22 MALDI biotyping of *Trypanosoma cruzi* using (**a**) CHCA DD, (**b**) SA DD, (**c**) SA TL, and (**d**) DHB DD (DD: dried droplet preparation, TL: thin layer method). SA TL delivers best results in terms of number of signals and intensity while DHB totally fails here (Adapted from Ref. [157] with permission. © Wiley, 2016)

11.6.3 Peptide Sequencing and Proteomics

Analysis of the total of all proteins expressed by a living organism, a type of tissue, or certain cells is a tremendous task, as we are dealing with thousands of proteins with relative abundances in range of $> 1000 : 1$. This field of research called *proteomics* aims at quantitative analysis of entire proteomes of individual organisms, ,and requires complex analytical approaches involving different separation techniques along with MS and MS/MS [160–169]. Of course, in proteomics there are no restrictions as to ionization methods, while MALDI (together with ESI; see Chap. 12) accomplish 99.9% of all MS analyses in proteomics.

A standardized workflow for the complete analysis of a protein by using a pure MALDI strategy comprises several steps (Fig. 11.23). It commences with the measurement of the intact protein's mass, preferably by MALDI-TOF-MS as this combination offers inexpensive and reliable access to the full m/z range where proteins may occur. Next, a proteolytic digestion is performed to cut the macromolecule into smaller peptide subunits, typically in the range of 800–2500 u. Generally, the enzyme trypsin is employed to deliver these peptides, a so-called *tryptic digest*, which are then analyzed in a survey measurement by MALDI-TOF-MS. The resulting MALDI spectrum presents a so-called *peptide mass map*. Such peptide mass maps usually suffice to identify the protein [170].

The next stage is to subject as many as possible peptides of the peptide mass map to tandem MS to reveal their individual amino acid sequences. Interpreting the amino acid sequences requires substantial knowledge of the fragmentation behavior of peptide ions [164, 168, 171]. Provided some basic information on the fragmentation pathways of peptide ions is available, computer algorithms can be developed that allow to derive substantial, however not necessarily complete, sequence information. Automated MALDI-TOF/TOF peptide sequencing is thus widely used. The procedure includes automated precursor ion selection for tandem MS, e.g., by selecting several abundant $[M + H]^+$ ions of a survey spectrum and generating peak lists from those tandem mass spectra. The experimental results are finally compared with large peptide databases. The number of potential proteins and its tryptic peptides can further be narrowed down using accurate mass data of the protein and the peptides. While MALDI-MS and MALDI-MS/MS could serve this pupose almost alone, electrospray ionization and liquid chromatography coupling to MS today contribute to a larger extent to the instrumental and methodological mix in proteomics, because the LC-MS technique is more efficient in detecting trace proteins than approaches starting from 2D gels [22–25, 152, 172, 173].

Only the peptide subunits of a protein can be efficiently fragmented by CID for tandem MS analysis. Identifying a protein from such a peptide "jumble" is called *bottom-up* protein analysis. The corresponding tandem MS of the entire protein ions is called *top-down* protein analysis. As the *top-down* approach requires larger amounts of purified protein, it is more widely applied in protein biochemistry. ECD-FT-ICR-MS, assisted by IRMPD heating of the protein ions, is currently the exclusive tool for this purpose (Sect. 9.14.4).

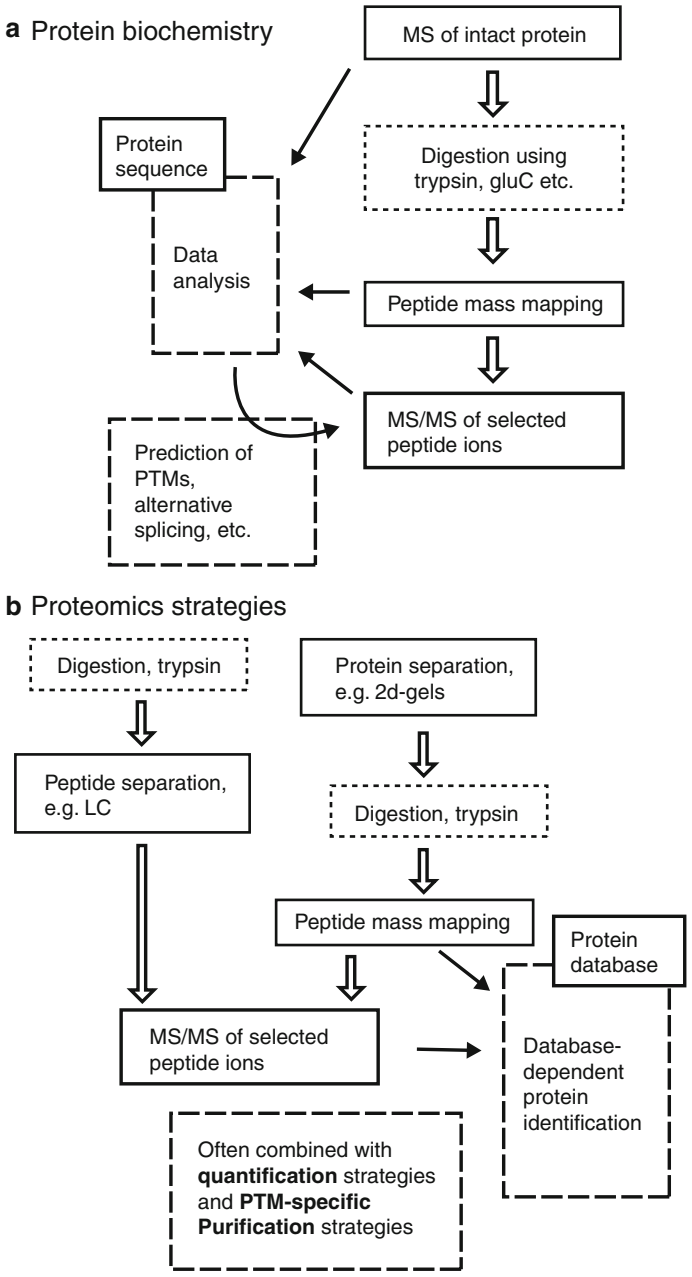

Fig. 11.23 Analytical strategies in (**a**) protein biochemistry requiring highly purified proteins and (**b**) proteomics addressing the entire proteome of a living cell. (Adapted from Chap. 3 by Hjernø and Jensen in Ref. [15] by permission. © Wiley-VCH, Weinheim, 2007)

Peptide fragmentations
Examples and mechanistic aspects of peptide fragmentation are also covered in the context of tandem MS (see Sects. 9.6.6, 9.8, and 9.10.1). The mechanism of peptide cleavage upon ECD is discussed in Sect. 9.13.2 with an example in Sect. 9.14.4; peptide ETD spectra are given in Sect. 9.15. Some further examples will follow in Chap. 12.

Peptide ions are comparatively large, and thus assume various fragmentation pathways. The most obvious and analytically useful fragmentation routes involve the cleavage of the peptide backbone. Following the nomenclature for peptide backbone cleavages originally suggested by Roepstoff and Fohlman [174] and modified by Biemann [175] fragments bearing the charge (due to protonation) at the N-terminus are denoted as a-, b-, and c-ions depending on the actual bond cleaved. If C-terminal fragment ions are formed, the ions are termed x-, y-, and z-ions, respectively (Scheme 11.1). Further, a number index counting from 1 to n–1 for a peptide composed of n amino acids is used to indicate which bond is cleaved. Within each ion series, peaks are seperated by $\Delta m/z$ values directly reflecting the amino acid residue (Table A.11 in Appendix) between them.

The base fragment ion series due to amide bond cleavages are formed by b-ions on the N-terminus and y-ions on the C-terminus. The signals of the a-ions are set off to lower mass by 28 u (CO loss) from the b-ions, while c-ions are 17 u (NH_3) heavier than b-ions as the adjacent N–C_α bond is cleaved. The x-ions of the C-terminal series are by 26 u lighter than y-ions (minus CO, plus H_2) and z-ions are again by 17 u (NH_3) heavier than y-ions.

CID of peptide ions Scheme 11.1 depicts the most likely structures for the main peptide fragment ions. For example, the nominal acylium form of the b_3 ions is not stable, rather it is stabilized by formation of a 5-membered oxazolone ring [176–179] at its C-terminus. Note that this ion contains the amino acid residues up to the third (R^3) including the carbonyl group of R^3 and that the charge is carried by the nitrogen of the ring. The corresponding a_3 ion is formed by elimination of the carbonyl group (CO) from the oxazolone ring.

Fragmentation of [QAMNKFTF–NH_2+H]$^+$ The purified octapeptide QAMNKFTF–NH_2 was subjected to positive-ion MALDI-TOF/TOF analysis. The spectrum shown (Fig. 11.24) was obtained from the $[M + H]^+$ precursor ion, m/z 985.53. The fragment at m/z 968.33 corresponds to ammonia loss from $[M + H]^+$. All seven ions belonging to the b-ion series are detected at m/z 821.25, 720.23, 573.19, 445.12, 331.08, 200.04, and 129.02. In addition b–NH_3 ions, referred to as b* ions, accompany the first four ions at m/z 804.24, 703.22, 556.17, and 428,10 because the N-terminal glutamine (Q) has a tendency to lose NH_3.Thus, we have ions consistent with the expected b_7 to b_1 and b_7* to b_4* fragments, although the ion at m/z 129 can also be formed from lysine (K). The four additional fragment ions at

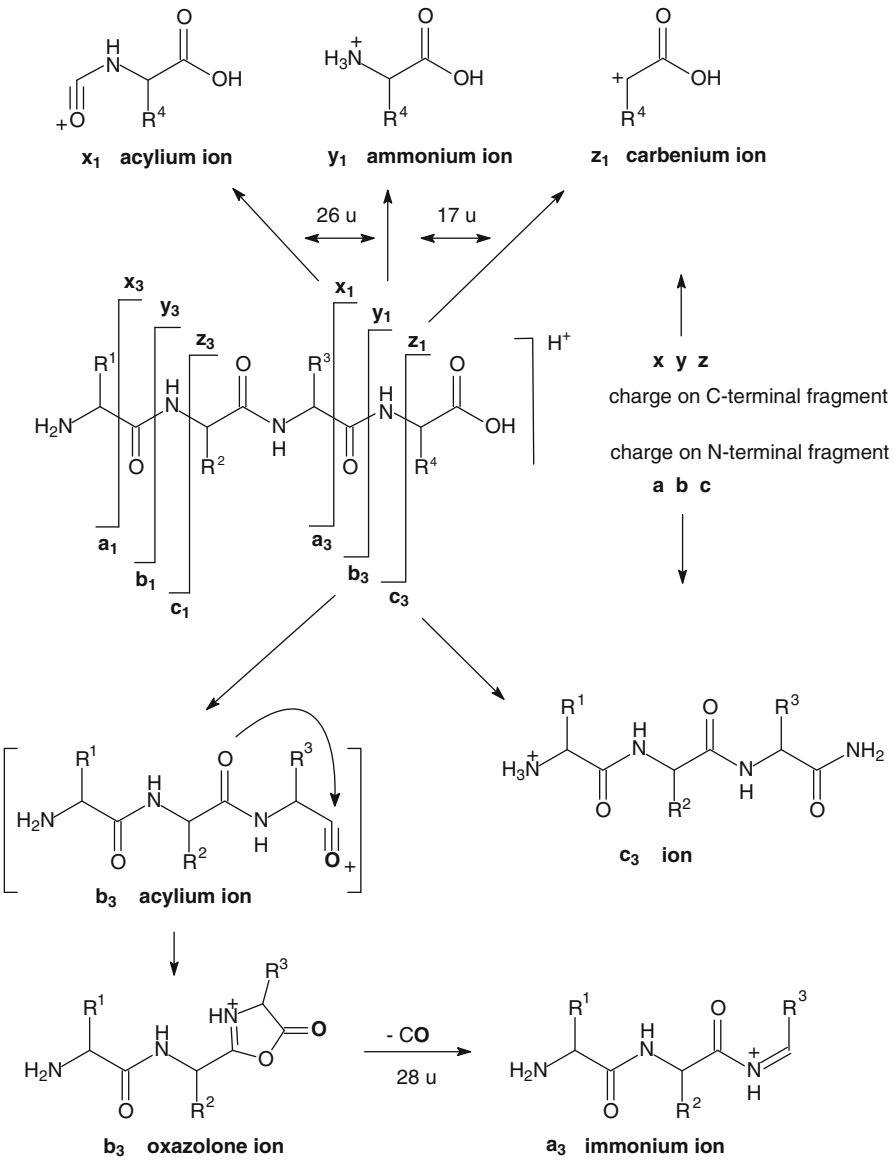

Scheme 11.1 (One carbonyl-*O* is set in bold for better tracking)

m/*z* 857.29, 786.25, 655.25, and 541.23 belong to the y-series and represent the y_7 to y_4 ions, whereas smaller y ions are absent (only their hypothetical positions are indicated as y_1^a to y_3^a) [180].

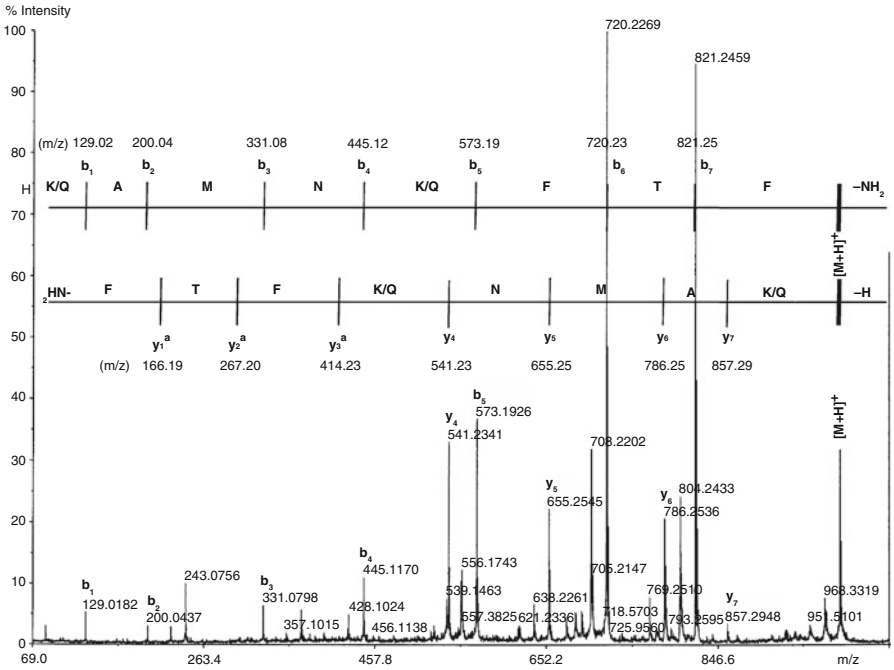

Fig. 11.24 MALDI-TOF/TOF mass spectrum of the purified octapeptide H-QAMNKFTF-NH_2 showing the experimental b_j and y_j peptide fragment ion series; y^a ions are only hypothetical in this case (Adapted from Ref. [180] with permission. © John Wiley & Sons, 2010)

It needs to be emphasized that the actual appearance of a tandem mass spectrum acquired of one and the same compound may be subject to substantial variation for several reasons:

- The spectrum depends to some extent on the ionization method employed to generate a $[M + H]^+$ precursor ion. Ions from MALDI are entering the activation stage with already somewhat higher internal energy than those from ESI.
- The charge state of the selected precursor ion is of utmost importance. With increasing number of charges the Coulombic repulsion also contributes to drive the incipient fragments apart, and thus, less energy needs to be provided by the activation method used.
- The particular activation technique, i.e., low-energy multiple-collision CID versus high-energy single-collision CID versus IRMPD, for example, influences the internal energy and lifetime of decomposing ions, and thus, the selection of fragmentation pathways and/or the relative abundance of fragment ions.
- Instrumental factors such as ion lifetime or internal energy distribution also effect the appearance of the spectrum. In tandem MS, quadrupole ion trap analyzers tend to suppress the lower third of the m/z range, whereas TOF and magnetic sector analyzers do not.

In combination with the intrinsic properties of the ion under study these specific differences introduced into the sequencing experiment cause certain fragments to occur in the final spectrum while others may be missed. This is commonly referred to as *sequence coverage* of a given instrumental configuration.

Peptides aren't all the same
Peptides show marked differences, though having a great deal in common. Biochemists always emphasize the enormous variability of peptides and proteins assembled from as just twenty amino acids and the plethora of resulting functional characteristics. Accordingly, one should stay aware of the fact, that every (peptide) molecule has intrinsic properties also determining their fragmentation into ions.

11.6.4 Carbohydrate Analysis by MALDI-MS

Starting from simple mono- and disaccharides to oligo- and polysaccharides, carbohydrates play an important role in organisms and nutrition. MALDI-MS (typically using DHB or some DHB-containing matrix [17, 82–84, 86]), is a powerful tool for their characterization [181]. Applications include the characterization of maltose chains in "gummy bears" [82], fructans in onions [182], high-molecular-weight oligosaccharides in human milk [83, 84], and others [117, 183]. MALDI-MS of carbohydrates from fungal spores [184] allows for the characterization of the corresponding fungus.

Carbohydrates form alkali adduct ions
Carbohydrates possess a high affinity towards alkali metal ions, and thus in MALDI spectra $[M + Na]^+$ and/or $[M + K]^+$ are normally observed instead of or sometimes in addition to $[M + H]^+$ ions of very low abundance. It generally depends on the relative amount of alkali ion impurities which ionic species will dominate within the spectrum. As NH_4^+ and K^+ ions share the same ionic radius, $[M + NH_4]^+$ adducts may also occur. Radical ions are not observed.

Gummy bear spectrum The maltose chains in the confectionery "gummy bears" consist of up to about 30 maltose units that can easily be extracted into water and analyzed by MALDI-MS [82]. To do so, it is sufficient to allow a gummy bear to take a short bath in water and to admix 1 µl of this extract to about 60 µl of 10 mg ml^{-1} DHB in water : acetonitrile = 1 : 1 (v/v) with 0.1 % of trifluoroacetic acid (Fig. 11.25). Next, 1 µl of this maltose–matrix solution is spotted onto a target and allowed to crystallize (Fig. 11.13). The positive-ion linear mode MALDI-TOF spectrum then exhibits signals due to $[M + Na]^+$ ions of the maltose chains. Linear mode is recommended, as oligosaccharides of > 2000 u tend to fragment even in

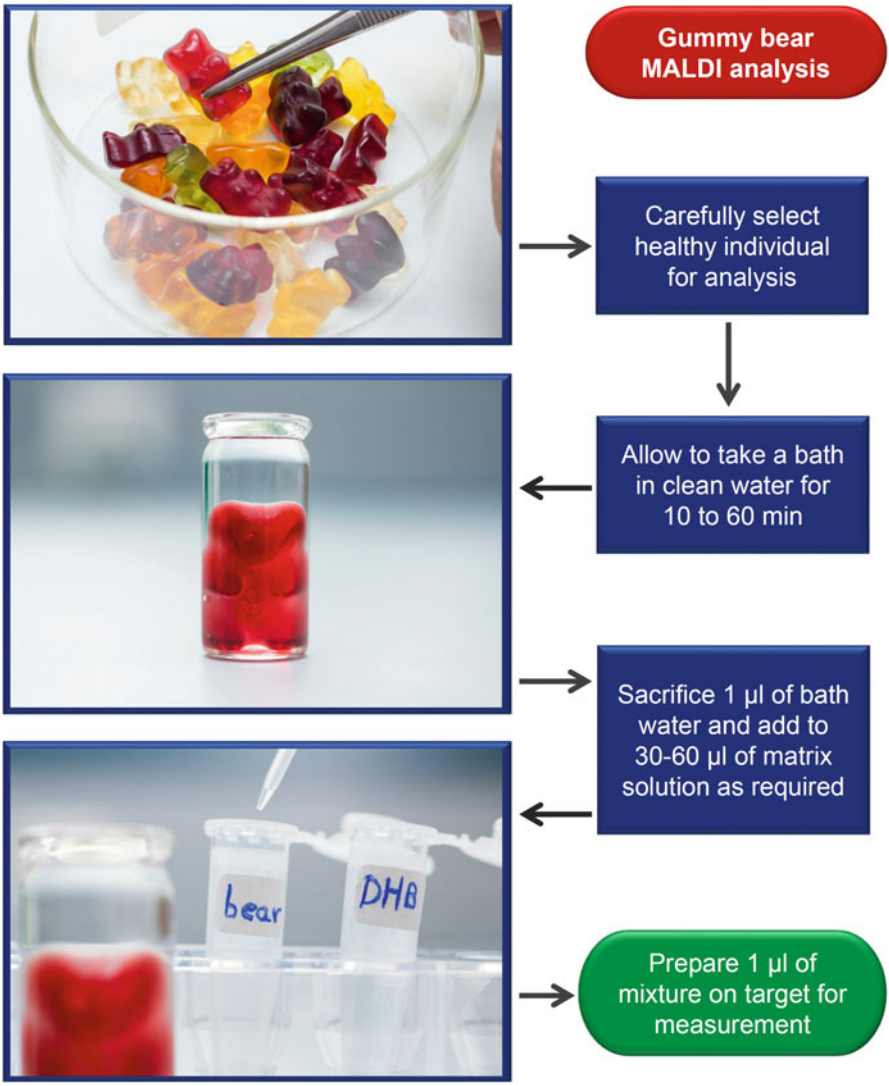

Fig. 11.25 Procedure to measure oligosaccharides of a gummy bear by MALDI-MS. The resulting spectrum is shown in Fig. 11.26

MALDI precluding their detection in reflector mode. Oligosaccharide ions have the formula $[C_6H_{12}O_6 + (C_6H_{10}O_5)_n + Na]^+$, and thus, occur in the spectrum at $\Delta(m/z) = 162$, i.e., by $C_6H_{10}O_5$ monomer units apart (Fig. 11.26). The MALDI-TOF spectrum covering the range m/z 400–5000 shows peaks belonging to the 3mer at m/z 527 up to the 30mer at m/z 4905.

The structure of linear as well as complex branched oligosaccharides can be sequenced by tandem MS analogous to peptide sequencing [181, 185]. If the

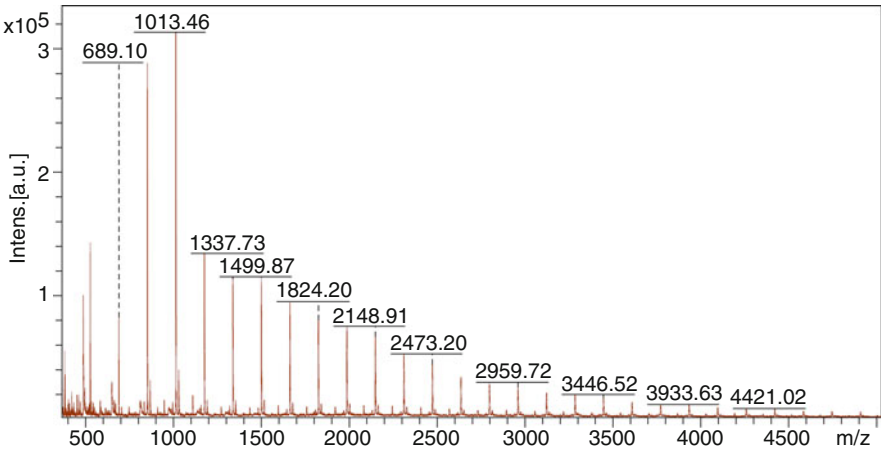

Fig. 11.26 Positive-ion linear mode MALDI-TOF spectrum of the maltose chains extracted from the red gummy bears shown in Fig. 11.25 in the range m/z 400–5000. The $[M + Na]^+$ ion peaks of the oligosaccharides occur at $\Delta(m/z) = 162$

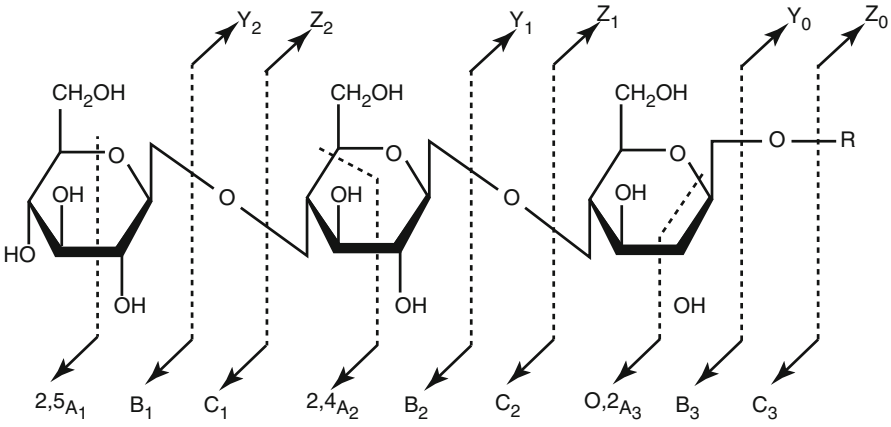

Scheme 11.2 Carbohydrate fragmentation and naming of fragment ions

carbohydrate ions are generated by MALDI, sufficient energy for their fragmentation can be provided in two ways: (*i*) Higher laser irradiance can effect *in-source decay* (ISD) or *metastable dissociation* [124]; the latter being termed *post-source decay* (PSD) in the MALDI-TOF community. (*ii*) *Collision-induced dissociation* (CID) of selected precursor ions can be employed alternatively. (Of course, other compound classes such as peptides, oligonucleotides, or synthetic polymers can be treated analogously.) The general scheme of carbohydrate fragmentation is as follows (from Ref. [181] by permission, © Elsevier Science, 2003) Scheme 11.2.

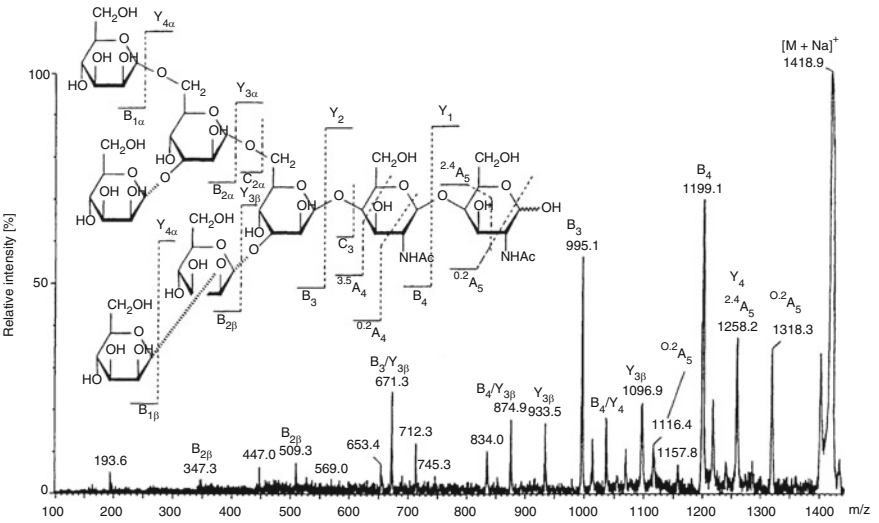

Fig. 11.27 PSD-MALDI-TOF spectrum of *N*-linked glycan $(Man)_6(GlcNAc)_2$ from chicken ovalbumin (Reproduced from Ref. [181] by permission. © Elsevier Science, 2003)

Fragmentation of a glycan The PSD-MALDI-TOF spectrum of the $[M + Na]^+$ ion, *m*/*z* 1418.9, of high-mannose *N*-linked glycan $(Man)_6(GlcNAc)_2$ from chicken ovalbumin shows distinct cleavages of the branched carbohydrate skeleton (Fig. 11.27) [181]. The spectrum was obtained using DHB matrix.

11.6.5 Oligonucleotide Analysis by MALDI-MS

Oligonucleotides and DNA represent the highest polarity class of biopolymers. Therefore, it is of special importance that isolation in an organic matrix allows to overcome their strong intermolecular interaction. MALDI analysis of oligonucleotides is further complicated by the numerous acidic hydrogens present in a single molecule. In particular the phosphate groups easily exchange protons with the ubiqitous alkali ions [30]. Thus, MALDI of this compound class requires to follow proven experimental protocols to obtain clean spectra of ions representing the intact macromolecules. The acidity of the phosphates makes oligonucleotides and DNA accessible as $[M - H]^-$ ions if measured in the negative ion mode [30].

Due to their numerous acidic hydrogens, oligonucleotides require desalting prior to MALDI, e.g., by using cation exchange resins [30]. Similar procedures are necessary when other ionization methods are applied to this compound class [81, 101, 186, 187].

Deoxynucleotide 5mer The negative- and positive-ion mode MALDI-TOF spectra of the solid-supported 5-meric oligodeoxynucleotide *po*-CNE 5′-GACTT-3′

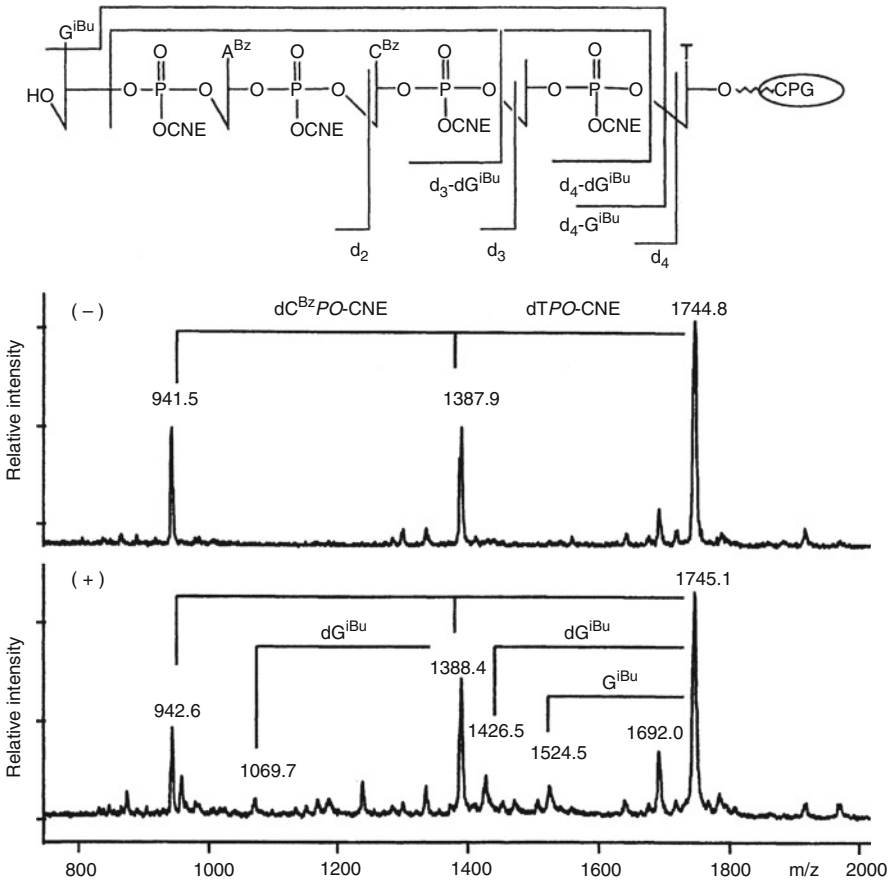

Fig. 11.28 Comparison of the negative- and positive-ion mode MALDI-TOF spectra of the 5-meric *po*-CNE 5′-GACTT-3′ oligodeoxynucleotide. Both show fragment ions by ISD (Adapted from Ref. [101] by permission. © John Wiley & Sons, 2000)

[101]: comparison shows that both exhibit fragment ions due to cleavages of the phosphotriester backbone (Fig. 11.28). As oligonucleotides normally do not exhibit such a distinct level of ISD in MALDI spectra, it has been argued that the linking to the solid support plays a role for the generation of this mass ladder of peaks which differ by one nucleotide residue.

11.6.6 MALDI-MS of Synthetic Polymers

MALDI is the method of choice for the analysis of synthetic polymers. MALDI is soft enough to provide intact molecular ions or intimately related ions by cationization and gives access to an essentially unlimited mass range [26, 27,

151]. As ions from MALDI are almost always singly charged [46] the spectrum may represent a very good approximation to the molecular weight distribution of the examined polymer. While polar polymers such as poly(methylmethacrylate) (PMMA) [102, 188], polyethylene glycol (PEG) [188, 189], and others [98, 190, 191] readily form $[M + H]^+$ or $[M + \text{alkali}]^+$ ions, nonpolar polymers like polystyrene (PS) [118, 119, 124, 125] or nonfunctionalized polymers like polyethylene (PE) [121, 122] can only be cationized by transition metal ions in their 1+ oxidation state [118, 119]. The formation of evenly spaced oligomer ion series can also be employed to establish an internal mass calibration of a spectrum [190].

The most important parameters that can be determined by MALDI are *number-average molecular weight* (M_n), *weight-average molecular weight* (M_w), and the molecular weight distribution expressed as *polydispersity* (*PD*) [125, 192]:

$$M_n = \frac{\sum M_i I_i}{\sum I_i} \tag{11.1}$$

$$M_w = \frac{\sum M_i^2 I_i}{\sum M_i I_i} \tag{11.2}$$

$$PD = \frac{M_w}{M_n} \tag{11.3}$$

where M_i and I_i represent the molecular weights of the oligomeric components and their signal intensities (assuming a linear relationship between number of ions and signal intensity) of the detected species. The formula for M_n is identical to that used for the calculation of the molecular weight from isotopic masses and their abundances as represented by an isotopic pattern (Eq. 3.2 in Sect. 3.1.5).

Silver adduct formation Polystyrenes ranging from PS 2200 to PS 12500 form $[M + \text{metal}]^+$ ions with Ag^+ and Cu^+ ions when silver or copper(I) salts are admixed to the sample preparation. In case of PS 12500, both metal ions were found to effect cationization equally well, i.e., without causing differences in average molecular weight or ionic abundances (Fig. 11.29) [125].

How to determine endgroups If the mass of the monomer is not already known prior to MALDI-MS, it is obtained from $\Delta(m/z)$ of adjacent peaks within the series of signals. Averaging of multiple measurements improves the accuracy of the value. Next, integer multiples of $\Delta(m/z)$ are subtracted from the m/z value of a peak at the low-mass side of the distribution until the remainder roughly attains the mass of the monomer. The mass of the sum of both endgroups, possibly including the charge bearing adduct ion, is thus obtained. However, the value is not unambiguous, because large endgroups may be misinterpreted as mass of a monomer plus a smaller endgroup. Polyethylene glycol 600 serves as a simple example: Peaks representing $[M + Na]^+$ ions at m/z 305.16, 349.19, 393.21, 437.24, ... deliver an average of $\Delta(m/z) = 44.03$. Subtracting 22.99 u for sodium and multiples (6) of

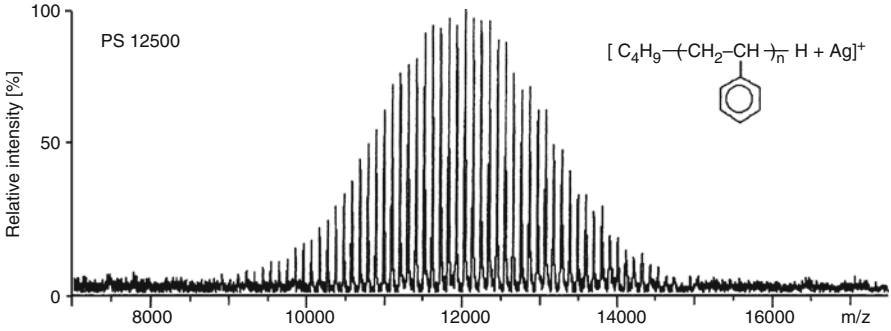

Fig. 11.29 Linear-mode positive-ion MALDI-TOF spectrum of polystyrene 12500 doped with Ag^+ ions. Subtraction of the Ag^+ ion mass (average of 108 u for the nonresolved pair of ^{107}Ag and ^{109}Ag) is therefore required to derive the correct molecular mass of the individual species. The isotopic pattern of silver does not affect the spectrum as isotopic resolution here is not achieved anyway (Adapted from Ref. [125] by permission. © John Wiley & Sons, 2001)

44.03 u from *m*/*z* 305.16 yields 17.99 u for the endgroups, i.e., 18 u point towards H and OH in this case.

In addition, the determination of a polymer's endgroup(s) [193, 194] and the analysis of random and block-copolymers [195, 196] can be achieved by MALDI. However, care has to be taken when judging the MALDI spectra because of the mass-dependent desorption and detection characteristics of the experiment. In case of higher polydispersity ($PD > 1.1$) high-mass ions are underestimated from MALDI spectra [112, 192]. The current practice to deal with such samples is to fractionate them by *gel permeation chromatography* (GPC) [191] or *size-exclusion chromatography* (SEC) prior to MALDI analysis [192, 197].

Polymer mixture Extracted and synthesized oligo(ethylene terephthalate)s were compared by MALDI-MS [194]. Using the symbols G for ethylene glycol units, GG for diethylene glycol units, and T for terephthalic acid units, the detected oligomers were (*i*) cyclic oligomers $[GT]_n$, (*ii*) linear chains H-$[GT]_n$-G, and (*iii*) some other distributions such as linear H-$[GH]_n$-OH and H-$[GGT]_1$-$[GT]_{n-1}$-G oligomers and cyclic H-$[GGT]_1$-$[GT]_{n-1}$ oligomers. Type (*i*) was mainly contained in technical yarns and tiles, whereas types (*ii*) and (*iii*) were constituents of the model oligomers (Fig. 11.30).

MALDI-MS of a block copolymer An ethylene oxide (EO)–propylene oxide (PO) block copolymer has been analyzed by MALDI-MS. Interferences are likely to occur, as ion series caused by different EO/PO ratios are going to superimpose in the spectrum. Using a JEOL SpiralTOF instrument, a design offering very high resolving power (Sect. 4.2.11) [198], allowed to separate overlapping isotopic patterns of the monoisotopic $[M+Na]^+$ ion of (EO_4–PO_{14}) and of the $^{13}C_2$ isotopic ion of (EO_0–PO_{17}) as present in the range *m*/*z* 1027.2–1033.2, for example. Due to $R = 80{,}000$, the instrument was still able to separate the doublet at *m*/*z* 1029.7 with peaks at $\Delta(m/z) = 0.03$ (Fig. 11.31).

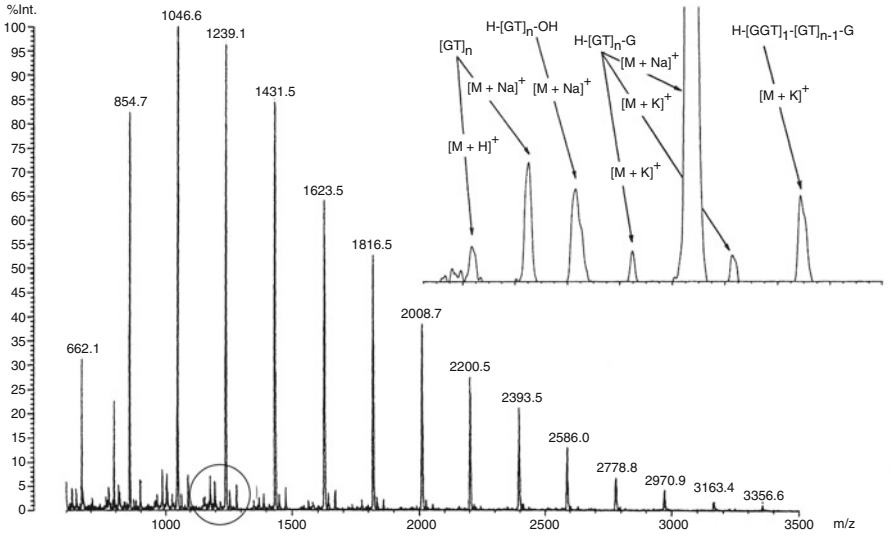

Fig. 11.30 Oligo(ethylene terephthalate diol)s: MALDI-TOF spectrum of the model compound. The *inset* shows an expanded view of the low-intensity peaks *m*/*z* 940–1120 (*circled*) (Adapted from Ref. [194] by permission. © John Wiley & Sons, 1995)

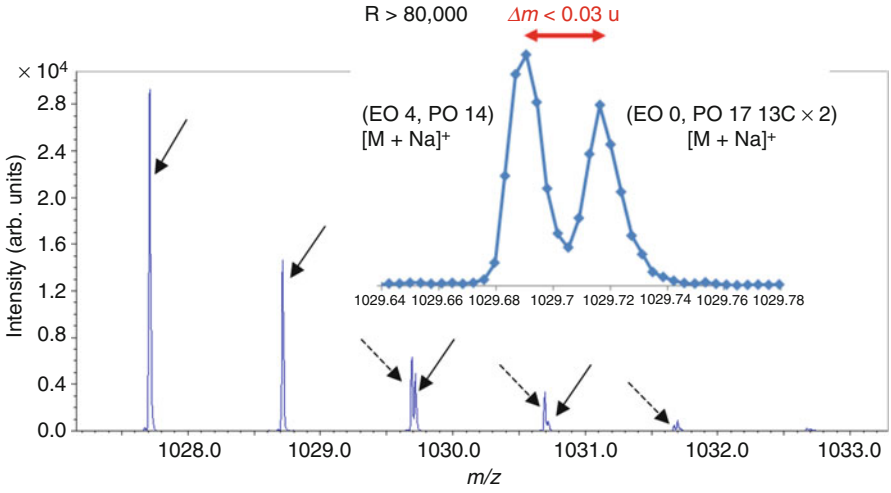

Fig. 11.31 Partial MALDI mass spectrum of an EO–PO block copolymer at *m*/*z* 1027.2–1033.2 as obtained on a JEOL SpiralTOF instrument. *Solid arrows* indicate the isotopic pattern of (EO0–PO17), and the *dotted arrows* indicate that of (EO4–PO14). The *inset* shows an expanded view of the doublet at *m*/*z* 1029.7; the *diamonds* on the line correspond to data points (Sect. 4.10) (Adapted with permission from Ref. [198] © Mass Spectrometry Society of Japan, 2014)

MALDI of dendrimers In terms of their behavior in MALDI-MS, dendrimers exhibit some resemblance to polymers. The molecular weight of dendrimers quickly increases as the molecules grow with each generation of branching. As dendrimer syntheses tend to yield "imperfect" by-products, the restriction of MALDI to form singly charged ions is beneficial in that it results in spectra that reveal all components at a glance. A MALDI-TOF spectrum of a dendrimer mixture has already been discussed in the context of mass calibration (Sect. 3.7.4) [199–201].

11.7 Special Surfaces to Mimic the Matrix Effect

MALDI is so unique in offering a wide range of applications from small molecule analysis over peptides and synthetic polymers to large biomacromolecules that efforts have been made to mimic the matrix effect in other ways without having the specific disadvantages of matrixes, such as background peaks (which are particularly disturbing in the low-mass range). Here, alternative techniques are briefly discussed.

11.7.1 Desorption/Ionization on Silicon

In *desorption/ionization on silicon* (DIOS), the analyte is absorbed by a micrometers-thick porous surface layer on a silicon chip, i.e., the porous silicon is used as substitute of an organic matrix [202, 203]. Porous silicon surfaces with high UV absorptivity can be generated with varying properties from flat crystalline silicon by using a galvanostatic etching procedure [204]. Stabilization of the freshly prepared surfaces is achieved by hydrosilylation. Porous silicon surfaces can be reused several times after washing. Arrays of 100–1000 sample positions can be realized on a 3 × 3 cm silicon chip [204]. The DIOS technique offers picomole detection limits for peptides, comparatively simple sample preparation, and – most importantly for small molecule analysis – the absence of matrix peaks in the spectra [205, 206].

DIOS of a tryptic digest DIOS-TOF/TOF experiments on the tryptic digest of 100 fmol of the protein bovine serum albumine (BSA) demonstrate this technique. Using conductive tape the DIOS chip was directly attached to the MALDI target plate of an Applied Biosystems 4700 tandem TOF instrument equipped with a frequency-tripled Nd:YAG laser (355 nm). The resulting DIOS-TOF spectrum of the digest and the DIOS-TOF/TOF spectrum of one selected peptide, $[YLYEIAR + H]^+$, m/z 927.5 are shown in Fig. 11.32. The tandem mass spectrum provides complete detection of the *y* and *b* ion series [206].

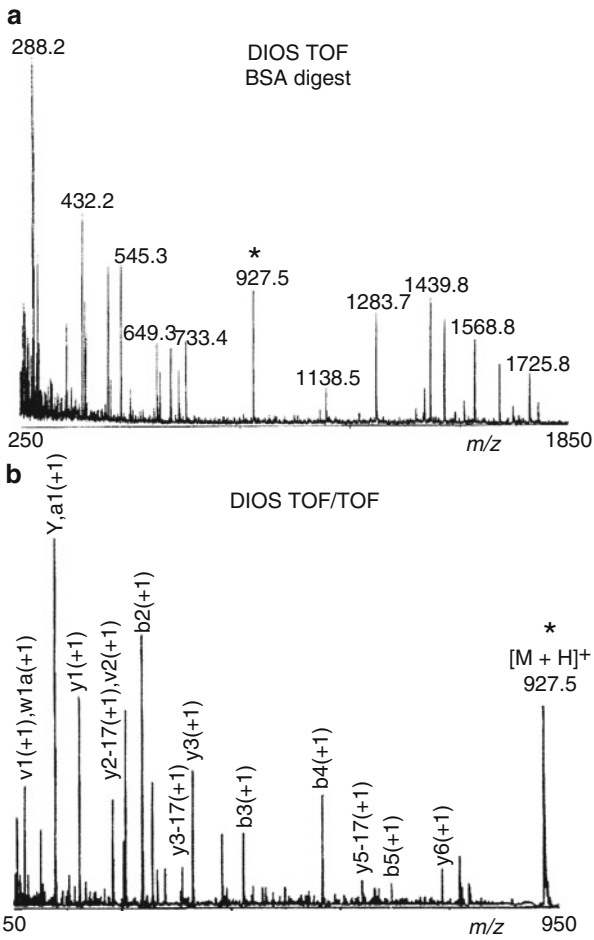

Fig. 11.32 DIOS applied to a tryptic BSA digest. (**a**) DIOS spectrum of the tryptic peptides from BSA; (**b**) DIOS tandem mass spectrum of the $[YLEIAR + H]^+$ peptide ion, *m*/*z* 927.5, to demonstrate sensitivity and sequence coverage of DIOS (Adapted from Ref. [206] with permission. © American Chemical Society, 2003)

11.7.2 Nano-assisted Laser Desorption/Ionization

A more recent approach, also from the Suizdak group, is to modify silicon surfaces with *single-crystal silicon nanowires* (SiNWs), which also happen to provide a good platform for surface-based mass spectrometry. Those silicon nanowires are directly synthesized on the surface of a silicon wafer. The formation of SiNW can be well controlled to define physical dimensions, composition, density, and position of the nanowires on the surface [207, 208].

The synthesis of SiNWs starts from gold nanoparticles with diameters of 10, 20, or 40 nm that are distributed on a silicon substrate. The nanoclusters are required to catalyze SiNW growth. The method employs an elaborate series of steps of growth, etching, oxidation, and finally silylation to generate a perfluorophenyl-derivatized SiNW surface. Like DIOS targets, the SiNW-coated plates are attached to a

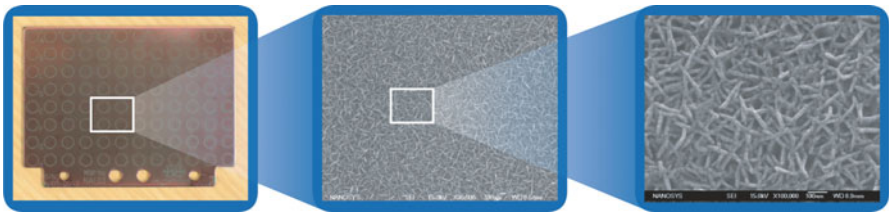

Fig. 11.33 NALDI target plate. The figure shows the NALDI target plate (*left*) and increasing magnification SEM images (*center* and *right*) of the nanostructured coating that provides the active surface for desorption/ionization of deposited analytes (Courtesy of Bruker Daltonik GmbH, Bremen)

modified sample plate. The procedure of measuring a spectrum is then analogous to LDI or DIOS, i.e., the special surface replaces the organic matrix.

The term *nano-assisted laser desorption/ionization* (NALDI) [209, 210] has been coined for techniques using nanostructured surfaces to mimic MALDI. The NALDI™ sample plates have become commerically available from a major manufacturer of MALDI-TOF instrumentation (Fig. 11.33). Like DIOS, NALDI is particularly useful for small molecule analysis in high-throughput analytics [209, 210]. In contrast to DIOS, NALDI is still in use.

11.7.3 Further Variations of the MALDI Theme

The properties of a surface may to a certain extent be tailored to optimize its performance for a particular field of application. Basically, the matrix–analyte pair is replaced by a customized surface–analyte pair that is subjected to laser irradiation. While this approach, on the one hand, simplifies sample preparation, on the other it necessitates preparation of a set of delicate surfaces to be used for different needs.

Silica gel can be derivatized in multiple ways, e.g., by covalently binding ligands via Si–O bonds to its surface. Both *surface-enhanced laser desorption/ionization* (SELDI) and *material-enhanced laser desorption/ionization* (MELDI) make use of the presence of metal complexes on a silica gel surface to selectively adsorb target compounds via complex formation from solution to a target surface [211]. Besides silica gel, also cellulose or glycidyl methacrylate particles, and even diamond powder have been employed as carriers for the metal complex-functionalized groups [212, 213].

Delicate surfaces
Surfaces for DIOS, NALDI, or MELDI are active and rather sensitive. They require proper storage, handling, and processing, e.g., washing, before use. As the sample holder is of one type of customized surface only, this sort of

(continued)

targets is merely useful when performing a large number of very similar analyses. Increased cost at reduced robustness as compared to simple stainless steel plates have to be taken into account.

11.8 MALDI Mass Spectral Imaging

11.8.1 Methodology of MALDI Imaging

MALDI-MS can be used to generate ion images of samples thus providing the capability of mapping specific molecules to two-dimensional coordinates of the original sample [214]. This approach to surface analysis has long been known in *secondary ion mass spectrometry* (SIMS, Sect. 15.6) and was introduced in MALDI-MS as *MALDI imaging* by the Caprioli group in 1997 [214]. Since then, MALDI imaging has undergone a tremendous development [215–218] (see Chap. 4 in [15] and Chap. 12 in [219]). The high sensitivity of the technique ranging down to the low femtomole to even attomole levels for proteins and peptides gives access to the study of intricate biochemical processes. In fact, MALDI imaging is most frequently used to map local concentrations of target analytes in tissue samples, but it can also be applied to analyze paint or ink on paper or valuable artwork.

IMS or IMS or MSI?
The term *imaging mass spectrometry* (IMS) is correlated to the same acronym as *ion mobility spectrometry* (IMS, Sect. 4.10), thus one must be aware of the context in which IMS is being used. The more recent term *mass spectral imaging* (MSI) resolves this ambiguity.

The preparation procedure is critical for the outcome of MALDI imaging. It consists of coating of the tissue section or a blotted imprint of the section with an evenly distributed thin matrix layer before the sample can be placed into the mass spectrometer (Fig. 11.34) [220]. The matrix solution is preferably sprayed onto the sample, e.g., by a pneumatic or electrostatic nebulizer delivering very fine droplets to assure homogeneous coating [221]. Alternatively, a picoliter volume spotter can be used to deposit matrix spots in a fixed pattern onto the sample slice [215]. Variations in matrix crystallization or layer thickness result in erroneous images, because the intensity of the signals would rather be determined by the quality of the matrix layer on the actual pixel than by the concentration of the analyte underneath. Microcrystalline layers and laser spot focus diameter also determine the spatial resolution of the imaging process, which can resolve structures to about 10 μm [216, 221, 222].

MALDI imaging creates an array of mass spectra, i.e., each “pixel” of the image, often of an 256 × 256 spot array, is represented by a MALDI spectrum of its own.

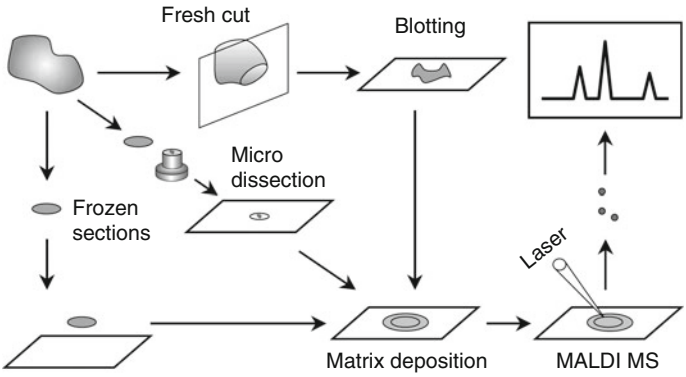

Fig. 11.34 Sample preparation strategies for MALDI imaging of tissues (Reprduced from Ref. [220] with permission. © John Wiley & Sons, Ltd., 2001)

Images are then obtained by extracting ionic abundances of certain m/z or eventually m/z ranges for display. In other words, reconstructed ion chromatograms (Sect. 1.5) are plotted two-dimensionally rather than just along a time axis. Often, color coding is used to simplify the recognition of patterns, e.g., a certain color may represent a certain compound or m/z range, its brightness may reveal the abundance of the compound. It is obvious from this approach that only a few components or compound groups can be displayed in one image at a time. This is why MALDI imaging results are often represented by a set of images each of them composed to highlight a topic of its own (Fig. 11.35). It is furthermore required to correlate the MALDI mass spectral image with the optical image of the sample as obtained by light microscopy immediately before matrix coating.

11.8.2 Instrumentation for MALDI-MSI

MSI instrumentation can be classified according to how ions are generated from the sample, i.e., either by irradiation with a pulsed laser as in MALDI or by bombardment with energetic particles as in SIMS [215]. SIMS uses a continuous particle beam that can be precisely focused, and thus, SIMS can deliver images offering a spatial resolution in the order of 100 nm, however, at the cost of fragmentation upon impact of the energetic particles. The lateral resolution of MALDI imaging is generally limited by both the laser focus and even more so by the homogeneity of the matrix coating. MALDI-MSI yields a lateral resolution of about 20 µm, but may resolve down to 5 µm in fortunate cases. As an advantage over SIMS, MALDI-TOF can access an essentially unlimited m/z range [215]. Most recently, a record of 1.4 µm lateral resolution has been achieved with an atmospheric pressure MALDI source [223].

While a few years back it took 4–12 h to acquire a MALDI image, an optimized imaging system like the Bruker rapifleX MALDI tissuetyper can collect the same amount of spectral data in about 1 h. To achieve this, the instrument has a dedicated laser optical system to allow for quick scanning of the sample surface and it

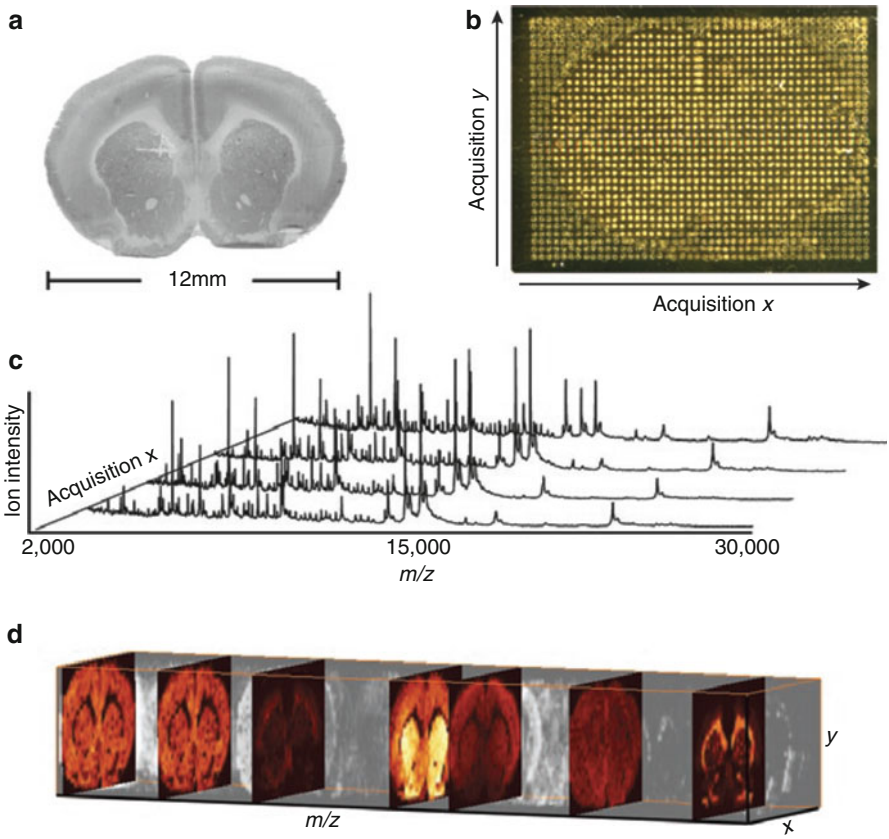

Fig. 11.35 Conceptual overview of MALDI imaging. (**a**) Freshly cut tissue section (here: mouse brain); (**b**) mounted section after application of matrix, here by a robotic picoliter volume spotter; (**c**) partial series of mass spectra along the *x*-axis of the sample; (**d**) three-dimensional volumetric plot of the complete dataset with selected *m*/*z* ranges per image (Reproduced from Ref. [215] with permission. © Nature Publishing Group, 2007)

operates a frequency tripled Nd:Yag laser at 10 kHz. Different from older approaches, the laser is set to deliver a 5 µm spot size and the lateral resolution of the intended image is then determined by setting the array size of the surface that is to be collected to yield data for one pixel of the MALDI image (Fig. 11.36) [224].

Even nowadays, with terabyte-capacities for data storage, MALDI-MSI presents a challenge in terms of data handling, because an array of 256 by 256 dots yields 65536 spectra. Assuming 2 MB of data per MALDI spectrum, such an image requires about 128 GB of hard disk storage. As an advantage, the data can retrospectively be interrogated for any *m*/*z* that turns out to be of interest.

It should also be noted that collecting such a large number of spectra goes along with a need for frequent ion source cleaning (up to daily) and with occasional replacement of the solid state laser.

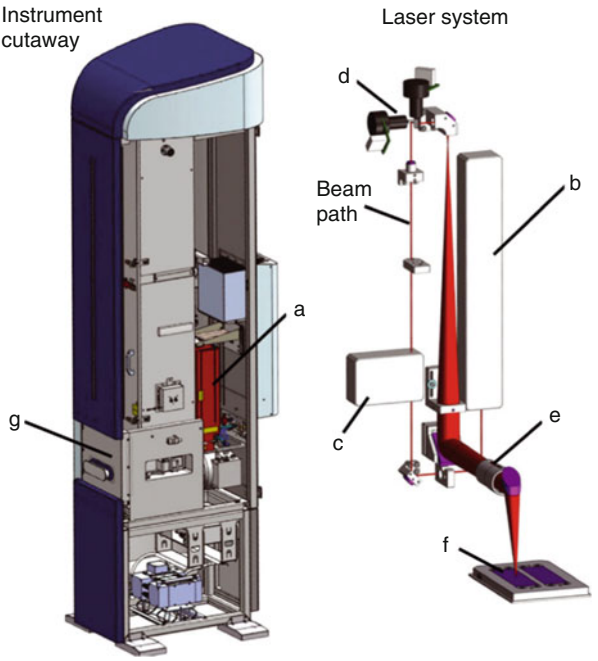

Fig. 11.36 Schematic of the RapifleX MALDI Tissuetyper instrument and its laser system employing two rotating mirrors. The laser system is mounted onto the flight tube as an enclosed box (**a**) containing the major optical elements. The beam is routed from the beam source (**b**) through the attenuator (**c**) onto the rotating mirrors (**d**) which allow fast and precise positioning of the laser spot. The laser is then focused (**e**) onto the target plate (**f**) inside the instruments source (**g**) (Adapted from Ref. [224] with permission. © Wiley, 2015)

11.8.3 Applications of MALDI-MSI

MALDI-MSI has a wide range of applications with an emphasis on intact tissue analysis. In analogy to MALDI biotyping, the field of MALDI-MSI tissuetyping has evolved. While the spectral information may be exactly the same, the imaging approach additionally delivers detailed information on the lateral distribution of the compounds of interest. An example of a MALDI image of tissue has already been shown (Fig. 11.35), another one is provided below (Fig. 11.37). The majority of MALDI-MSI applications certainly is in the life sciences and pharmaceutical development as it permits to track drugs and metabolites across organs and tissue regions [225–227].

MALDI imaging of fingerprints has evolved as an important tool in forensic science [228, 229]. In addition to an optical image of a fingerprint, the MALDI imaging approach enables to selectively interrogate fingerprint for compound classes. While the lipids image basically reflects the conventional fingerprint, MALDI offers enhanced levels of detection [228–230]. Further, MALDI-MSI enables the analysis of proteins from blood stains [231], traces of medication or illicit drugs [232], and other target compounds that may be of interest in a specific case [25].

Fingerprint MALDI images Ungroomed fingerprints obtained from different surfaces including glass, metal, wood, plastic, and leather were recovered and subjected to MALDI imaging. Rather than using conventional TiO_2 powder, the contrast-enhancing dusting was performed using CHCA matrix [228]. Then MALDI images were collected and reconstructed ion currents were plotted for selected compounds such as m/z 118 as marker of an endogenous amino acid (valine), m/z 283 for an endogenous fatty acid (oleic acid), and m/z 304 for

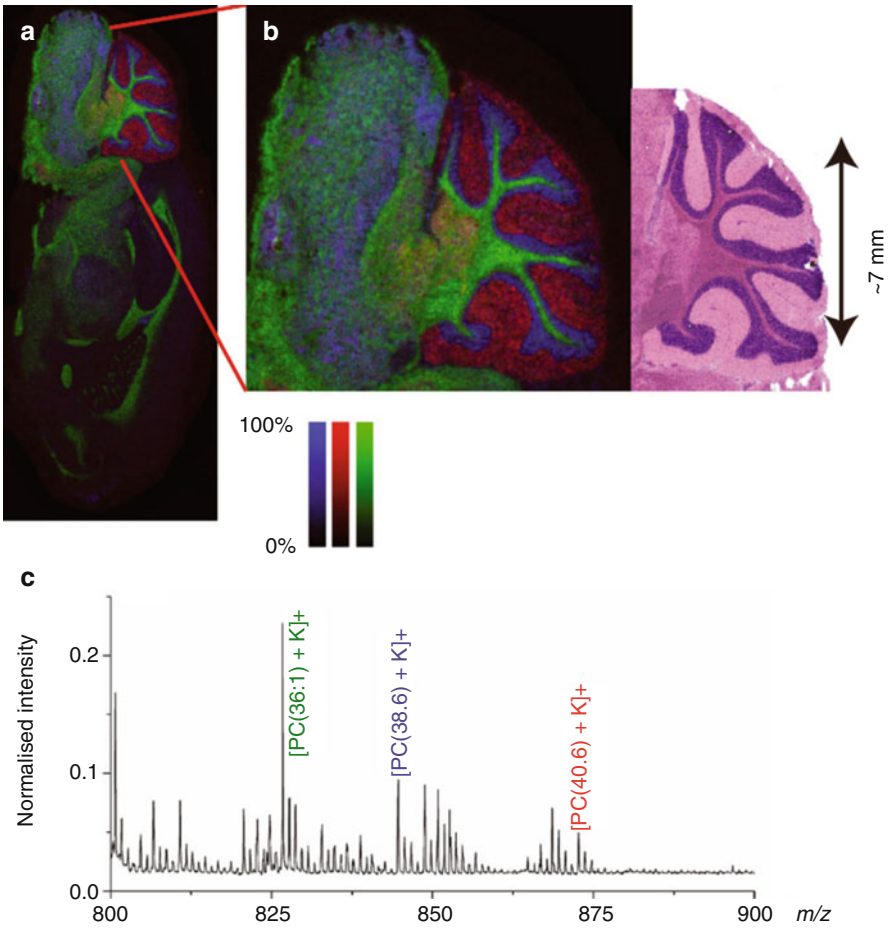

Fig. 11.37 (**a**) Positive-ion images of phosphatidylcholines (PC) in cerebellum tissue. Compounds $[PC(40:6) + K]^+$, $[PC(38:6) + K]^+$, and $[PC(36:1) + K]^+$ were observed at *m/z* 972, 844, and 826 and shown in *red*, *blue*, and *green*, respectively, acquired with a 20 × 20 μm raster. This image contained 181,723 pixels. (**b**) Enlarged region showing the complementary distributions of these ions in the cerebellum. The corresponding microscopic image of the stained section is shown on the right. (**c**) Overall average on tissue spectrum (Reproduced from Ref. [224] with permission. © Wiley, 2015)

dimethylbenzylammonium ion (DBA) as an exogenous compound (Fig. 11.38). It should be noted that, for ease of comparison with the dusted optical images, MALDI images were flipped left to right.

More than just nice pictures

Clearly, MALDI imaging provides pictures that often have esthetic appeal and may even have artistic quality. No wonder that such material is often showcased during conferences and company presentations. The preceding

(continued)

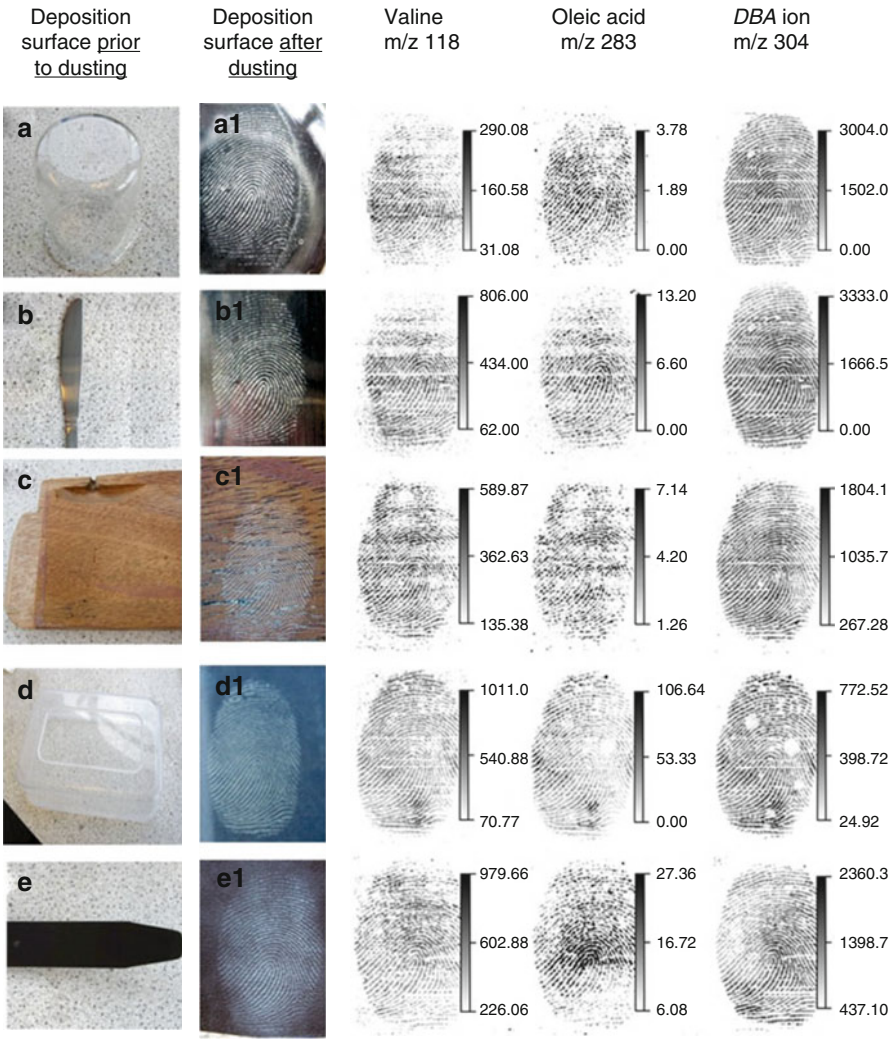

Fig. 11.38 Recovery and MALDI MSI analysis of ungroomed fingerprints obtained from (**a**) glass, (**b**) metal, (**c**) wood, (**d**) plastic, and (**e**) leather. MALDI images of three selected compounds are shown on the right of each fingerprint (Reproduced from Ref. [228] with permission. © American Chemical Society, 2011)

section should also have pointed out that these pictures are connected to a wealth of analytical information as each pixel is backed up by a complete mass spectrum. It is just not possible to depict all this information in a single picture. Typically, they display spatial distributions of a few selected compounds in a color-coded fashion; one would have to generate large numbers of them to address every possible facet of such a data set.

11.9 Atmospheric Pressure MALDI

In *atmospheric pressure MALDI* (AP-MALDI) the MALDI process takes place in dry nitrogen gas under atmospheric pressure. The desorbed ions are then transferred into the vacuum of the mass analyzer by means of an *atmospheric pressure ionization* (API) interface which is provided by any electrospray ionization (ESI, Chap. 12) interface. AP-MALDI was first presented in combination with an orthogonal acceleration TOF (oaTOF, Sect. 4.2.8) analyzer where the original ESI ion interface was modified to accommodate a MALDI target plus a laser light source instead of the ESI spray capillary [233]. While the coherence of the laser light is preserved in vacuum MALDI, the use of an optical fiber to guide the light from the laser to the sample layer results in a loss of coherence.

AP-MALDI has been adapted to a quadrupole ion trap (QIT, Sect. 4.6) [234] where an improved design was realized by extending the heated transfer capillary of a Finnigan LCQ ion trap instrument toward the MALDI target. Thus, a multi-sample target on an *xy*-movable target holder and observation optics could be incorporated on the atmospheric pressure side (Fig. 11.39) [235]. The entrance of the capillary extender is held at 1.5–3 kV to attract the ions from the target surface located about 2 mm away. Based on this development, AP-MALDI can now also be attached to QIT, LIT, Q-TOF, and Orbitrap analyzers.

Compared to vacuum MALDI, AP-MALDI has a larger tolerance to laser fluence variations and exhibits reduced fragmentation due to the collisional cooling of the expanding plume. As a result of this cooling process, clustering between

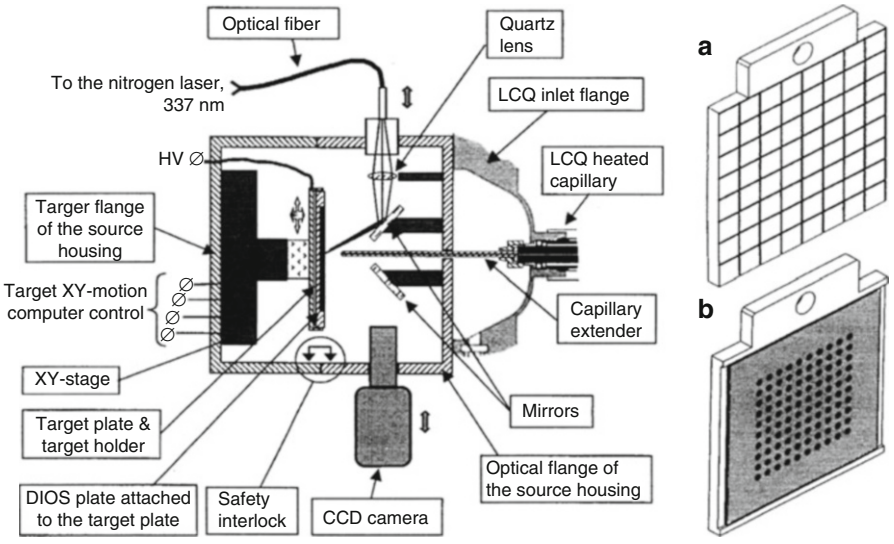

Fig. 11.39 AP-MALDI ion source with extended transfer capillary. *Insets*: (**a**) the target holder can be equipped with a 64-spot MALDI target or (**b**) a 10 × 10-spot DIOS chip (Adapted from Ref. [205] by permission. © John Wiley & Sons, 2002)

matrix and analyte ions is more pronounced. Declustering can be achieved by employing higher laser fluences or adapting the parameters of the atmospheric pressure interface [236].

AP-MALDI presents an add-on to any instrument with atmospheric pressure interface, i.e., mass spectrometers with ESI, APCI, or APPI source can also accommodate an AP-MALDI source. The limit of detection (LOD) of vacuum MALDI is 5–10 fold lower than in AP-MALDI and the laser threshold fluence is about 1.5 fold lower in vacuum MALDI compared to AP-MALDI (Fig. 11.40) [237]. Thus, AP-MALDI can increase the versatility of mass spectrometers without sacrificing too much performance.

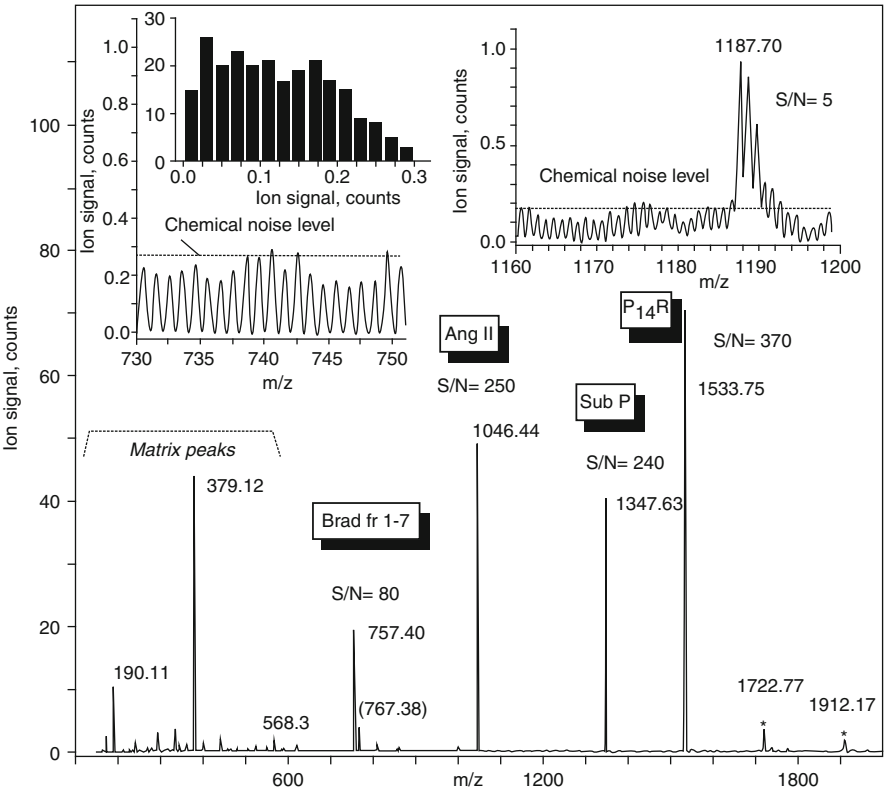

Fig. 11.40 AP-MALDI spectrum of four synthetic peptides in CHCA as obtained in a 1-min scan of a spot containing 300 fmol of bradykinin fr. 1–7 (*m/z* 757), 100 fmol of angiotensin II (*m/z* 1046), 100 fmol of $P_{14}R$ (*m/z* 1534), and 50 fmol of substance P (*m/z* 1348). Single and double matrix adducts of $P_{14}R$ are indicated by *asterisks* (*m/z* 1723, 1912). Note the doubly charged ion of $P_{14}R$ at *m/z* 767. *Inserts* show representative patterns of chemical noise in the vicinity of bradykinin and angiotensin II. The *left insert* also shows the histogram for the chemical noise signal. The *insert on the right* shows a peptide contaminant with the intensity slightly above the limit of detection (Reproduced from Ref. [237] with permission. © Elsevier, 2016)

11.10 Essentials of MALDI

Basic Principle
Laser desorption/ionization (LDI) and matrix-assisted laser desorption/ionization (MALDI) rely on the absorption of energy from light by a thin crystalline layer of sample or sample–matrix mixture, respectively. The laser may be of infrared (IR) or ultraviolet (UV) wavelength; UV lasers are by far most common. The uptake of energy from a large number of photons irradiated within several nanoseconds locally leads to the formation of a plasma. Depending on the actual analyte–matrix combination, ionization occurs via different channels such as multi-photonionization, charge transfer, protonation or deprotonation, addition of cations or anions, or electron capture. MALDI generally yields singly charged ions.

Sample Preparation and Measurement
For LDI, the analyte is preferably provided as dilute solution, about 1 µl of which is applied onto a (stainless steel) sample plate and allowed to dry.

For MALDI, a dilute sample solution (0.01–1.0 mg ml^{-1}) is admixed to an excess of matrix solution (ca. 10 mg ml^{-1}) as to achieve an analyte-to-matrix ratio preferably in the range of 1:1000 to 1:10,000. About 1 µl of the combined solutions is then pipetted onto a sample plate, allowed to dry, and crystallize.

Thin layers of homogenously distributed microcrystals are preferred for good shot-to-shot reproducibility, and thus, high mass resolution and accuracy. The laser fluence is adjusted slightly above threshold for ion formation. Individual spectra by thousands of laser shots are accumulated to yield the final MALDI spectrum.

Sample Consumption and Detection Limit
In MALDI-MS, the combination of the actual analyte, the selection of the matrix, and the procedure of sample preparation essentially represent the limiting factors for sample consumption and detection limit.

The minimum sample load or the detection limit is usually specified instead of sensitivity. Sample loads of 1 fmol of a protein can normally be achieved. As thousands of single-shot spectra can be obtained from one preparation spread over some square millimeters, the sample consumption has been estimated to approximate 10^{-17} mol per laser shot, i.e., normally more than 99% of the sample can theoretically be recovered from the target. Improved ion extraction and detection as well as miniaturized sample preparation, e.g., by means of the anchor target technology, can provide attomole detection limits for peptides.

Analytes for MALDI
For standard MALDI sample preparation, the analyte should be soluble to about 0.1 mg ml^{-1} in some solvent. If an analyte is completely insoluble, solvent-free sample preparation may alternatively be applied (Sect. 11.4.3). The analyte may be medium polar to highly polar, neutral or ionic. Nonpolar compounds are hardest to analyze. Solutions containing metal salts, e.g., from buffers or excess of

Table 11.5 Ions formed by LDI and MALDI

Analytes	Positive ions	Negative ions
Nonpolar	$M^{+\bullet}$, $[M + Ag]^+$, $[M + Cs]^+$ [a]	$M^{-\bullet}$
Medium polarity	$M^{+\bullet}$ and/or $[M + H]^+$, $[M + alkali]^+$, {*clusters* $[2M]^{+\bullet}$ and/or $[2M + H]^+$, $[2M + alkali]^+$, *adducts* $[M + Ma + H]^+$, $[M + Ma + alkali]^+$}[c]	$M^{-\bullet}$ and/or $[M - H]^-$, {*clusters* $[2M]^{-\bullet}$ and/or $[2M - H]^-$*adducts* $[M + Ma]^{-\bullet}$, $[M + Ma - H]^-$}
Polar	$[M + H]^+$, $[M + alkali]^+$, *exchange* $[M - H_n + alkali_{n+1}]^+$ *high-mass anal.* $[M + 2H]^{2+}$, $[M + 2alkali]^{2+}$ {*clusters* $[nM + H]^+$, $[nM + alkali]^+$, *adducts* $[M + Ma + H]^+$, $[M + Ma + alkali]^+$}	$[M - H]^-$, *exchange* $[M - H_n + alkali_{n-1}]^-$ {*clusters* $[nM - H]^-$ *adducts* $[M + Ma - H]^-$}
Ionic [b]	C^+, $[C_n + A_{n-1}]^+$, $\{[CA]^{+\bullet}\}$	A^-, $[C_{n-1} + A_n]^-$, $\{[CA]^{-\bullet}\}$

[a]Silver and cesium ions can serve as a workaround for nonpolar analytes
[b]Comprising of cation C^+ and anion A^-
[c]Braces denote rarely observed species

noncomplexed metals, may cause a confusingly large number of signals due to multiple proton/metal exchange and adduct ion formation; even complete suppression of the analyte can occur.

The mass range of MALDI is theoretically almost unlimited; in practice, limits strongly depend on the compound class to be analyzed.

Types of Ions in LDI and MALDI

LDI and MALDI produce a variety of ions depending on the polarity of the analyte, its ionization energy, the characteristics of the matrix (if any) and on the presence or absence of impurities such as alkali metal ions [20, 36, 37]. The tendency to form radical ions is somewhat lower than in case of FAB/LSIMS (Table 11.5).

Mass Analyzers for MALDI-MS

Laser desorption intrinsically is a pulsed ionization process, which is therefore ideally combined with time-of-flight (TOF) analyzers (Sect. 4.2) [17, 56]. Ever since the first MALDI experiments, MALDI and TOF have been forming a unit, and the majority of MALDI applications are MALDI-TOF measurements. Vice versa, it was the success of MALDI that pushed forth the tremendous delevopment of TOF mass analyzers. More recently, MALDI has also been adapted to orthogonal acceleration TOF analyzers [238].

Fourier transform ion cyclotron resonance (FT-ICR, Sect. 4.7) can be used in combination with an external ion source [239], and thus, MALDI-FT-ICR has become a mature combination [240, 241]. Modern MALDI-FT-ICR instruments make use of collisional cooling of the plasma plume before transferring the ions into the ICR cell [242, 243].

AP-MALDI may be attached to any instrument with an atmospheric pressure ionization interface.

References

1. Fenner NC, Daly NR (1966) Laser Used for Mass Analysis. Rev Sci Instrum 37:1068–1070. doi:10.1063/1.1720410
2. Vastola FJ, Pirone AJ (1968) Ionization of Organic Solids by Laser Irradiation. Adv Mass Spectrom 4:107–111
3. Vastola FJ, Mumma RO, Pirone AJ (1970) Analysis of Organic Salts by Laser Ionization. Org Mass Spectrom 3:101–104. doi:10.1002/oms.1210030112
4. Posthumus MA, Kistemaker PG, Meuzelaar HLC, Ten Noever de Brauw MC (1978) Laser Desorption-Mass Spectrometry of Polar Nonvolatile Bio-Organic Molecules. Anal Chem 50:985–991. doi:10.1021/ac50029a040
5. Wilkins CL, Weil DA, Yang CLC, Ijames CF (1985) High Mass Analysis by Laser Desorption Fourier Transform Mass Spectrometry. Anal Chem 57:520–524. doi:10.1021/ac50001a046
6. Coates ML, Wilkins CL (1985) Laser Desorption Fourier Transform Mass Spectra of Malto-Oligosaccharides. Biomed Mass Spectrom 12:424–428. doi:10.1002/bms.1200120812
7. Macfarlane RD (1999) Mass Spectrometry of Biomolecules: From PDMS to MALDI. Brazilian J Phys 29:415–421. doi:10.1590/S0103-97331999000300003
8. Tanaka K, Waki H, Ido Y, Akita S, Yoshida Y, Yhoshida T (1988) Protein and Polymer Analyses Up to *M*/*z* 100,000 by Laser Ionization Time-of-Flight Mass Spectrometry. Rapid Commun Mass Spectrom 2:151–153. doi:10.1002/rcm.1290020802
9. Tanaka K (2003) The Origin of Macromolecule Ionization by Laser Irradiation (Nobel Lecture). Angew Chem Int Ed 42:3861–3870. doi:10.1002/anie.200300585
10. Karas M, Bachmann D, Hillenkamp F (1985) Influence of the Wavelength in High-Irradiance Ultraviolet Laser Desorption Mass Spectrometry of Organic Molecules. Anal Chem 57:2935–2939. doi:10.1021/ac00291a042
11. Karas M, Bachmann D, Bahr U, Hillenkamp F (1987) Matrix-Assisted Ultraviolet Laser Desorption of Non-Volatile Compounds. Int J Mass Spectrom Ion Proc 78:53–68. doi:10.1016/0168-1176(87)87041-6
12. Karas M, Hillenkamp F (1988) Laser Desorption Ionization of Proteins with Molecular Masses Exceeding 10,000 Daltons. Anal Chem 60:2299–2301. doi:10.1021/ac00171a028
13. Karas M, Bahr U, Ingendoh A, Hillenkamp F (1989) Laser-Desorption Mass Spectrometry of 100,000–250,000-Dalton Proteins. Angew Chem Int Ed 28:760–761. doi:10.1002/anie.198907601
14. Karas M, Ingendoh A, Bahr U, Hillenkamp F (1989) Ultraviolet-Laser Desorption/Ionization Mass Spectrometry of Femtomolar Amounts of Large Proteins. Biomed Environ Mass Spectrom 18:841–843. doi:10.1002/bms.1200180931
15. Hillenkamp F, Peter-Katalinic J (eds) (2007) MALDI-MS. A Practical Guide to Instrumentation, Methods and Applications. Wiley-VCH, Weinheim
16. Karas M, Bahr U, Gießmann U (1991) Matrix-Assisted Laser Desorption Ionization Mass Spectrometry. Mass Spectrom Rev 10:335–357. doi:10.1002/mas.1280100503
17. Hillenkamp F, Karas M, Beavis RC, Chait BT (1991) Matrix-Assisted Laser Desorption/Ionization Mass Spectrometry of Biopolymers. Anal Chem 63:1193A–1203A. doi:10.1021/ac00024a716
18. Beavis RC (1992) Matrix-Assisted Ultraviolet Laser Desorption: Evolution and Principles. Org Mass Spectrom 27:653–659. doi:10.1002/oms.1210270602
19. Hillenkamp F, Karas M (2000) Matrix-Assisted Laser Desorption/Ionisation, an Experience. Int J Mass Spectrom 200:71–77. doi:10.1016/S1387-3806(00)00300-6
20. Lehmann WD (1996) Massenspektrometrie in der Biochemie. Spektrum Akademischer Verlag, Heidelberg
21. Cotter RJ (1997) Time-of-Flight Mass Spectrometry: Instrumentation and Applications in Biological Research. American Chemical Society, Washington, DC

22. Siuzdak G (2006) The Expanding Role of Mass Spectrometry in Biotechnology. MCC Press, San Diego
23. Cole RB (ed) (2010) Electrospray and MALDI Mass Spectrometry: Fundamentals, Instrumentation, Practicalities, and Biological Applications. Wiley, Hoboken
24. Hillenkamp F, Peter-Katalinic J (eds) (2013) MALDI MS: A Practical Guide to Instrumentation, Methods and Applications. Wiley-VCH, Weinheim
25. Cramer R (ed) (2016) Advances in MALDI and Laser-Induced Soft Ionization Mass Spectrometry. Springer, Cham. doi:10.1007/978-3-319-04819-2
26. Montaudo G, Lattimer RP (eds) (2001) Mass Spectrometry of Polymers. CRC Press, Boca Raton
27. Murgasova R, Hercules DM (2003) MALDI of Synthetic Polymers – An Update. Int J Mass Spectrom 226:151–162. doi:10.1016/S1387-3806(02)00971-5
28. Mamyrin BA (1994) Laser Assisted Reflectron Time-of-Flight Mass Spectrometry. Int J Mass Spectrom Ion Proc 131:1–19. doi:10.1016/0168-1176(93)03891-O
29. Dreisewerd K, Schürenberg M, Karas M, Hillenkamp F (1995) Influence of the Laser Intensity and Spot Size on the Desorption of Molecules and Ions in Matrix-Assisted Laser Desorption/Ionization with a Uniform Beam Profile. Int J Mass Spectrom Ion Proc 141:127–148. doi:10.1016/0168-1176(94)04108-J
30. Nordhoff E, Ingendoh A, Cramer R, Overberg A, Stahl B, Karas M, Hillenkamp F, Crain PF (1992) Matrix-Assisted Laser Desorption/Ionization Mass Spectrometry of Nucleic Acids with Wavelengths in the Ultraviolet and Infrared. Rapid Commun Mass Spectrom 6:771–776. doi:10.1002/rcm.1290061212
31. Overberg A, Karas M, Bahr U, Kaufmann R, Hillenkamp F (1990) Matrix-Assisted Infrared-Laser (2.94 μm) Desorption/Ionization Mass Spectrometry of Large Biomolecules. Rapid Commun Mass Spectrom 4:293–296. doi:10.1002/rcm.1290040808
32. Overberg A, Karas M, Hillenkamp F (1991) Matrix-Assisted Laser Desorption of Large Biomolecules with a TEA-CO_2-Laser. Rapid Commun Mass Spectrom 5:128–131. doi:10.1002/rcm.1290050308
33. Berkenkamp S, Menzel C, Hillenkamp F, Dreisewerd K (2002) Measurements of Mean Initial Velocities of Analyte and Matrix Ions in Infrared Matrix-Assisted Laser Desorption Ionization Mass Spectrometry. J Am Soc Mass Spectrom 13:209–220. doi:10.1016/S1044-0305(01)00355-5
34. Zenobi R, Knochenmuss R (1999) Ion Formation in MALDI Mass Spectrometry. Mass Spectrom Rev 17:337–366. doi:10.1002/(SICI)1098-2787(1998)17:5<337::AID-MAS2>3.0.CO;2-S
35. Menzel C, Dreisewerd K, Berkenkamp S, Hillenkamp F (2001) Mechanisms of Energy Deposition in Infrared Matrix-Assisted Laser Desorption/Ionization Mass Spectrometry. Int J Mass Spectrom 207:73–96. doi:10.1016/S1387-3806(01)00363-3
36. Dreisewerd K, Berkenkamp S, Leisner A, Rohlfing A, Menzel C (2003) Fundamentals of Matrix-Assisted Laser Desorption/Ionization Mass Spectrometry with Pulsed Infrared Lasers. Int J Mass Spectrom 226:189–209. doi:10.1016/S1387-3806(02)00977-6
37. Dreisewerd K (2003) The Desorption Process in MALDI. Chem Rev 103:395–425. doi:10.1021/cr010375i
38. Karas M, Krüger R (2003) Ion Formation in MALDI: The Cluster Ionization Mechanism. Chem Rev 103:427–439. doi:10.1021/cr010376a
39. Dreisewerd K (2014) Recent Methodological Advances in MALDI Mass Spectrometry. Anal Bioanal Chem 406:2261–2278. doi:10.1007/s00216-014-7646-6
40. Westmacott G, Ens W, Hillenkamp F, Dreisewerd K, Schürenberg M (2002) The Influence of Laser Fluence on Ion Yield in Matrix-Assisted Laser Desorption Ionization Mass Spectrometry. Int J Mass Spectrom 221:67–81. doi:10.1016/S1387-3806(02)00898-9
41. Menzel C, Dreisewerd K, Berkenkamp S, Hillenkamp F (2002) The Role of the Laser Pulse Duration in Infrared Matrix-Assisted Laser Desorption/Ionization Mass Spectrometry. J Am Soc Mass Spectrom 13:975–984. doi:10.1016/S1044-0305(02)00397-5

42. Juhasz P, Vestal ML, Martin SA (1997) On the Initial Velocity of Ions Generated by Matrix-Assisted Laser Desorption Ionization and Its Effect on the Calibration of Delayed Extraction Time-of-Flight Mass Spectra. J Am Soc Mass Spectrom 8:209–217. doi:10.1016/S1044-0305(96)00256-5
43. Karas M, Bahr U, Fournier I, Glückmann M, Pfenninger A (2003) The Initial Ion Velocity as a Marker for Different Desorption-Ionization Mechanisms in MALDI. Int J Mass Spectrom 226:239–248. doi:10.1016/S1387-3806(02)01062-X
44. Horneffer V, Dreisewerd K, Ludemann H-C, Hillenkamp F, Lage M, Strupat K (1999) Is the Incorporation of Analytes into Matrix Crystals a Prerequisite for Matrix-Assisted Laser Desorption/Ionization Mass Spectrometry? A Study of Five Positional Isomers of Dihydroxybenzoic Acid. Int J Mass Spectrom 185(186/187):859–870. doi:10.1016/S1387-3806(98)14218-5
45. Glückmann M, Pfenninger A, Krüger R, Thierolf M, Karas M, Horneffer V, Hillenkamp F, Strupat K (2001) Mechanisms in MALDI Analysis: Surface Interaction or Incorporation of Analytes? Int J Mass Spectrom 210(211):121–132. doi:10.1016/S1387-3806(01)00450-X
46. Karas M, Gluckmann M, Schäfer J (2000) Ionization in Matrix-Assisted Laser Desorption/Ionization: Singly Charged Molecular Ions Are the Lucky Survivors. J Mass Spectrom 35:1–12. doi:10.1002/(SICI)1096-9888(200001)35:1<1::AID-JMS904>3.0.CO;2-0
47. Ens W, Mao Y, Mayer F, Standing KG (1991) Properties of Matrix-Assisted Laser Desorption. Measurements with a Time-to-Digital Converter. Rapid Commun Mass Spectrom 5:117–123. doi:10.1002/rcm.1290050306
48. Medina N, Huth-Fehre T, Westman A, Sundqvist BUR (1994) Matrix-Assisted Laser Desorption: Dependence of the Threshold Fluence on Analyte Concentration. Org Mass Spectrom 29:207–209. doi:10.1002/oms.1210290410
49. Quist AP, Huth-Fehre T, Sundqvist BUR (1994) Total Yield Measurements in Matrix-Assisted Laser Desorption Using a Quartz Crystal Microbalance. Rapid Commun Mass Spectrom 8:149–154. doi:10.1002/rcm.1290080204
50. Beavis RC, Chait BT (1989) Factors Affecting the Ultraviolet Laser Desorption of Proteins. Rapid Commun Mass Spectrom 3:233–237. doi:10.1002/rcm.1290030708
51. Ingendoh A, Karas M, Hillenkamp F, Giessmann U (1994) Factors Affecting the Resolution in Matrix-Assisted Laser Desorption-Ionization Mass Spectrometry. Int J Mass Spectrom Ion Proc 131:345–354. doi:10.1016/0168-1176(93)03873-K
52. Aksouh F, Chaurand P, Deprun C, Della-Negra S, Hoyes J, Le Beyec Y, Pinho RR (1995) Influence of the Laser Beam Direction on the Molecular Ion Ejection Angle in Matrix-Assisted Laser Desorption/Ionization. Rapid Commun Mass Spectrom 9:515–518. doi:10.1002/rcm.1290090609
53. Liao P-C, Allison J (1995) Dissecting Matrix-Assisted Laser Desorption/Ionization Mass Spectra. J Mass Spectrom 30:763–766. doi:10.1002/jms.1190300517
54. Strupat K, Karas M, Hillenkamp F (1991) 2,5-Dihydroxybenzoic Acid: A New Matrix for Laser Desorption-Ionization Mass Spectrometry. Int J Mass Spectrom Ion Proc 111:89–102. doi:10.1016/0168-1176(91)85050-V
55. Holle A, Haase A, Kayser M, Hoehndorf J (2006) Optimizing UV Laser Focus Profiles for Improved MALDI Performance. J Mass Spectrom 41:705–716. doi:10.1002/jms.1041
56. Cotter RJ (1987) Laser Mass Spectrometry: An Overview of Techniques, Instruments and Applications. Anal Chim Acta 195:45–59. doi:10.1016/S0003-2670(00)85648-2
57. Pan Y, Cotter RJ (1992) Measurement of Initial Translational Energies of Peptide Ions in Laser Desorption/Ionization Mass Spectrometry. Org Mass Spectrom 27:3–8. doi:10.1002/oms.1210270103
58. Glückmann M, Karas M (1999) The Initial Ion Velocity and Its Dependence on Matrix, Analyte and Preparation Method in Ultraviolet Matrix-Assisted Laser Desorption/Ionization. J Mass Spectrom 34:467–477. doi:10.1002/(SICI)1096-9888(199905)34:5<467::AID-JMS809>3.0.CO;2-8

59. Puretzky AA, Geohegan DB, Hurst GB, Buchanan MV, Luk'yanchuk BS (1999) Imaging of Vapor Plumes Produced by Matrix Assisted Laser Desorption: A Plume Sharpening Effect. Phys Rev Lett 83:444–447. doi:10.1103/PhysRevLett.83.444
60. Leisner A, Rohlfing A, Berkenkamp S, Röhling U, Dreisewerd K, Hillenkamp F (2003) IR-MALDI with the Matrix Glycerol: Examination of the Plume Expansion Dynamics for Lasers of Different Pulse Duration. 36. DGMS Jahrestagung: Poster
61. Leisner A, Rohlfing A, Roehling U, Dreisewerd K, Hillenkamp F (2005) Time-Resolved Imaging of the Plume Dynamics in Infrared Matrix-Assisted Laser Desorption/Ionization with a Glycerol Matrix. J Phys Chem B 109:11661–11666. doi:10.1021/jp0509941
62. Chen LC, Rahman MM, Hiraoka K (2014) Super-Atmospheric Pressure Ion Sources: Application and Coupling to API Mass Spectrometer. Mass Spectrom 3:S0024. doi:10.5702/massspectrometry.S0024
63. Wang BH, Dreisewerd K, Bahr U, Karas M, Hillenkamp F (1993) Gas-Phase Cationization and Protonation of Neutrals Generated by Matrix-Assisted Laser Desorption. J Am Soc Mass Spectrom 4:393–398. doi:10.1016/1044-0305(93)85004-H
64. Liao P-C, Allison J (1995) Ionization Processes in Matrix-Assisted Laser Desorption/Ionization Mass Spectrometry: Matrix-Dependent Formation of $[M+H]^+$ Vs. $[M+Na]^+$ Ions of Small Peptides and Some Mechanistic Comments. J Mass Spectrom 30:408–423. doi:10.1002/jms.1190300304
65. Gimon ME, Preston LM, Solouki T, White MA, Russel DH (1992) Are Proton Transfer Reactions of Excited States Involved in UV Laser Desorption Ionization? Org Mass Spectrom 27:827–830. doi:10.1002/oms.1210270711
66. Juhasz P, Costello CE (1993) Generation of Large Radical Ions from Oligometallocenes by Matrix-Assisted Laser Desorption Ionization. Rapid Commun Mass Spectrom 7:343–351. doi:10.1002/rcm.1290070508
67. Lidgard RO, McConnell BD, Black DSC, Kumar N, Duncan MW (1996) Fragmentation Observed in Continuous Extraction Linear MALDI: A Cautionary Note. J Mass Spectrom 31:1443–1445. doi:10.1002/(SICI)1096-9888(199612)31:12<1443::AID-JMS448>3.0.CO;2-J
68. Irngartinger H, Weber A (1996) Twofold Cycloaddition of [60]Fullerene to a Bifunctional Nitrile Oxide. Tertrahedron Lett 37:4137–4140. doi:10.1016/0040-4039(96)00779-4
69. Gromov A, Ballenweg S, Giesa S, Lebedkin S, Hull WE, Krätschmer W (1997) Preparation and Characterization of C_{119}. Chem Phys Lett 267:460–466. doi:10.1016/S0009-2614(97)00129-2
70. Giesa S, Gross JH, Hull WE, Lebedkin S, Gromov A, Krätschmer W, Gleiter R (1999) C_{120}OS: The First Sulfur-Containing Dimeric [60]Fullerene Derivative. Chem Commun:465–466. doi:10.1039/a809831j
71. Juhasz P, Costello CE, Biemann K (1993) Matrix-Assisted Laser Desorption Ionization Mass Spectrometry with 2-(4-Hydroxyphenylazo)benzoic acid Matrix. J Am Soc Mass Spectrom 4:399–409. doi:10.1016/1044-0305(93)85005-I
72. Hopwood FG, Michalak L, Alderdice DS, Fisher KJ, Willett GD (1994) C_{60}-Assisted Laser Desorption/Ionization Mass Spectrometry in the Analysis of Phosphotungstic Acid. Rapid Commun Mass Spectrom 8:881–885. doi:10.1002/rcm.1290081105
73. Jones RM, Lamb JH, Lim CK (1995) 5,10,15,20-*Meso*-Tetra(hydroxyphenyl)-chlorin as a Matrix for the Analysis of Low Molecular Weight Compounds by Matrix-Assisted Laser Desorption/Ionization Time-of-Flight Mass Spectrometry. Rapid Commun Mass Spectrom 9:968–969. doi:10.1002/rcm.1290091020
74. Armstrong DW, Zhang LK, He L, Gross ML (2001) Ionic Liquids As Matrixes for Matrix-Assisted Laser Desorption/Ionization Mass Spectrometry. Anal Chem 73:3679–3686. doi:10.1021/ac010259f
75. Li YL, Gross ML (2004) Ionic-Liquid Matrices for Quantitative Analysis by MALDI-TOF Mass Spectrometry. J Am Soc Mass Spectrom 15:1833–1837. doi:10.1016/j.jasms.2004.08.011

76. Tang K, Taranenko NI, Allman SL, Chen CH, Chang LY, Jacobson KB (1994) Picolinic Acid as a Matrix for Laser Mass Spectrometry of Nucleic Acids and Proteins. Rapid Commun Mass Spectrom 8:673–677. doi:10.1002/rcm.1290080902
77. Wu KJ, Steding A, Becker CH (1993) Matrix-Assisted Laser Desorption Time-of-Flight Mass Spectrometry of Oligonucleotides Using 3-Hydroxypicolinic Acid as an Ultraviolet-Sensitive Matrix. Rapid Commun Mass Spectrom 7:142–146. doi:10.1002/rcm.1290070206
78. Taranenko NI, Tang K, Allman SL, Ch'ang LY, Chen CH (1994) 3-Aminopicolinic Acid As a Matrix for Laser Desorption Mass Spectrometry of Biopolymers. Rapid Commun Mass Spectrom 8:1001–1006. doi:10.1002/rcm.1290081219
79. Terrier P, Tortajada J, Zin G, Buchmann W (2007) Noncovalent Complexes Between DNA and Basic Polypeptides or Polyamines by MALDI-TOF. J Am Soc Mass Spectrom 18:1977–1989. doi:10.1016/j.jasms.2007.07.028
80. Lecchi P, Le HM, Pannell LK (1995) 6-Aza-2-thiothymine: a Matrix for MALDI Spectra of Oligonucleotides. Nucl Acids Res 23:1276–1277. doi:10.1093/nar/23.7.1276
81. Taranenko NI, Potter NT, Allman SL, Golovlev VV, Chen CH (1999) Gender Identification by Matrix-Assisted Laser Desorption/Ionization Time-of-Flight Mass Spectrometry. Anal Chem 71:3974–3976. doi:10.1021/ac990150w
82. Mohr MD, Börnsen KO, Widmer HM (1995) Matrix-Assisted Laser Desorption/Ionization Mass Spectrometry: Improved Matrix for Oligosaccharides. Rapid Commun Mass Spectrom 9:809–814. doi:10.1002/rcm.1290090919
83. Finke B, Stahl B, Pfenninger A, Karas M, Daniel H, Sawatzki G (1999) Analysis of High-Molecular-Weight Oligosaccharides from Human Milk by Liquid Chromatography and MALDI-MS. Anal Chem 71:3755–3762. doi:10.1021/ac990094z
84. Pfenninger A, Karas M, Finke B, Stahl B, Sawatzki G (1999) Matrix Optimization for Matrix-Assisted Laser Desorption/Ionization Mass Spectrometry of Oligosaccharides from Human Milk. J Mass Spectrom 34:98–104. doi:10.1002/(SICI)1096-9888(199902)34:2<98::AID-JMS767>3.0.CO;2-N
85. Laugesen S, Roepstorff P (2003) Combination of Two Matrices Results in Improved Performance of MALDI MS for Peptide Mass Mapping and Protein Analysis. J Am Soc Mass Spectrom 14:992–1002. doi:10.1016/S1044-0305(03)00262-9
86. Karas M, Ehring H, Nordhoff E, Stahl B, Strupat K, Hillenkamp F, Grehl M, Krebs B (1993) Matrix-Assisted Laser Desorption/Ionization Mass Spectrometry with Additives to 2,5-Dihydroxybenzoic Acid. Org Mass Spectrom 28:1476–1481. doi:10.1002/oms.1210281219
87. Rohmer M, Meyer B, Mank M, Stahl B, Bahr U, Karas M (2010) 3-Aminoquinoline Acting As Matrix and Derivatizing Agent for MALDI MS Analysis of Oligosaccharides. Anal Chem 82:3719–3726. doi:10.1021/ac1001096
88. Stahl B, Thurl S, Zeng J, Karas M, Hillenkamp F, Steup M, Sawatzki G (1994) Oligosaccharides from Human Milk As Revealed by Matrix-Assisted Laser Desorption/Ionization Mass Spectrometry. Anal Biochem 223:218–226. doi:10.1006/abio.1994.1577
89. Metzger JO, Woisch R, Tuszynski W, Angermann R (1994) New Type of Matrix for Matrix-Assisted Laser Desorption Mass Spectrometry of Polysaccharides and Proteins. Fresenius J Anal Chem 349:473–474. doi:10.1007/BF00322937
90. Beavis RC, Chaudhary T, Chait BT (1992) α-Cyano-4-hydroxycinnamic acid As a Matrix for Matrix-Assisted Laser Desorption Mass Spectrometry. Org Mass Spectrom 27:156–158. doi:10.1002/oms.1210270217
91. Ayorinde FO, Elhilo E, Hlongwane C (1999) Matrix-Assisted Laser Desorption/Ionization Time-of-Flight Mass Spectrometry of Canola, Castor and Olive Oils. Rapid Commun Mass Spectrom 13:737–739. doi:10.1002/(SICI)1097-0231(19990430)13:8<737::AID-RCM552>3.0.CO;2-L
92. George M, Wellemans JMY, Cerny RL, Gross ML, Li K, Cavalieri EL (1994) Matrix Design for Matrix-Assisted Laser Desorption Ionization: Sensitive Determination of PAH-DNA Adducts. J Am Soc Mass Spectrom 5:1021–1025. doi:10.1016/1044-0305(94)80021-9

93. Lidgard RO, Duncan MW (1995) Utility of Matrix-Assisted Laser Desorption/Ionization Time-of-Flight Mass Spectrometry for the Analysis of Low Molecular Weight Compounds. Rapid Commun Mass Spectrom 9:128–132. doi:10.1002/rcm.1290090205
94. Soltwisch J, Jaskolla TW, Hillenkamp F, Karas M, Dreisewerd K (2012) Ion Yields in UV-MALDI Mass Spectrometry As a Function of Excitation Laser Wavelength and Optical and Physico-Chemical Properties of Classical and Halogen-Substituted MALDI Matrixes. Anal Chem 84:6567–6576. doi:10.1021/ac3008434
95. Wiegelmann M, Soltwisch J, Jaskolla TW, Dreisewerd K (2013) Matching the Laser Wavelength to the Absorption Properties of Matrices Increases the Ion Yield in UV-MALDI Mass Spectrometry. Anal Bioanal Chem 405:6925–6932. doi:10.1007/s00216-012-6478-5
96. Beavis RC, Chait BT (1989) Cinnamic Acid Derivatives as Matrices for Ultraviolet Laser Desorption Mass Spectrometry of Proteins. Rapid Commun Mass Spectrom 3:432–435. doi:10.1002/rcm.1290031207
97. Montaudo G, Montaudo MS, Puglisi C, Samperi F (1994) 2-(4-Hydroxyphenylazo)benzoic acid: A Solid Matrix for Matrix-Assisted Laser Desorption/Ionization of Polystyrene. Rapid Commun Mass Spectrom 8:1011–1015. doi:10.1002/rcm.1290081221
98. Xu N, Huang ZH, Watson JT, Gage DA (1997) Mercaptobenzothiazoles: A New Class of Matrixes for Laser Desorption Ionization Mass Spectrometry. J Am Soc Mass Spectrom 8:116–124. doi:10.1016/S1044-0305(96)00233-4
99. Pitt JJ, Gorman JJ (1996) Matrix-Assisted Laser Desorption/Ionization Time-of-Flight Mass Spectrometry of Sialylated Glycopeptides and Proteins Using 2,6-Dihydroxyacetophenone as a Matrix. Rapid Commun Mass Spectrom 10:1786–1788. doi:10.1002/(SICI)1097-0231(199611)10:14<1786::AID-RCM751>3.0.CO;2-I
100. Gorman JJ, Ferguson BL, Nguyen TB (1996) Use of 2,6-Dihydroxyacetophenone for Analysis of Fragile Peptides, Disulfide Bonding and Small Proteins by Matrix-Assisted Laser Desorption/Ionization. Rapid Commun Mass Spectrom 10:529–536. doi:10.1002/(SICI)1097-0231(19960331)10:5<529::AID-RCM522>3.0.CO;2-9
101. Meyer A, Spinelli N, Imbach JL, Vasseur J-J (2000) Analysis of Solid-Supported Oligonucleotides by Matrix-Assisted Laser Desorption/Ionization Time-of-Flight Mass Spectrometry. Rapid Commun Mass Spectrom 14:234–242. doi:10.1002/(SICI)1097-0231(20000229)14:4<234::AID-RCM874>3.0.CO;2-1
102. Kassis CM, DeSimone JM, Linton RW, Lange GW, Friedman RM (1997) An Investigation into the Importance of Polymer-Matrix Miscibility Using Surfactant Modified Matrix-Assisted Laser Desorption/Ionization Mass Spectrometry. Rapid Commun Mass Spectrom 11:1462–1466. doi:10.1002/(SICI)1097-0231(19970830)11:13<1462::AID-RCM44>3.0.CO;2-2
103. Carr RH, Jackson AT (1998) Preliminary Matrix-Assisted Laser Desorption Ionization Time-of-Flight and Field Desorption Mass Spectrometric Analyses of Polymeric Methylene Diphenylene Diisocyanate, Its Amine Precursor and a Model Polyether Prepolymer. Rapid Commun Mass Spectrom 12:2047–2050. doi:10.1002/(SICI)1097-0231(19981230)12:24<2047::AID-RCM428>3.0.CO;2-9
104. Lebedkin S, Ballenweg S, Gross JH, Taylor R, Krätschmer W (1995) Synthesis of $C_{120}O$: A New Dimeric [60]Fullerene Derivative. Tetrahedron Lett 36:4971–4974. doi:10.1016/0040-4039(95)00784-A
105. Ballenweg S, Gleiter R, Krätschmer W (1996) Chemistry at Cyclopentene Addends on [60] Fullerene. Matrix-Assisted Laser Desorption-Ionization Time-of-Flight Mass Spectrometry (MALDI-TOF MS) As a Quick and Facile Method for the Characterization of Fullerene Derivatives. Synth Met 77:209–212. doi:10.1016/0379-6779(96)80089-0
106. Ulmer L, Mattay J, Torres-Garcia HG, Luftmann H (2000) The Use of 2-[(2*E*)-3-(4-*tert*-Butylphenyl)-2-methylprop-2-enylidene]malononitrile as a Matrix for Matrix-Assisted Laser Desorption/Ionization Mass Spectrometry. Eur J Mass Spectrom 6:49–52. doi:10.1255/ejms.329
107. Brown T, Clipston NL, Simjee N, Luftmann H, Hungebühler H, Drewello T (2001) Matrix-Assisted Laser Desorption/Ionization of Amphiphilic Fullerene Derivatives. Int J Mass Spectrom 210(211):249–263. doi:10.1016/S1387-3806(01)00429-8

108. Mirza SP, Raju NP, Vairamani M (2004) Estimation of the Proton Affinity Values of Fifteen Matrix-Assisted Laser Desorption/Ionization Matrices Under Electrospray Ionization Conditions Using the Kinetic Method. J Am Soc Mass Spectrom 15:431–435. doi:10.1016/j.jasms.2003.12.001
109. Burton RD, Watson CH, Eyler JR, Lang GL, Powell DH, Avery MY (1997) Proton Affinities of Eight Matrixes Used for Matrix-Assisted Laser Desorption/Ionization. Rapid Commun Mass Spectrom 11:443–446. doi:10.1002/(SICI)1097-0231(199703)11:5<443::AID-RCM897>3.0.CO;2-3
110. Nordhoff E, Schürenberg M, Thiele G, Lübbert C, Kloeppel K-D, Theiss D, Lehrach H, Gobom J (2003) Sample Preparation Protocols for MALDI-MS of Peptides and Oligonucleotides Using Prestructured Sample Supports. Int J Mass Spectrom 226:163–180. doi:10.1016/S1387-3806(02)00978-8
111. Westman A, Huth-Fehre T, Demirev PA, Sundqvist BUR (1995) Sample Morphology Effects in Matrix-Assisted Laser Desorption/Ionization Mass Spectrometry of Proteins. J Mass Spectrom 30:206–211. doi:10.1002/jms.1190300131
112. Arakawa R, Watanabe S, Fukuo T (1999) Effects of Sample Preparation on Matrix-Assisted Laser Desorption/Ionization Time-of-Flight Mass Spectra for Sodium Polystyrene Sulfonate. Rapid Commun Mass Spectrom 13:1059–1062. doi:10.1002/(SICI)1097-0231(19990615)13:11<1059::AID-RCM608>3.0.CO;2-1
113. Chan PK, Chan T-WD (2000) Effect of Sample Preparation Methods on the Analysis of Dispersed Polysaccharides by Matrix-Assisted Laser Desorption/Ionization Time-of-Flight Mass Spectrometry. Rapid Commun Mass Spectrom 14:1841–1847. doi:10.1002/1097-0231(20001015)14:19<1841::AID-RCM104>3.0.CO;2-Q
114. Vorm O, Mann M (1994) Improved Mass Accuracy in Matrix-Assisted Laser Desorption/Ionization Time-of-Flight Mass Spectrometry of Peptides. J Am Soc Mass Spectrom 5:955–958. doi:10.1016/1044-0305(94)80013-8
115. Ayorinde FO, Keith QL Jr, Wan LW (1999) Matrix-Assisted Laser Desorption/Ionization Time-of-Flight Mass Spectrometry of Cod Liver Oil and the Effect of Analyte/Matrix Concentration on Signal Intensities. Rapid Commun Mass Spectrom 13:1762–1769. doi:10.1002/(SICI)1097-0231(19990915)13:17<1762::AID-RCM711>3.0.CO;2-8
116. Vorm O, Roepstorff P, Mann M (1994) Improved Resolution and Very High Sensitivity in MALDI-TOF of Matrix Surfaces Made by Fast Evaporation. Anal Chem 66:3281–3287. doi:10.1021/ac00091a044
117. Bashir S, Derrick PJ, Critchley P, Gates PJ, Staunton J (2003) Matrix-Assisted Laser Desorption/Ionization Time-of-Flight Mass Spectrometry of Dextran and Dextrin Derivatives. Eur J Mass Spectrom 9:61–70. doi:10.1255/ejms.510
118. Rashidezadeh H, Baochuan G (1998) Investigation of Metal Attachment to Polystyrenes in Matrix-Assisted Laser Desorption Ionization. J Am Soc Mass Spectrom 9:724–730. doi:10.1016/S1044-0305(98)00038-5
119. Rashidezadeh H, Hung K, Baochuan G (1998) Probing Polystyrene Cationization in Matrix-Assisted Laser/Desorption Ionization. Eur Mass Spectrom 4:429–433. doi:10.1255/ejms.267
120. Kühn G, Weidner S, Decker R, Holländer A (1997) Derivatization of Double Bonds Investigated by Matrix-Assisted Laser Desorption/Ionization Mass Spectrometry. Rapid Commun Mass Spectrom 11:914–918. doi:10.1002/(SICI)1097-0231(199705)11:8<914::AID-RCM920>3.0.CO;2-2
121. Kühn G, Weidner S, Just U, Hohner S (1996) Characterization of Technical Waxes. Comparison of Chromatographic Techniques and Matrix-Assisted Laser-Desorption/Ionization Mass Spectrometry. J Chromatogr A 732:111–117. doi:10.1016/0021-9673(95)01255-9
122. Pruns JK, Vietzke J-P, Strassner M, Rapp C, Hintze U, König WA (2002) Characterization of Low Molecular Weight Hydrocarbon Oligomers by Laser Desorption/Ionization Time-of-Flight Mass Spectrometry Using a Solvent-Free Sample Preparation Method. Rapid Commun Mass Spectrom 16:208–211. doi:10.1002/rcm.568

123. Mowat IA, Donovan RJ (1995) Metal-Ion Attachment to Non-Polar Polymers During Laser Desorption/Ionization at 337 Nm. Rapid Commun Mass Spectrom 9:82–90. doi:10.1002/rcm.1290090118
124. Goldschmitt RJ, Wetzel SJ, Blair WR, Guttman CM (2000) Post-Source Decay in the Analysis of Polystyrene by Matrix-Assisted Laser Desorption/Ionization Time-of-Flight Mass Spectrometry. J Am Soc Mass Spectrom 11:1095–1106. doi:10.1016/S1044-0305(00)00177-X
125. Kéki S, Deák G, Zsuga M (2001) Copper(I) Chloride: A Simple Salt for Enhancement of Polystyrene Cationization in Matrix-Assisted Laser Desorption/Ionization Mass Spectrometry. Rapid Commun Mass Spectrom 15:675–678. doi:10.1002/rcm.284
126. Zhang J, Zenobi R (2004) Matrix-Dependent Cationization in MALDI Mass Spectrometry. J Mass Spectrom 39:808–816. doi:10.1002/jms.657
127. Thurman EM, Ferrer I (2010) The Isotopic Mass Defect: a Tool for Limiting Molecular Formulas by Accurate Mass. Anal Bioanal Chem 397:2807–2816. doi:10.1007/s00216-010-3562-6
128. Salplachta J, Rehulka P, Chmelik J (2004) Identification of Proteins by Combination of Size-Exclusion Chromatography with Matrix-Assisted Laser Desorption/Ionization Time-of-Flight Mass Spectrometry and Comparison of Some Desalting Procedures for Both Intact Proteins and Their Tryptic Digests. J Mass Spectrom 39:1395–1401. doi:10.1002/jms.700
129. Jensen ON, Wilm M, Shevchenko A, Mann M (1999) Sample Preparation Methods for Mass Spectrometric Peptide Mapping Directly from 2-DE Gels. Methods Mol Biol 112:513–530
130. Rehulka P, Salplachta J, Chmelik J (2003) Improvement of Quality of Peptide Mass Spectra in Matrix-Assisted Laser Desorption/Ionization Time-of-Flight Mass Spectrometry and Post-Source Decay Analysis of Salty Protein Digests by Using on-Target Washing. J Mass Spectrom 38:1267–1269. doi:10.1002/jms.548
131. Zhang L, Orlando R (1999) Solid-Phase Extraction/MALDI-MS: Extended Ion-Pairing Surfaces for the On-Target Cleanup of Protein Samples. Anal Chem 71:4753–4757. doi:10.1021/ac990328e
132. Gobom J, Nordhoff E, Mirgorodskaya E, Ekman R, Roepstorff P (1999) Sample Purification and Preparation Technique Based on Nano-Scale Reversed-Phase Columns for the Sensitive Analysis of Complex Peptide Mixtures by Matrix-Assisted Laser Desorption/Ionization Mass Spectrometry. J Mass Spectrom 34:105–116. doi:10.1002/(SICI)1096-9888(199902)34:2<105::AID-JMS768>3.0.CO;2-4
133. Leite JF, Hajivandi MR, Diller T, Pope RM (2004) Removal of Sodium and Potassium Adducts Using a Matrix Additive During Matrix-Associated Laser Desorption/Ionization Time-of-Flight Mass Spectrometric Analysis of Peptides. Rapid Commun Mass Spectrom 18:2953–2959. doi:10.1002/rcm.1711
134. Puchades M, Westman A, Blennow K, Davidsson P (1999) Removal of Sodium Dodecyl Sulfate from Protein Samples Prior to Matrix-Assisted Laser Desorption/Ionization Mass Spectrometry. Rapid Commun Mass Spectrom 13:344–349. doi:10.1002/(SICI)1097-0231(19990315)13:5<344::AID-RCM489>3.0.CO;2-V
135. Trimpin S, Grimsdale AC, Räder HJ, Müllen K (2002) Characterization of an Insoluble Poly(9,9-diphenyl-2,7-fluorene) by Solvent-Free Sample Preparation for MALDI-TOF Mass Spectrometry. Anal Chem 74:3777–3782. doi:10.1021/ac0111863
136. Trimpin S, Rouhanipour A, Az R, Räder HJ, Müllen K (2001) New Aspects in Matrix-Assisted Laser Desorption/Ionization Time-of-Flight Mass Spectrometry: a Universal Solvent-Free Sample Preparation. Rapid Commun Mass Spectrom 15:1364–1373. doi:10.1002/rcm.372
137. Guittard J, Hronowski XL, Costello CE (1999) Direct Matrix-Assisted Laser Desorption/Ionization Mass Spectrometric Analysis of Glycosphingolipids on Thin Layer Chromatographic Plates and Transfer Membranes. Rapid Commun Mass Spectrom 13:1838–1849. doi:10.1002/(SICI)1097-0231(19990930)13:18<1838::AID-RCM726>3.0.CO;2-9

138. McCrery DA, Ledford EB Jr, Gross ML (1982) Laser Desorption Fourier Transform Mass Spectrometry. Anal Chem 54:1435–1437. doi:10.1021/ac00245a040
139. Claereboudt J, Claeys M, Geise H, Gijbels R, Vertes A (1993) Laser Microprobe Mass Spectrometry of Quaternary Phosphonium Salts: Direct Versus Matrix-Assisted Laser Desorption. J Am Soc Mass Spectrom 4:798–812. doi:10.1016/1044-0305(93)80038-Z
140. Gromer S, Gross JH (2002) Methylseleninate Is a Substrate Rather Than an Inhibitor of Mammalian Thioredoxin Reductase: Implications for the Antitumor Effects of Selenium. J Biol Chem 277:9701–9706. doi:10.1074/jbc.M109234200
141. Wood TD, Van Cleef GW, Mearini MA, Coe JV, Marshall AG (1993) Formation of Giant Fullerene Gas-Phase Ions (C_{2n}^+, $n = 60$–500): Laser Desorption/Electron Ionization Fourier-Transform Ion Cyclotron Resonance Mass Spectrometric Evidence. Rapid Commun Mass Spectrom 7:304–311. doi:10.1002/rcm.1290070408
142. Beck RD, Weis P, Hirsch A, Lamparth I (1994) Laser Desorption Mass Spectrometry of Fullerene Derivatives: Laser-Induced Fragmentation and Coalescence Reactions. J Phys Chem 98:9683–9687. doi:10.1021/j100090a001
143. Wolkenstein K, Gross JH, Oeser T, Schöler HF (2002) Spectroscopic Characterization and Crystal Structure of the 1,2,3,4,5,6-Hexahydrophenanthro[1,10,9,8-*opqra*]Perylene. Tetrahedron Lett 43:1653–1655. doi:10.1016/S0040-4039(02)00085-0
144. Grim DM, Siegel J, Allison J (2002) Does Ink Age Inside of a Pen Cartridge? J Forensic Sci 47:1294–1297. doi:10.1520/JFS15563J
145. Jones RM, Lamb JH, Lim CK (1995) Urinary Porphyrin Profiles by Laser Desorption/Ionization Time-of-Flight Mass Spectrometry Without the Use of Classical Matrixes. Rapid Commun Mass Spectrom 9:921–923. doi:10.1002/rcm.1290091011
146. Krätschmer W, Lamb LD, Fostiropoulos K, Huffman DR (1990) Solid C_{60}: A New Form of Carbon. Nature 347:354–358. doi:10.1038/347354a0
147. Kroto H (1997) Symmetry, Space, Stars and C_{60}. Rev Mod Phys 69:703–722. doi:10.1103/RevModPhys.69.703
148. Gross JH (2009) Mass Spectrometry. In: Andrews DL (ed) Encyclopedia of Applied Spectroscopy. Wiley-VCH, Weinheim
149. Chapman JR (ed) (2000) Mass Spectrometry of Proteins and Peptides. Humana Press, Totowa
150. Snyder AP (2000) Interpreting Protein Mass Spectra. Oxford University Press, New York
151. Pasch H, Schrepp W (2003) MALDI-TOF Mass Spectrometry of Synthetic Polymers. Springer, Heidelberg
152. Barner-Kowollik C, Gruendling T, Falkenhagen J, Weidner S (eds) (2012) Mass Spectrometry in Polymer Chemistry. Wiley-VCH, Weinheim
153. Angeletti R, Gioacchini AM, Seraglia R, Piro R, Traldi P (1998) The Potential of Matrix-Assisted Laser Desorption/Ionization Mass Spectrometry in the Quality Control of Water Buffalo Mozzarella Cheese. J Mass Spectrom 33:525–531. doi:10.1002/(SICI)1096-9888(199806)33:6<525::AID-JMS655>3.0.CO;2-S
154. Fanton C, Delogu G, Maccioni E, Podda G, Seraglia R, Traldi P (1998) Matrix-Assisted Laser Desorption/Ionization Mass Spectrometry in the Dairy Industry 2. The Protein Fingerprint of Ewe Cheese and Its Application to Detection of Adulteration by Bovine Milk. Rapid Commun Mass Spectrom 12:1569–1573. doi:10.1002/(SICI)1097-0231(19981030)12:20<1569::AID-RCM341>3.0.CO;2-F
155. Krishnamurthy T, Ross PL, Rajamani U (1996) Detection of Pathogenic and Non-Pathogenic Bacteria by Matrix-Assisted Laser Desorption/Ionization Time-of-Flight Mass Spectrometry. Rapid Commun Mass Spectrom 10:883–888. doi:10.1002/(SICI)1097-0231(19960610)10:8<883::AID-RCM594>3.0.CO;2-V
156. Egert M, Spaeth K, Weik K, Kunzelmann H, Horn C, Kohl M, Blessing F (2015) Bacteria on Smartphone Touchscreens in a German University Setting and Evaluation of Two Popular Cleaning Methods Using Commercially Available Cleaning Products. Folia Microbiol 60:159–164. doi:10.1007/s12223-014-0350-2

157. Avila CC, Almeida FG, Palmisano G (2016) Direct Identification of Trypanosomatids by Matrix-Assisted Laser Desorption Ionization–Time-of-Flight Mass Spectrometry (DIT MALDI-TOF MS). J Mass Spectrom 51:549–557. doi:10.1002/jms.3763
158. Mestas J, Quias T, Dien Bard J (2016) Direct Identification of Aerobic Bacteria by Matrix-Assisted Laser Desorption Ionization Time-of-Flight Mass Spectrometry Is Accurate and Robust. J Clin Lab Anal 30:543–551. doi:10.1002/jcla.21900
159. Bohme K, Fernandez-No IC, Barros-Velazquez J, Gallardo JM, Calo-Mata P, Canas B (2010) Species Differentiation of Seafood Spoilage and Pathogenic Gram-Negative Bacteria by MALDI-TOF Mass Fingerprinting. J Proteome Res 9:3169–3183. doi:10.1021/pr100047q
160. Gevaert K, Vandekerckhove J (2000) Protein Identification Methods in Proteomics. Electrophoresis 21:1145–1154. doi:10.1002/(SICI)1522-2683(20000401)21:6<1145::AID-ELPS1145>3.0.CO;2-Z
161. Peng J, Gygi SP (2001) Proteomics: The Move to Mixtures. J Mass Spectrom 36:1083–1096. doi:10.1002/jms.229
162. Aebersold R, Mann M (2003) Mass Spectrometry-Based Proteomics. Nature 422:198–207. doi:10.1038/nature01511
163. Reinders J, Lewandrowski U, Moebius J, Wagner Y, Sickmann A (2004) Challenges in Mass Spectrometry-Based Proteomics. Proteomics 4:3686–3703. doi:10.1002/pmic.200400869
164. Paizs B, Suhai S (2005) Fragmentation Pathways of Protonated Peptides. Mass Spectrom Rev 24:508–548. doi:10.1002/mas.20024
165. Khidekel N, Ficarro SB, Clark PM, Bryan MC, Swaney DL, Rexach JE, Sun YE, Coon JJ, Peters EC, Hsieh-Wilson LC (2007) Probing the Dynamics of *O*-GlcNAc Glycosylation in the Brain Using Quantitative Proteomics. Nature Chem Biol 3:339–348. doi:10.1038/nchembio881
166. Vestal M, Hayden K (2007) High Performance MALDI-TOF Mass Spectrometry for Proteomics. Int J Mass Spectrom 268:83–92. doi:10.1016/j.ijms.2007.06.21
167. Nesvizhskii AI, Vitek O, Aebersold R (2007) Analysis and Validation of Proteomic Data Generated by Tandem Mass Spectrometry. Nature Methods 4:787–797. doi:10.1038/nmeth1088
168. Paizs B, Van SM (2008) Editorial: Focus Issue on Peptide Fragmentation. J Am Soc Mass Spectrom 19:1717–1718. doi:10.1016/j.jasms.2008.10.009
169. Seidler J, Zinn N, Boehm ME, Lehmann WD (2010) De Novo Sequencing of Peptides by MS/MS. Proteomics 10:634–649. doi:10.1002/pmic.200900459
170. Henzel WJ, Watanabe C, Stults JT (2003) Protein Identification: The Origins of Peptide Mass Fingerprinting. J Am Soc Mass Spectrom 14:931–942. doi:10.1016/S1044-0305(03)00214-9
171. Bleiholder C, Osburn S, Williams TD, Suhai S, Van SM, Harrison AG, Paizs B (2008) Sequence-Scrambling Fragmentation Pathways of Protonated Peptides. J Am Chem Soc 130:17774–17789. doi:10.1021/ja805074d
172. Kinter M, Sherman NE (2000) Protein Sequencing and Identification Using Tandem Mass Spectrometry. Wiley, Chichester
173. Kaltashov IA, Eyles SJ (2005) Mass Spectrometry in Biophysics: Conformation and Dynamics of Biomolecules. John Wiley & Sons Inc., Hoboken
174. Roepstorff P (1984) Proposal for a Common Nomenclature for Sequence Ions in Mass Spectra of Peptides. Biomed Mass Spectrom 11:601. doi:10.1002/bms.1200111109
175. Biemann K (1988) Contributions of Mass Spectrometry to Peptide and Protein Structure. Biomed Environ Mass Spectrom 16:99–111. doi:10.1002/bms.1200160119
176. Yalcin T, Khouw C, Csizmadia IG, Peterson MR, Harrison AG (1995) Why Are b Ions Stable Species in Peptide Spectra? J Am Soc Mass Spectrom 6:1165–1174. doi:10.1016/1044-0305(95)00569-2
177. Yalcin T, Csizmadia IG, Peterson MR, Harrison AG (1996) The Structure and Fragmentation of B_n (n >= 3) Ions in Peptide Spectra. J Am Soc Mass Spectrom 7:233–242. doi:10.1016/1044-0305(95)00677-X

178. Harrison AG (2008) Peptide Sequence Scrambling Through Cyclization of B5 Ions. J Am Soc Mass Spectrom 19:1776–1780. doi:10.1016/j.jasms.2008.06.025
179. Harrison AG (2009) To b or Not to B: the Ongoing Saga of Peptide b Ions. Mass Spectrom Rev 28:640–654. doi:10.1002/mas.20228
180. Amadei GA, Cho CF, Lewis JD, Luyt LG (2010) A Fast, Reproducible and Low-Cost Method for Sequence Deconvolution of "on-Bead" Peptides via "on-Target" Maldi-TOF/TOF Mass Spectrometry. J Mass Spectrom 45:241–251. doi:10.1002/jms.1708
181. Harvey DJ (2003) Matrix-Assisted Laser Desorption/Ionization Mass Spectrometry of Carbohydrates and Glycoconjugates. Int J Mass Spectrom 226:1–35. doi:10.1016/S1387-3806(02)00968-5
182. Stahl B, Linos A, Karas M, Hillenkamp F, Steup M (1997) Analysis of Fructans from Higher Plants by Matrix-Assisted Laser Desorption/Ionization Mass Spectrometry. Anal Biochem 246:195–204. doi:10.1006/abio.1997.2011
183. Garrozzo D, Impallomeni G, Spina E, Sturiale L, Zanetti F (1995) Matrix-Assisted Laser Desorption/Ionization Mass Spectrometry of Polysaccharides. Rapid Commun Mass Spectrom 9:937–941. doi:10.1002/rcm.1290091014
184. Welham KJ, Domin MA, Johnson K, Jones L, Ashton DS (2000) Characterization of Fungal Spores by Laser Desorption/Ionization Time-of-Flight Mass Spectrometry. Rapid Commun Mass Spectrom 14:307–310. doi:10.1002/(SICI)1097-0231(20000315)14:5<307::AID-RCM823>3.0.CO;2-3
185. Harvey DJ, Naven TJP, Küster B, Bateman R, Green MR, Critchley G (1995) Comparison of Fragmentation Modes for the Structural Determination of Complex Oligosaccharides Ionized by Matrix-Assisted Laser Desorption/Ionization Mass Spectrometry. Rapid Commun Mass Spectrom 9:1556–1561. doi:10.1002/rcm.1290091517
186. Lin H, Hunter JM, Becker CL (1999) Laser Desorption of DNA Oligomers Larger than One Kilobase from Cooled 4-Nitrophenol. Rapid Commun Mass Spectrom 13:2335–2340. doi:10.1002/(SICI)1097-0231(19991215)13:23<2335::AID-RCM794>3.0.CO;2-1
187. Bartolini WP, Johnston MV (2000) Characterizing DNA Photo-Oxidation Reactions by High-Resolution Mass Measurements with Matrix-Assisted Laser Desorption/Ionization Time-of-Flight Mass Spectrometry. J Mass Spectrom 35:408–416. doi:10.1002/(SICI)1096-9888(200003)35:3<408::AID-JMS951>3.0.CO;2-0
188. Jackson AT, Yates HT, Scrivens JH, Critchley G, Brown J, Green MR, Bateman RH (1996) The Application of Matrix-Assisted Laser Desorption/Ionization Combined with Collision-Induced Dissociation to the Analysis of Synthetic Polymers. Rapid Commun Mass Spectrom 10:1668–1674. doi:10.1002/(SICI)1097-0231(199609)10:12<1459::AID-RCM630>3.0.CO;2-Q
189. Tang X, Dreifuss PA, Vertes A (1995) New Matrixes and Accelerating Voltage Effects in Matrix-Assisted Laser Desorption/Ionization of Synthetic Polymers. Rapid Commun Mass Spectrom 9:1141–1147. doi:10.1002/rcm.1290091212
190. Montaudo G, Montaudo MS, Puglisi C, Samperi F (1994) Self-Calibrating Property of Matrix-Assisted Laser Desorption/Ionization Time-of-Flight Spectra of Polymeric Materials. Rapid Commun Mass Spectrom 8:981–984. doi:10.1002/rcm.1290081215
191. Williams JB, Chapman TM, Hercules DM (2003) Matrix-Assisted Laser Desorption/Ionization Mass Spectrometry of Discrete Mass Poly(butylene glutarate) Oligomers. Anal Chem 75:3092–3100. doi:10.1021/ac030061q
192. Nielen MFW, Malucha S (1997) Characterization of Polydisperse Synthetic Polymers by Size-Exclusion Chromatography/Matrix-Assisted Laser Desorption/Ionization Time-of-Flight Mass Spectrometry. Rapid Commun Mass Spectrom 11:1194–1204. doi:10.1002/(SICI)1097-0231(199707)11:11<1194::AID-RCM935>3.0.CO;2-L
193. de Koster CG, Duursma MC, van Rooij GJ, Heeren RMA, Boon JJ (1995) Endgroup Analysis of Polyethylene Glycol Polymers by Matrix-Assisted Laser Desorption/Ionization Fourier-Transform Ion Cyclotron Resonance Mass Spectrometry. Rapid Commun Mass Spectrom 9:957–962. doi:10.1002/rcm.1290091018

194. Weidner S, Kühn G, Just U (1995) Characterization of Oligomers in Poly(Ethylene Terephthalate) by Matrix-Assisted Laser Desorption/Ionization Mass Spectrometry. Rapid Commun Mass Spectrom 9:697–702. doi:10.1002/rcm.1290090813
195. Montaudo MS (1999) Sequence Constraints in a Glycine-Lactic Acid Copolymer Determined by Matrix-Assisted Laser Desorption/Ionization Mass Spectrometry. Rapid Commun Mass Spectrom 13:639–644. doi:10.1002/(SICI)1097-0231(19990430)13:8<639::AID-RCM513>3.0.CO;2-J
196. Montaudo MS (2002) Mass Spectra of Copolymers. Mass Spectrom Rev 21:108–144. doi:10.1002/mas.10021
197. Murgasova R, Hercules DM (2003) Quantitative Characterization of a Polystyrene/Poly (α-methylstyrene) Blend by MALDI Mass Spectrometry and Size-Exclusion Chromatography. Anal Chem 75:3744–3750. doi:10.1021/ac020593r
198. Satoh T, Kubo A, Hazama H, Awazu K, Toyoda M (2014) Separation of Isobaric Compounds Using a Spiral Orbit Type Time-of-Flight Mass Spectrometer, MALDI-SpiralTOF. Mass Spectrom 3:S0027-1-S0027/5. doi:10.5702/massspectrometry.S0027
199. Grayson SM, Myers BK, Bengtsson J, Malkoch M (2014) Advantages of Monodisperse and Chemically Robust "SpheriCal" Polyester Dendrimers as a "Universal" MS Calibrant. J Am Soc Mass Spectrom 25:303–309. doi:10.1007/s13361-013-0777-8
200. Casey BK, Grayson SM (2015) Letter: The Potential of Amine-Containing Dendrimer Mass Standards for Internal Calibration of Peptides. Eur J Mass Spectrom 21:747–752. doi:10.1255/ejms.1394
201. Gross JH (2016) Improved Procedure for Dendrimer-Based Mass Calibration in Matrix-Assisted Laser Desorption/Ionization-Time-of-Flight-Mass Spectrometry. Anal Bioanal Chem 408:5945–5951. doi:10.1007/s00216-016-9714-6
202. Wei J, Buriak JM, Siuzdak G (1999) Desorption-Ionization Mass Spectrometry on Porous Silicon. Nature 399:243–246. doi:10.1038/20400
203. Go EP, Shen Z, Harris K, Siuzdak G (2003) Quantitative Analysis with Desorption/Ionization on Silicon Mass Spectrometry Using Electrospray Deposition. Anal Chem 75:5475–5479. doi:10.1021/ac034376h
204. Shen Z, Thomas JJ, Averbuj C, Broo KM, Engelhard M, Crowell JE, Finn MG, Siuzdak G (2001) Porous Silicon as a Versatile Platform for Laser Desorption/Ionization Mass Spectrometry. Anal Chem 73:612–619. doi:10.1021/ac000746f
205. Laiko VV, Taranenko NI, Berkout VD, Musselman BD, Doroshenko VM (2002) Atmospheric Pressure Laser Desorption/Ionization on Porous Silicon. Rapid Commun Mass Spectrom 16:1737–1742. doi:10.1002/rcm.781
206. Go EP, Prenni JE, Wei J, Jones A, Hall SC, Witkowska HE, Shen Z, Siuzdak G (2003) Desorption/Ionization on Silicon Time-of-Flight/Time-of-Flight Mass Spectrometry. Anal Chem 75:2504–2506. doi:10.1021/ac026253n
207. Kang MJ, Pyun JC, Lee JC, Choi YJ, Park JH, Park JG, Lee JG, Choi HJ (2005) Nanowire-Assisted Laser Desorption and Ionization Mass Spectrometry for Quantitative Analysis of Small Molecules. Rapid Commun Mass Spectrom 19:3166–3170. doi:10.1002/rcm.2187
208. Go EP, Apon JV, Luo G, Saghatelian A, Daniels RH, Sahi V, Dubrow R, Cravatt BF, Vertes A, Siuzdak G (2005) Desorption/Ionization on Silicon Nanowires. Anal Chem 77:1641–1646. doi:10.1021/ac048460o
209. Vidova V, Novak P, Strohalm M, Pol J, Havlicek V, Volny M (2010) Laser Desorption-Ionization of Lipid Transfers: Tissue Mass Spectrometry Imaging Without MALDI Matrix. Anal Chem 82:4994–4997. doi:10.1021/ac100661h
210. Shenar N, Cantel S, Martinez J, Enjalbal C (2009) Comparison of Inert Supports in Laser Desorption/Ionization Mass Spectrometry of Peptides: Pencil Lead, Porous Silica Gel, DIOS-Chip and NALDI Target. Rapid Commun Mass Spectrom 23:2371–2379. doi:10.1002/rcm.4158
211. Hashir MA, Stecher G, Bakry R, Kasemsook S, Blassnig B, Feuerstein I, Abel G, Popp M, Bobleter O, Bonn GK (2007) Identification of Carbohydrates by Matrix-Free Material-

Enhanced Laser Desorption/Ionisation Mass Spectrometry. Rapid Commun Mass Spectrom 21:2759–2769. doi:10.1002/rcm.3147
212. Rainer M, Muhammad NNH, Huck CW, Feuerstein I, Bakry R, Huber LA, Gjerde DT, Zou X, Qian H, Du X, Fang WG, Ke Y, Bonn GK (2006) Ultra-Fast Mass Fingerprinting by High-Affinity Capture of Peptides and Proteins on Derivatized Poly(Glycidyl Methacrylate/Divinylbenzene) for the Analysis of Serum and Cell Lysates. Rapid Commun Mass Spectrom 20:2954–2960. doi:10.1002/rcm.2673
213. Feuerstein I, Najam-ul-Haq M, Rainer M, Trojer L, Bakry R, Aprilita NH, Stecher G, Huck CW, Bonn GK, Klocker H, Bartsch G, Guttman A (2006) Material-Enhanced Laser Desorption/Ionization (MELDI)-A New Protein Profiling Tool Utilizing Specific Carrier Materials for Time-of-Flight Mass Spectrometric Analysis. J Am Soc Mass Spectrom 17:1203–1208. doi:10.1016/j.jasms.2006.04.032
214. Caprioli RM, Farmer TB, Gile J (1997) Molecular Imaging of Biological Samples: Localization of Peptides and Proteins Using MALDI-TOF MS. Anal Chem 69:4751–4760. doi:10.1021/ac970888i
215. Cornett DS, Reyzer ML, Chaurand P, Caprioli RM (2007) MALDI Imaging Mass Spectrometry: Molecular Snapshots of Biochemical Systems. Nat Methods 4:828–833. doi:10.1038/nmeth1094
216. Chaurand P, Schriver KE, Caprioli RM (2007) Instrument Design and Characterization for High Resolution MALDI-MS Imaging of Tissue Sections. J Mass Spectrom 42:476–489. doi:10.1002/jms.1180
217. Franck J, Arafah K, Elayed M, Bonnel D, Vergara D, Jacquet A, Vinatier D, Wisztorski M, Day R, Fournier I, Salzet M (2009) MALDI Imaging Mass Spectrometry: State of the Art Technology in Clinical Proteomics. Mol Cell Proteom 8:2023–2033. doi:10.1074/mcp.R800016-MCP200
218. Francese S, Dani FR, Traldi P, Mastrobuoni G, Pieraccini G, Moneti G (2009) MALDI Mass Spectrometry Imaging, from Its Origins Up to Today: The State of the Art. Comb Chem High Throughput Screening 12:156–174. doi:10.2174/138620709787315454
219. Ramanathan R (ed) (2009) Mass Spectrometry in Drug Metabolism and Pharmacokinetics. John Wiley & Sons, Inc., Hoboken
220. Todd PJ, Schaaff TG, Chaurand P, Caprioli RM (2001) Organic Ion Imaging of Biological Tissue with Secondary Ion Mass Spectrometry and Matrix-Assisted Laser Desorption/Ionization. J Mass Spectrom 36:355–369. doi:10.1002/jms.153
221. Sugiura Y, Shimma S, Setou M (2006) Two-Step Matrix Application Technique to Improve Ionization Efficiency for Matrix-Assisted Laser Desorption/Ionization in Imaging Mass Spectrometry. Anal Chem 78:8227–8235. doi:10.1021/ac060974v
222. Guenther S, Koestler M, Schulz O, Spengler B (2010) Laser Spot Size and Laser Power Dependence of Ion Formation in High Resolution MALDI Imaging. Int J Mass Spectrom 294:7–15. doi:10.1016/j.ijms.2010.03.014
223. Kompauer M, Heiles S, Spengler B (2017) Atmospheric Pressure MALDI Mass Spectrometry Imaging of Tissues and Cells at 1.4-μm Lateral Resolution. Nat Methods 14:90–96. doi:10.1038/nmeth.4071
224. Ogrinc Potocnik N, Porta T, Becker M, Heeren RMA, Ellis SR (2015) Use of Advantageous, Volatile Matrices Enabled by Next-Generation High-Speed Matrix-Assisted Laser Desorption/Ionization Time-of-Flight Imaging Employing a Scanning Laser Beam. Rapid Commun Mass Spectrom 29:2195–2203. doi:10.1002/rcm.7379
225. Spengler B (2015) Mass Spectrometry Imaging of Biomolecular Information. Anal Chem 87:64–82. doi:10.1021/ac504543v
226. Grey AC (2016) MALDI Imaging of the Eye: Mapping Lipid, Protein and Metabolite Distributions in Aging and Ocular Disease. Int J Mass Spectrom 401:31–38. doi:10.1016/j.ijms.2016.02.017
227. Heyman HM, Dubery IA (2016) The Potential of Mass Spectrometry Imaging in Plant Metabolomics: A Review. Phytochemistry Reviews 15:297–316. doi:10.1007/s11101-015-9416-2

228. Ferguson L, Bradshaw R, Wolstenholme R, Clench M, Francese S (2011) Two-Step Matrix Application for the Enhancement and Imaging of Latent Fingermarks. Anal Chem 83:5585–5591. doi:10.1021/ac200619f
229. Bradshaw R, Denison N, Francese S (2016) Development of Operational Protocols for the Analysis of Primary and Secondary Fingermark Lifts by MALDI-MS Imaging. Anal Methods 8:6795–6804. doi:10.1039/c6ay01406b
230. Emerson B, Gidden J, Lay JO Jr, Durham B (2011) Laser Desorption/Ionization Time-of-Flight Mass Spectrometry of Triacylglycerols and Other Components in Fingermark Samples. J Forensic Sci 56:381–389. doi:10.1111/j.1556-4029.2010.01655.x
231. Deininger L, Patel E, Clench MR, Sears V, Sammon C, Francese S (2016) Proteomics Goes Forensic: Detection and Mapping of Blood Signatures in Fingermarks. Proteomics 16:1707–1717. doi:10.1002/pmic.201500544
232. Groeneveld G, de Puit M, Bleay S, Bradshaw R, Francese S (2015) Detection and Mapping of Illicit Drugs and Their Metabolites in Fingermarks by MALDI MS and Compatibility with Forensic Techniques. Scientific Reports 5:11716. doi:10.1038/srep11716
233. Laiko VV, Baldwin MA, Burlingame AL (2000) Atmospheric Pressure Matrix-Assisted Laser Desorption/Ionization Mass Spectrometry. Anal Chem 72:652–657. doi:10.1021/ac990998k
234. Laiko VV, Moyer SC, Cotter RJ (2000) Atmospheric Pressure MALDI/Ion Trap Mass Spectrometry. Anal Chem 72:5239–5243. doi:10.1021/ac000530d
235. Moyer SC, Marzilli LA, Woods AS, Laiko VV, Doroshenko VM, Cotter RJ (2003) Atmospheric Pressure Matrix-Assisted Laser Desorption/Ionization (AP MALDI) on a Quadrupole Ion Trap Mass Spectrometer. Int J Mass Spectrom 226:133–150. doi:10.1016/S1387-3806(02)00972-7
236. Doroshenko VM, Laiko VV, Taranenko NI, Berkout VD, Lee HS (2002) Recent Developments in Atmospheric Pressure MALDI Mass Spectrometry. Int J Mass Spectrom 221:39–58. doi:10.1016/S1387-3806(02)00893-X
237. Moskovets E, Misharin A, Laiko V, Doroshenko V (2016) A Comparative Study on the Analytical Utility of Atmospheric and Low-Pressure MALDI Sources for the Mass Spectrometric Characterization of Peptides. Methods 104:21–32. doi:10.1016/j.ymeth.2016.02.009
238. Krutchinsky AN, Loboda AV, Spicer VL, Dworschak R, Ens W, Standing KG (1998) Orthogonal Injection of Matrix-Assisted Laser Desorption/Ionization Ions into a Time-of-Flight Spectrometer Through a Collisional Damping Interface. Rapid Commun Mass Spectrom 12:508–518. doi:10.1002/(SICI)1097-0231(19980515)12:9<508::AID-RCM197>3.0.CO;2-L
239. McIver RT Jr, Li Y, Hunter RL (1994) Matrix-Assisted Laser Desorption/Ionization with an External Ion Source Fourier-Transform Mass Spectrometer. Rapid Commun Mass Spectrom 8:237–241. doi:10.1002/rcm.1290080303
240. Li Y, McIver RT Jr, Hunter RL (1994) High-Accuracy Molecular Mass Determination for Peptides and Proteins by Fourier Transform Mass Spectrometry. Anal Chem 66:2077–2083. doi:10.1021/ac00085a024
241. Li Y, Tang K, Little DP, Koester H, McIver RT Jr (1996) High-Resolution MALDI Fourier Transform Mass Spectrometry of Oligonucleotides. Anal Chem 68:2090–2096. doi:10.1021/ac9601268
242. Baykut G, Jertz R, Witt M (2000) Matrix-Assisted Laser Desorption/Ionization Fourier Transform Ion Cyclotron Resonance Mass Spectrometry with Pulsed In-Source Collision Gas and In-Source Ion Accumulation. Rapid Commun Mass Spectrom 14:1238–1247. doi:10.1002/1097-0231(20000730)14:14<1238::AID-RCM17>3.0.CO;2-H
243. O'Connor PB, Costello CE (2001) A High Pressure Matrix-Assisted Laser Desorption/Ionization Fourier Transform Mass Spectrometry Ion Source for Thermal Stabilization of Labile Biomolecules. Rapid Commun Mass Spectrom 15:1862–1868. doi:10.1002/rcm.447